UNIVERSITÀ
DEGLI STUDI
DI PADOVA

Sede Amministrativa: Università degli Studi di Padova

Dipartimento di Tecnica e Gestione dei Sistemi Industriali

CORSO DI DOTTORATO DI RICERCA IN: ING. MECCATRONICA E DELL'INNOVAZIONE MECCANICA DEL PRODOTTO
CURRICOLO: MECCANICA DEI MATERIALI
CICLO: XXX

CORRELATIONS BETWEEN DEFECT CONTENT, MICROSTRUCTURE AND CASTING QUALITY IN HPDC AlSi ALLOYS

Coordinatore: Ch.mo Prof. Roberto Caracciolo
Supervisore: Ch.mo Prof. Franco Bonollo

Dottorando: Eleonora Battaglia

Abstract

Two are the key players of this doctoral thesis: secondary AlSi alloys and the High Pressure Die Casting (HPDC) process.

As the levels of CO2 and other greenhouse gasses increase, the industry sector is called to reduce the emissions produced and to contain the energy consumptions. Therefore, secondary Al ingot production shows a 6% annual rate growth, mainly drawn by the transport sector.

In particular, automotive industry and, in general, transportation one increasingly needs light components in order to reduce total weights and therefore limit harmful emissions and fuel consumption. To this end, HPDC process is getting more and more crucial. It is, on one hand, versatile and highly productive but, on the other, the elevated amount of defects found in the castings sometimes compromises the characteristics of the final product.

The research activities performed during the Ph.D. years focused on the High Pressure Die Casting (HPDC) process and the assessment of the correlations between process parameters, casting quality and mechanical response improvement. The research work comprises three interconnected topics: (i) the effect of the process on the casting quality in terms of defect generation and eutectic Si morphology, (ii) how defects and microstructure influence the mechanical response of the components and (iii) how the mechanical properties can be improved through specific heat treatments.

The thesis starts dealing with the work developed within the EU MUSIC project aimed at transforming a production-rate-dominated manufacturing process into a quality/efficiency-driven and integration-oriented one. In the frame of the EU MUSIC project, an investigation procedure was developed which led to the definition of preliminary correlations between process parameters, defect content and static mechanical properties obtained analyzing both reference castings and commercialized industrial demonstrators.

A specific focus was always devoted to the possible industrial application in order to narrow down the gap between academic research and industry.

The second section deals with the definition of a so-called *Penalty Index* based on FE simulation model and fractographic investigations. It gave satisfactory predictions of both static strength and fatigue life of castings based on defect locations on the fracture surfaces and their projected areas. The elaborated criterion gives good results even though it does not take into account the real morphology of defects (which can be a very complex 3D morphology in the case of irregular flaws); its main drawback is that it is a "post-mortem" application. However, this limit can be overcome thanks to the wider diffusion of industrial high-resolution Computed Tomography (CT).

The third section is mainly dedicated to the study of HPDC microstructure. Two secondary Al-Si alloys, an AlSi12(b) and an AlSi12Cu1(Fe), were used to produce HPDCs. In both cases, there was an evident non-homogeneity of the microstructure, in particular of the eutectic Si morphology which could be correlated, to some extent, to the different as-cast mechanical

response of the castings. Heat treatments at 350°C and soaking times ranging from1 to 8 hours were performed

Mechanical testing, hardness and metallographic investigations were carried out in order to understand the effect of the heat treatments. Microstructural observations using OM, SEM, TEM and EBSD investigations were also performed.

Based on the obtained results, the heat treating procedure was effective since it did not cause surface blistering (a real issue in the heat treatment of die castings) or component distortion.

The visible mechanical improvement in terms of both static and fatigue response was determined by Si crystals' size and morphology. Thanks to heat treatment, the Si particle morphology changed from an interconnected 'network' to a more fragmented and smooth one. In terms of mechanical behavior, from a rapid crack propagation which led to a drastic reduction of the load-bearing area during the component use, the heat treatment caused a less instantaneous failure since the crack had to propagate through the ductile Al matrix.

The best solution was assessed and proposed to obtain significant mechanical properties and low costs.

Preliminary lab tests aimed at verifying the effect on the eutectic Si of common alloying elements such as Cu and Fe were finally conducted. A small mold was designed and manufactured in order to produce castings with solidification velocities comparable with those typical of the HPDC process. The base alloy was an AlSi12(b) ingot which was melt and several elements (i.e. Cu, Fe, Mn) were added to reach the AlSi12Cu1(Fe) alloy ranges. A refining effect of Cu was observed, however further investigations are necessary in order to better understand its joined effect with Fe.

This doctoral thesis deals with a complex topic; a high number of sequential actions are involved in the process. This is the reason why the developed work brought interesting and useful results, but it can also be considered a starting point for further investigations. Further analyses can be conducted to understand the causes of the non-uniform eutectic Si morphology and the nature of the Si precipitates within the α-Al phase as well as an enhancement of the elaborated Penalty Index can be obtained.

KEYWORDS:
High pressure die casting; secondary Aluminum alloys; process parameters; defects; mechanical testing; FE analysis; penalization criterion

Acknowledgements

There are many people that I want to acknowledge; they are special not only from a professional point of view but most importantly, from a personal one.

I want to express my deep gratitude and appreciation to Prof. Franco Bonollo, my advisor, for the opportunity he gave me three years ago to join the DTG Metallurgy group, for his endless support during my study, for his patience and for providing me with the opportunity to pursue my academic studies in the metallurgy field, not only here in Vicenza but also in the US.

I extend my sincere gratitude to Giacomo Mazzacavallo, for his technical assistance in the lab, for his valuable comments and advice and for his brilliant ideas during my work.
During these past three years, a good working relationship has become a sincere friendship.

I would like to thank Prof. Giulio Timelli, Prof. Paolo Ferro and Dr. Alberto Fabrizi for very helpful discussions, useful comments and technical assistance. They've always inspired me with intelligent ideas and comments and they've become more than just reliable professors and colleagues.

I offer my sincere gratitude to the whole technician and metallurgy team, in particular to Enrico Della Rovere, for his technical assistance. I would like to thank Elena Fiorese, Giorgio Kral and the bachelor and master students, who helped me with the experimental work and all the present and former Ph.D. students for making a vibrant and joyful working atmosphere.

Last but not least, I would like to express my immense gratitude and love to my family who always supported me and believed in me. My parents, always by my side, my sister, my brother and their families with their many children, my joy, and especially my beloved Stefano who is a constant source of love and support. I am so incredibly blessed having you in my life and calling you husband at the end of this journey.

Ringraziamenti

Ci sono molte persone che voglio ringraziare; tutte speciali non solo da un punto di vista professionale ma, soprattutto, da un punto di vista umano e personale.

Voglio iniziare esprimendo la mia profonda gratitudine e il mio profondo apprezzamento nei confronti del Prof. Franco Bonollo, il mio supervisore, per avermi dato l'opportunità, tre anni fa, di entrare a far parte del gruppo di Metallurgia del DTG, per il continuo supporto nella ricerca, per la pazienza e per la possibilità che mi ha dato di fare ricerca in quest'ambito sia qui a Vicenza che, per alcuni mesi, negli USA.

Estendo la mia sincera gratitudine verso Giacomo Mazzacavallo, per la sua assistenza tecnica in laboratorio, per i suoi commenti e suggerimenti sempre utili e per le brillanti idee che mi hanno aiutata nel mio lavoro. In questi tre anni un buon rapporto lavorativo è diventato una sincera amicizia.

Voglio ringraziare il Prof. Giulio Timelli, il Prof. Paolo Ferro e il Dt. Alberto Fabrizi per le conversazioni sempre utilissime, per i commenti e i suggerimenti che mi hanno sempre aiutata e per la fondamentale assistenza tecnica. Mi hanno sempre ispirata con idee e commenti intelligenti e sono diventati, nel tempo, più che semplicemente professori e colleghi.

Devo un ringraziamento speciale ai tecnici del DTG e a tutti i membri del gruppo di metallurgia, in particolare ad Enrico Della Rovere per l'assistenza tecnica. Vorrei ringraziare Elena Fiorese e Giorgio Kral così come tutti gli studenti triennali e magistrali che mi hanno aiutata nell'attività sperimentale e tutti gli attuali e passati dottorandi che hanno reso l'ambiente lavorativo allegro e piacevole.

Ultima ma non per importanza, voglio esprimere la mia immensa gratitudine nei confronti della mia amata famiglia che mi ha supportata e ha creduto in me. I miei genitori, sempre al mio fianco, mia sorella e mio fratello e le loro famiglie con i molti nipotini, che sono la mia gioia, e soprattutto il mio amato Stefano, che sempre mi ama e mi sostiene. Sono incredibilmente fortunata ad averti ad averti nella mia vita e a poterti chiamare marito alla fine di questo viaggio.

Preface

This thesis outlines research carried out at the Department of Management and Engineering (DTG), School of Mechatronics and Product Innovation Engineering, Padua University, Vicenza, Italy. The work was conducted under the supervision of Professor Franco Bonollo. It was developed within the EU MUSIC project (MUlti-layers control& cognitive System to drive metal and plastic production line for Injected Components), supported by the European Union - FP7-2012-NMP-ICT-FoF - under grant agreement No. 3141. There have also been collaborations with Italian and European industrial partners as well as the Worcester Polytechnic Institute, USA. It is expected that the findings presented in this study can expand knowledge on the effect of HPDC process parameters on the quality of the AlSi castings as well as provide suggestions to improve their aesthetic and mechanical properties. It is the author's expectation that both industry and its customers can benefit from the presented findings.

Table of contents

INTRODUCTION

This chapter deals with a background on what has already known about Aluminum casting alloys, High Pressure Die Casting, defect assessment and microstructure. The standardized defect classification approach, the already known methods to predict the mechanical response of a die casting on the basis of its defect content and how the in-service behavior can be improved are also described. In the last segment, the research that has been developed in this work is introduced.

1 THE FOUNDRY INDUSTRY

Metal castings are essential features of everyday life. Analyses conducted by CAEF – umbrella organization of the European Foundry Association - indicate that there are more than 4,000 foundries processing iron or non-ferrous metals in Europe alone, with over 200,000 employees overall.

The biggest costumers of the foundry industry are car and machine manufacturers, plant engineering companies, railway and aerospace industries, the power generation industry, shipbuilding and marine engineering. These industries - particularly the automotive one - act as "innovation drivers" for the foundry industry [1].

Indeed, the automotive industry is the major end-market served by the Aluminum die casting industry since it recognizes the need for a drastic reduction of the emissions to face ongoing climate changes. The choice of alloy and casting process will play a major role in affecting both component properties and costs.

In the future, only about one-fifth of the total materials used in automotive applications will be conventional steel, a fifth will be accounted for by high-tensile steel and another fifth will be made up by plastics and composites (only a small share is attributable to carbon fibers, mainly used in luxury class). On the other side, light Aluminum and magnesium components will significantly gain in importance, as shown in Fig. 1.

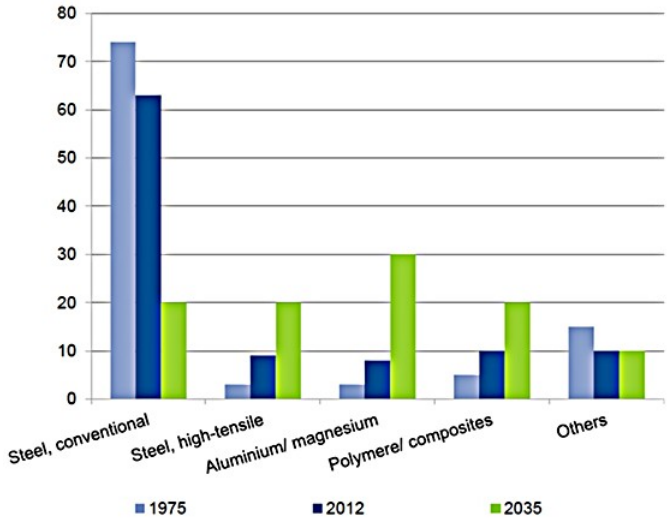

Fig. 1 Material split in light vehicles [%] [1].

Specifically, the global Aluminum cast production is expected to grow; it is very likely that Germany will gain market within Europe at the expense of Western European competitors, NAFTA states will grow due to investments of foreign OEMs and Korea and Japan will lose market shares to China, which will for sure dominate its competitors.

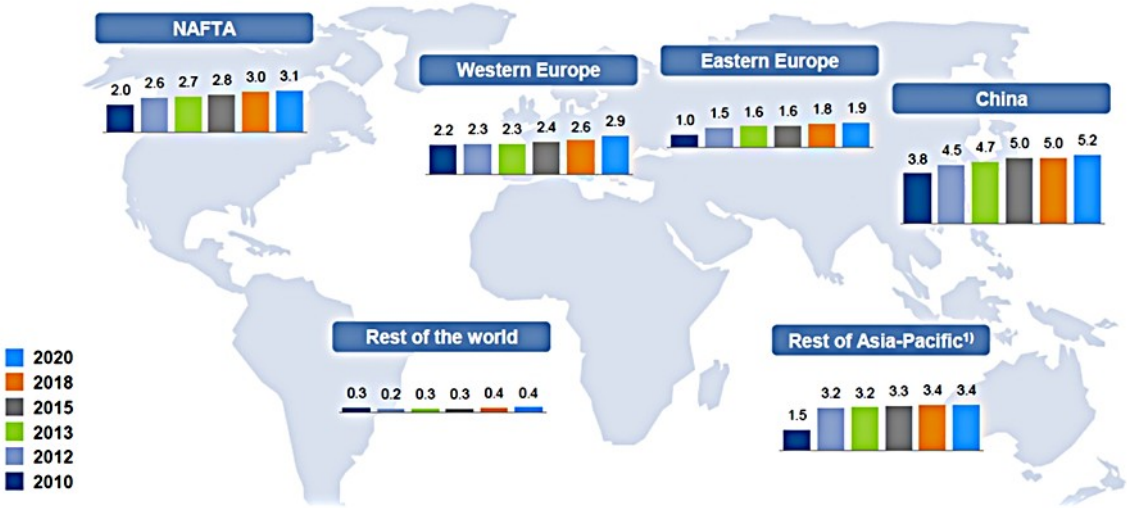

Fig. 2 Global Al cast production (in million tons) [1].

However, according to "*2016 State of the Die Casting Industry*", a report about the state-of-the-art of U.S. Die Casting Industry edited by NADCA [2], right now Aluminum is the material of choice for the automotive industry only because they have not found anything to replace it, *yet*. For expanding Aluminum die castings application, crash and strength relevant die-castings are going to have to be made and new alloys with higher elongation will need to be used.

1.1 Aluminum casting alloys

On average, the production of Aluminum castings counts for a quarter of annual Aluminum world production, 60% of which are die castings.
The most important production processes are: High Pressure Die Casting (HPDC), by far the preferred technology for large production volumes of high integrity products; low pressure die casting (LPDC), permanent mold and sand casting used for smaller production and investment casting, normally used for the production of some components.

The Aluminum alloys used in the various casting processes should offer certain microstructural advantages, good feeding and filling characteristics to provide a good castability. An Aluminum casting alloy should guarantee, at least, a relatively high solubility, a low melting point, relative low tendency for hot cracking, good as-cast surface finish and chemical stability. To these, other advantages depend upon the specific alloy chosen [3].

The specification of an Aluminum casting alloy is based on the mechanical properties it can achieve. Indeed, casting properties result from three primary factors: (i) the alloy, (ii) the melting and casting operations and (iii) the heat treatment [4]. For this reason casting alloys are tailored to the casting process; the basic casting process used is part of the casting alloy designation system.

Contrary to the international system of wrought Aluminum alloy designation (AA, ISO, CEN), the designation system for casting alloys and castings differ significantly.
Specifically the AA system - American Association system - defines 8 groups of casting alloys as listed in Table 1, whereas the EN system - European standard - only differentiate between 4 alloy groups and excludes the tin-containing bearing alloys.
In the latter designation system, the alloy composition is specified either by 5 digits or by chemical symbols, followed by a letter for the casting process and possibly by a letter and/or digit for temper designation (see Table 2).

Table 1 Aluminum Association designation system for Aluminum casting alloys

Designation	Main elements
1XX	> 99% Al
2XX	Al-Cu
3XX	Al-Si-Mg, Al-Si-Cu, Al-Si-Cu-Mg
4XX	Al-Si
5XX	Al-Mg
7XX	Al-Zn
8XX	Al-Sn

Table 2 Aluminum casting alloys designation according to European Standard

1st digit	2nd digit	Chemical symbols	Main elements
2XXXX	21XXX	AlCu	Al-Cu
4XXXX	41XXX	AlSiMgTi	Al-Si
	42XXX	AlSi7Mg	
	43XXX	AlSi10Mg	
	44XXX	AlSi	
	45XXX	AlSi5Cu	
	46XXX	AlSi9Cu	
	47XXX	AlSi(Cu)	
	48XXX	AlSiCuNiMg	
5XXXX	51XXX	AlMg	Al-Mg
7XXXX	71XXX	AlZnMg	Al-Zn

During molten Aluminum processing, the percentages of alloying elements and impurities must be controlled carefully. For example, in HPDCs, Fe and Mn are strictly regulated in order to avoid the component embrittlement or die soldering issues [5-10]. Also, Mg is precisely controlled because of its hardening effect. In addition to these elements, molten Aluminum is also sensitive to trace elements that can have a strong impact on castability.

Among the Aluminum casting alloys, the AlSi based alloys are the most widely used in foundry mainly because Si provides a good castability. As a rule of thumb, the Si content ranges between 8-13wt% for HPDCs and it increases to 16-20wt% for certain applications that require elevated wear resistance. Lower ranges, i.e. 5-8wt%, are normally used for sand or gravity castings.

A recent survey carried out within the European Stacast project, revealed that the most diffused alloy in the European foundries is EN AB46000 (AlSi9Cu3(Fe)), used by 58.6% of them, followed by EN AB43400 (AlSi10Mg(Fe)), used in 37.9% of the foundries.
Four of the five most used alloys (EN AB46000, EN AB43400, EN AB47100 and EN AB46100) are typical HPDC alloys, in agreement with the fact that this is the most adopted process in Al alloys foundry [11].

As previously stated, the Aluminum casting alloys offer different microstructural features depending on the alloy composition and the adopted production process.
In most cases, however, in the as-cast condition, they comprise a α-Al matrix and a eutectic mixture. Morphological transformations resulting from grain refinement and chemical modification are not always required, however, they could be necessary for premium Aluminum castings mainly to improve mechanical properties.

The most common grain refiners are based on the Al-Ti-B system; among them, the mainly used is the Al5Ti1B. These grain refiners typically contain TiB_2 and Al_3Ti which can act as nucleating points of Aluminum.

Furthermore, the addition of chemical modifiers (often in the form of master alloys), i.e. Na or Sr, is very common in sand and permanent mold cast AlSi alloys in which there is the need for a more fine and fibrous Si morphology. Nevertheless, the exact mechanism of modification is still not well understood despite decades of research.

In addition, another important element that must be taken into account is hydrogen as it is the main cause of entrapped porosity in solidified castings. The main source of hydrogen comes from the reaction of Aluminum with moisture in the melting environment. It is the only gas having a measurable solubility in Aluminum and it shows a solubility in the solid Aluminum much smaller than that in the molten state, as shown in Fig. 3. Thus, for high integrity applications, it is necessary to degas the molten metal and have a good control over the process.

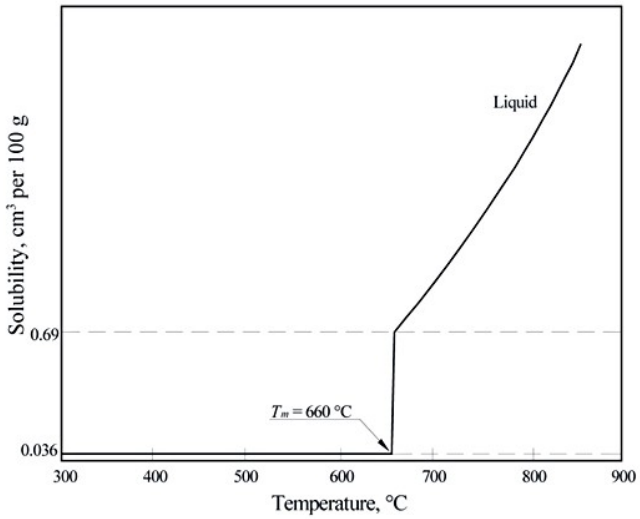

Fig. 3 Hydrogen solubility in Aluminum [12]

Degassing with an inert gas, which is typically part of the melting practices, is extremely useful not only to remove hydrogen but also to clean the molten Aluminum of oxides and other inclusions prior to pouring. Indeed, both gas porosity and inclusions have a negative impact on the casting quality and can compromise its in-service performance.

1.1.1 The AlSi based casting alloys

Si is the main and most important alloying element in Aluminum casting alloys. It provides good castability and slightly enhances strength and ductility (see Fig. 4) [13]. Its contribution to strength improvement is due to the load transfer from the α-Al matrix to the rigid, highly interconnected Si particles [14]; therefore alloys with a low Si content show poorer mechanical properties. Moreover, increasing the Si content, the favorable effect of this alloying element on alloy castability is more evident; Si allows a rapid filling of the die and a solidification with no hot tearing or hot cracking issues.

Referring to the phase diagram of AlSi binary system the alloys can be divided into:

- hypoeutectic alloys - the Si content is lower than 12-13wt%. The typical microstructure shows a primary α-Al phase surrounded by an Al-Si eutectic, i.e. a mixture of the two alloying elements. These alloys, due to their excellent castability, corrosion resistance and higher specific strength in the heat treated condition, are most widely used in automotive and aerospace industries.
- hypereutectic alloys - the Si content exceeds 12-13wt%. The microstructure is characterized by two major components: the primary Si crystals and the eutectic phase. The former consists of large particles exhibiting a variety of morphologies such as coarser platelets - star-like and blocky – and they may form before the eutectic while the latter consists of an Aluminum-rich solid solution of silicon and virtually pure silicon, forming the matrix of the microstructure.

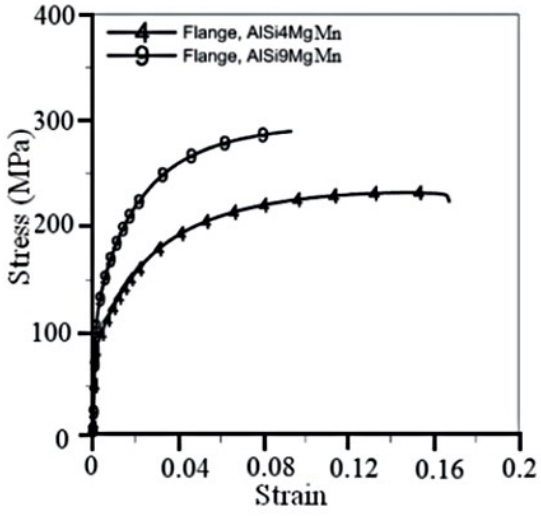

Fig. 4 Engineering stress-strain curves of high-pressure die-cast AlSi4MgMn and AlSi9MgMn alloys [15].

1.2 Primary vs secondary Aluminum alloys

More than half of the Aluminum currently produced in the European Union originates from recycled raw materials. In view of a growing end-use demand and a lack of sufficient domestic primary Aluminum production, Europe has a great steak in maximizing the collection of all available Aluminum and developing the most resource-efficient scrap treatments and melting processes [16].

It is particularly appropriate to focus on automotive recycling in addressing this subject as the high volume of recycled Aluminum coming from automotive components already exceeded the recycled metal coming from used beverage cans in 2005 [17]. This increased adoption of recycled Aluminum in manufacturing has created significant economic and environmental advantages for both industry and consumers.

The use of recycled-grade alloys implies important and ecological advantages as the production of recycled Aluminum alloys require 95% less energy and CO_2 emissions than primary alloys according to Das, Green and Kaufman [18]. Recycled Al alloys offer economical and environmental advantages compared to primary production: Rombach [19] estimated an energy reduction from 174 GJ/ton to 20 GJ/ton.

Thus, as worldwide Aluminum foundries benefit from the trend toward light-weight construction supported by increasing requirements for energy efficiency, cost saving and emission reduction, the automotive industry is providing the driving force for the development and production of new solutions.

1.2.1 Sectorial analysis

Primary Aluminum

Primary Aluminum production involves two independent processes to transform the ore, i.e. bauxite, into metal. The Bayer process makes alumina from bauxite and the Hall-Héroult process gives molten Aluminum by electrolytic reduction of alumina.

According to a survey conducted by AluPlanet [20], in EU-28, primary Aluminum production decreased by 32% in 2000-2013. This reduction was due primarily to the economic downturn started in 2008, but also to the de-localization conducted by EU smelters in cheaper countries such as the Middle East or China.

About 70% of primary Aluminum needs are satisfied by importation and the EU primary Aluminum production is not sufficient to cover EU demand. In 2013 only 10 countries owned smelting plants: Germany, Spain, France, Romania, Slovak Republic, Greece, Sweden, Italy (5%), the Netherlands and the UK.

In Fig.5 the global primary Aluminum production for 2016 is shown [21].

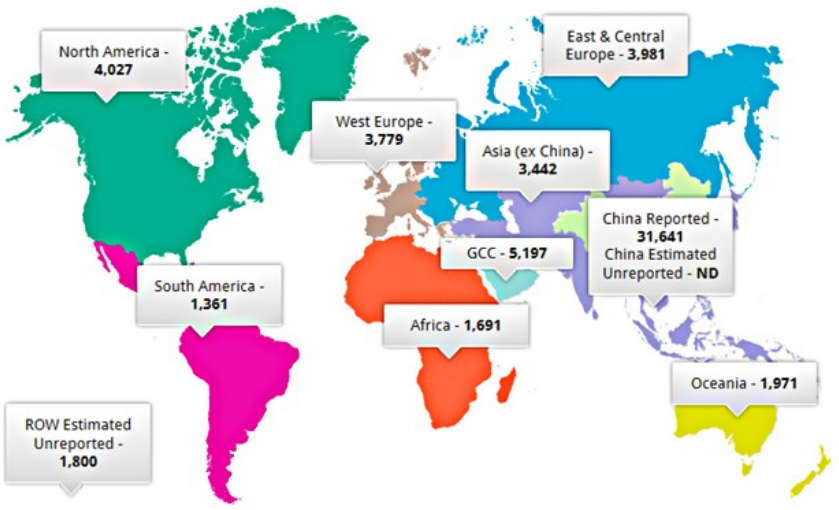

Fig. 5 2016 global Aluminum production – 58,890 thousand metric tons [22]

Secondary Aluminum

Currently, secondary Aluminum accounts for about one-third of world Aluminum consumption. Almost 100% of the scrap arising from manufacturing of Aluminum products is recycled with an approximate 70% of recycled Aluminum used in the production of Aluminum-Silicon casting alloys.

According to the abovementioned survey [20], also secondary production fell between 2007 and 2009 and its levels have not matched yet pre-crisis ones (roughly 3 million tons).
Within EU, Germany and Italy are the two countries with the largest share of production. In 2013, they both produced more than 60% of secondary Aluminum in Western Europe.

Aluminum global demand is expected to grow at a 6% annual rate mainly drawn by transport sector since the pressure from governments for lower emission vehicles has been significant in the growth of secondary Aluminum as automotive producers strive for lighter weight. Market analysists highlight that Aluminum is winning market share from galvanized steel in the transport industry and copper in the electricity cable industry [20].

When dealing with secondary alloys, what must be seriously taken into account are the factors which define the value of the scrap: (i) if the scrap is a single known alloy, (ii) if it is free of contaminants, (iii) if dangerous items are present and (iv) if some sort of pre-processing is required.

In Table 3 the comparison, conducted by the European Aluminum Association, between primary and secondary production of 1 ton of Aluminum ingot is displayed. It shows, in particular, that the emissions of GHG – Green House Gas - is 30 times higher in the case of primary production than scrap remelting.

Table 3 Environmental indicators to produce 1 ton of primary and secondary Al ingot - EU

EAA indicators (per ton of primary ingot)	**Primary Al production**	**Secondary Al production**
GHG emissions (GWP 100 years) [kg CO_2-Equiv.]	9677	317
Ozone Layer Depletion Potential (ODP, steady state) [kg R11-Equiv.]	9.79E-04	1.98E-05
Primary energy from renewable raw materials (net cal. Value) [MJ]	42386	125
Primary energy from non-renewable resources (net cal. Value) [MJ]	130699	5464

1.3 The High Pressure Die Casting process

The casting processes have been around for millennia since the first metal mold application in China in about 2000 BC. Metal molds became very common in the 1800s to cast complex and repeatable parts. At the time, the molds were generally made by two halves with a sand core to make any inside cavity. The invention of the printing press brought forward the need for higher detail; in order to produce smaller font, it was necessary to cast smaller letters. This proved quite difficult with gravity casting. The obvious solution was to push the metal into the die through a piston and a cylinder, but also metal molds that could withstand the extra pressure were needed. This technology development led to the first patent for a manually operated die casting machine, dated back to 1849. This first application was followed by many others, till the first Aluminum machine developed in 1915.

High Pressure Die Casting (HPDC) is a casting process particularly suited for mass production of small to medium-sized metal components. A continuously growing population, coupled with an increase in living standards especially in emerging markets, are boosting automobile sales. A consequence of this trend is that manufacturers are looking for ways to make their products more efficient and reduce fuel consumption as well as CO_2 emission. Lightweight construction using efficient, highly automated and cost-optimized Aluminum die casting plays a key role in achieving this goal.

Thus, the main market for die cast parts, since its very beginning, has always been the automotive industry, form the Model T Ford to the present. The die casting machine changed over the years to the form used today in which two types of systems are applied for injecting the molten metal into the die cavity:

1. *Hot chamber* system consisting of an injection mechanism immersed in the molten metal bath of the melting furnace. It is typically used with metals such as zinc, magnesium and lead, that show a low melting point (see Fig.6a).

2. *Cold chamber* system used for metals with a high melting temperature, as Aluminum, brass and magnesium. The metal poured manually or automatically into the cold chamber sleeve, is forced by the piston into the die cavity at high speed and pressure (see Fig.6b).

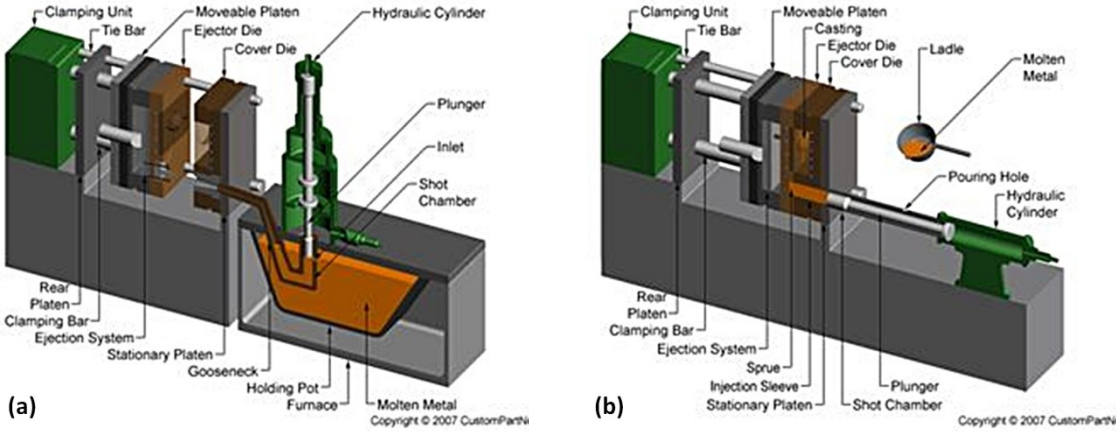

Fig. 6 Schematic representation of (a) hot chamber system, (b) cold chamber system[22]

In both configurations, the metal is forced at a velocity in a range of 30-100 m/s into the die cavity at a temperature between 943-983 K (670-710°C), where it is held by a powerful press (i.e. 50-80 MPa) until completely solidified. The capacity of HPDC machine is described by their locking force, typically in the range of 100-2000 tonnes. The dies are costly but they can last for more than 100,000 shots.

The process consists of three main phases, as illustrated in Fig. 7:

- *First phase* - the molten metal fills the shot sleeve, the plunger starts its movement with a speed that is not too high in order to force the air on the front by a molten metal wave which is built up. To avoid turbulence, and thus air entrapment, an optimal plunger first phase speed ranges between 0.25 - 0.35 m s^{-1}.

- *Second phase* - when the metal is at the die gate, the plunger switches its velocity to higher values in order to ensure rapid filling since the narrower section of the gate causes a counter-pressure.

- *Third phase* - this phase starts when the molten metal has completely filled the die cavity. An extremely high pressure is applied, i.e. intensification pressure, until complete casting solidification is reached.

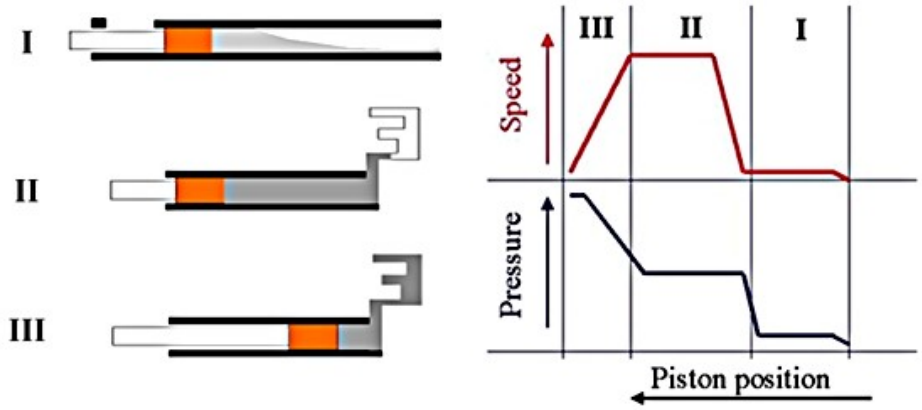

Fig. 7 HPDC piston positions [23]

Once the solidification is completed, the piston is retracted, the die opened, the component ejected and the system is ready for the following cycle.

1.3.1 HPDC Al alloys for automotive applications

Until the end of the 1990s, HPDC was considered to be appropriate only for simple castings made of low-cost secondary alloys, where in most cases, a high productivity was the main concern. Thanks to the *boom* in the automotive industry, HPDCs were suddenly required to be ductile, stronger, heat-treated or welded. A number of high integrity HPDC processes have been developed to meet these requirements, but at present, none of them is 100% satisfactory.

Nowadays, the main applications for automotive Aluminum HPDCs can be divided into four categories:

1) Engine and auxiliary systems
2) Powertrain
3) Interiors and electronics
4) Chassis and body structure.

Among them, the latter is the most relevant area of progress in terms of the development of new alloys since body structure applications normally require very good mechanical properties [24]. This is why the production of structural components with recycled Aluminum alloys remains a major challenge; indeed, the higher amounts of Fe (0.8-1.1wt% in secondary alloys vs 0.6-0.8wt% in primary alloys) tends to form brittle Fe-rich intermetallic compounds which can cause the in-service failure of the components if it is subjected to a certain amount of cyclic load [25,26].

Moreover, both investment and production costs are generally higher for high integrity HPDC than for their conventional counterpart, mainly because the use of primary alloys is necessary [27].

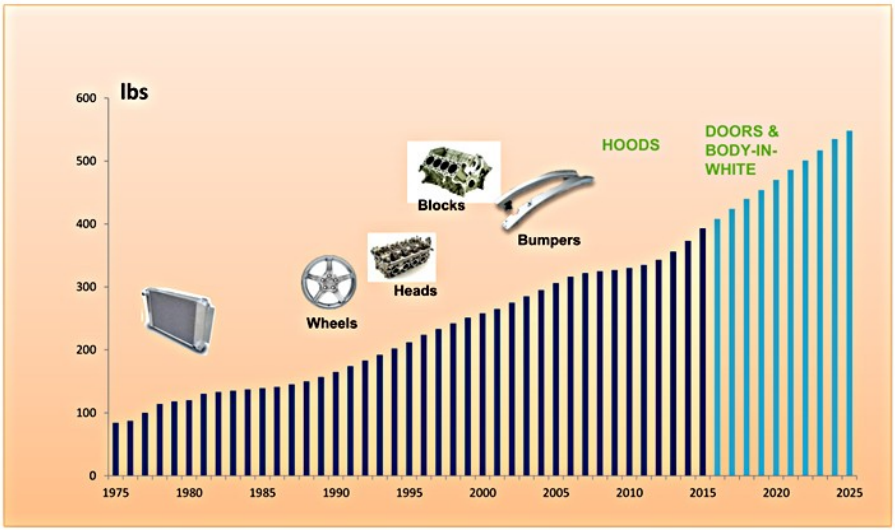

Fig. 8 Aluminum trend in cars [28]

2 DEFECTS IN HPDC

The final quality and mechanical properties of die castings are determined by microstructure and defect content. These two features are strongly influenced by the high number of sequential actions involved in High Pressure Die Casting process. As stated by Campbell [29], the directness of the process from the liquid metal to the finished product involves the greatest difficulty as many aspects must be controlled simultaneously. Injection of molten metal, solidification, casting extraction, lubrication system, die temperature, mold filling capacity of the molten metal, cooling rate, geometrical complexity of the casting and many other aspects may affect the integrity of the component [30]. Therefore, the presence of surface and internal defects in HPDCs is almost inevitable, mainly if all these parameters are not adequately controlled, leading to a casting scrap rate measured in part per million [30-33].

According to EN 12258-1:2012 standard [34], a *defect* is a quality characteristic which does not allow the product to carry out the requested function. On the contrary, what is called *imperfection* is something that does not necessarily compromises the product use.

A recent survey, carried out among European foundries, providers of materials and services, die-makers, end-users, universities and RTD centers, highlighted that the most common defects in HPDC are air/gas porosity, metal-die interaction defects, shrinkage and filling related defects, cracks and inclusions (see Fig. 9a,b) [35].

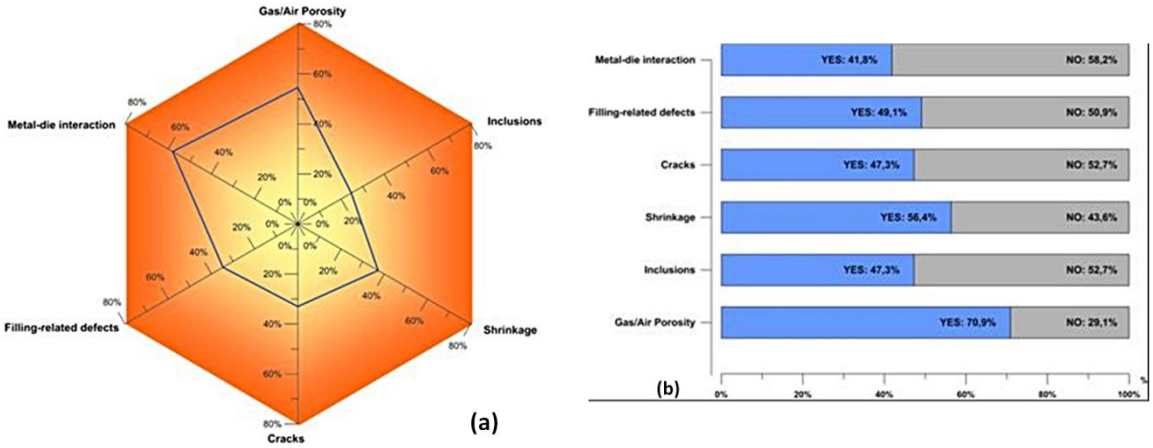

Fig.9 (a) Frequency of defects in die castings and (b) extent of measurement/quantification of defects in die castings, as estimated by European HPDC foundries.

Thanks to the same survey, a defect classification for HPDC components was elaborated [33,36] which has recently been published as CEN/TR 16749:2014 [37].

2.1 Defect origin

2.1.1 High speed

In HPDC it is important to fill the die cavity very rapidly (10-150 ms depending on the part dimension and alloy used) and, in order to achieve a good surface finish, it is also important to have the metal entering the die at high speed. According to Herman [38], the molten metal atomizes because of the high velocities and the narrow gate through which it has to enter the die cavity. These metal droplets impact the inside of the cavity and rapidly freeze, forming a skin of metal on the cavity face that can make up 30-60% of the overall casting thickness.

Moreover, such a turbulent and chaotic flow results in small vortices that trap air in the liquid Aluminum, with the obvious result of approximately 1-2% or entrapped air in the form of small bubbles or gas pores [27].

2.1.2 Heat transfer

The intensification pressure applied during the third phase of the process forces the metal against the die and provides a very good heat transfer with the die. The component solidification proceeds from the skin towards the center of the part, causing shrinkage and therefore a reduction of the pressure of the metal against the mold walls. As so, the heat transfer is not constant during the solidification.

Dour et al. [39] demonstrated that the heat flux density reaches a peak at $10^5 W/m^2$ when the pressure is first applied and then decreases at $5x10^3 W/m^2$ after four seconds. This explains why it is common to have a finer structure on the surface of the casting and a coarser/dendritic one in the center.

When steel cores are used, they rapidly reach high temperatures but soon they cannot accept further heat, leading to areas around them that do not solidify for some time and, as a result, formation of Al-Fe intermetallics on the surface of the core. This, in turn, can generate die soldering issues [27].

2.1.3 Solidification prior to entering the cavity

During the process, the molten Aluminum gets in contact with surfaces that are relatively cold. This leads to the formation of a skin and, sometimes, dendrites that break up into small particles causing a spread of nuclei into the cavity. This can have a large effect on the resultant microstructure of the component.

2.1.4 Hydrogen

As already explained in Section 1.1 of Chapter 1, hydrogen has a high solubility in the molten Aluminum and a low solubility in the solid. This can result in hydrogen porosity.

Therefore, on one hand, it should continuously be removed from the bath, on the other, appropriate die sprays must be chosen in order to avoid its picking up from the humidity left in the die after spraying [27].

2.2 Defect classification

Three main approaches for the classification of defects in cast components can be found in the literature.

1. Cocks' approach
   This first approach distinguishes only between surface and internal defects. The former are visible by naked eye and affect both aesthetic and functionality; on the contrary, the latter only affect the component mechanical behavior [40].

2. Campbell's approach
   It discerns defects on the basis of their metallurgical origin/cause. The main advantage is the possibility to design and adopt strategies for improving the product quality. However, two main drawbacks must be pointed out. On one hand, origin/cause of defects are discovered concurrently to defect identification and the same defect can be due to several factors; on the other, this approach is less suitable for application in foundries [29, 41].

3. NADCA approach
   This third approach is based on defect morphology. Defects are divided into seven categories that are distinguished with a letter among them. Each category shows more groups and, in turn, each group is divided into different subgroups [42].

The new approach presented in [33, 36] and published as CEN/TR 16749:2014 [37], aims at helping die casting facilities to address defects-related issues with increased confidence and ability in order to assure quality and reliability of the produced components. Starting from the three previously described approaches, it classifies defects and imperfections into three main levels:

I) **Morphology/location of defects**: internal, external or geometrical defects.
   This first level also suggests the investigation techniques suitable for their detection.
II) **Metallurgical origin of defects**.
   Defects are divided into several categories and the knowledge of their metallurgical origin supplies a starting point for corrective actions on the process.
III) **The specific type of defects** (i.e. the same metallurgical phenomenon can generate different kinds of defects).

In Tables 4-6 the classification structure is better illustrated.

Table 4 Classification of internal defects and imperfections

1st level	**2nd level**		**3rd level**	
A Internal defects and imperfections	A1	Shrinkage	A1.1	Macro-shrinkage
			A1.2	Interdendritic shrinkage
			A1.3	Layer porosity
	A2	Gas-related	A2.1	Air entrapment porosity
			A2.2	Hydrogen porosity
			A2.3	Vapor entrapment porosity
			A2.4	Lubricant and/or die release agent entrapment porosity
	A3	Filling-related	A3.1	Cold joint
			A3.2	Lamination
			A3.3	Cold shot
	A4	Undesired phase	A4.1	Inclusion
			A4.2	Undesired structure
	A5	Thermal contraction	A5.1	Cold crack
			A5.2	Hot tear, hot crack

Table 5 Classification of surface defects and imperfections

1st level	**2nd level**		**3rd level**	
B Surface defects and imperfections	B1	Shrinkage	B1.1	Sink
	B2	Gas-related	B2.1	Blister
			B2.2	Pinhole
	B3	Filling-related	B3.1	Cold joint, vortex
			B3.2	Lamination
			B3.3	Cold shot
	B4	Undesired phase	B4.1	Surface deposit
			B4.2	Contamination, inclusion
	B5	Thermal contraction	B5.1	Cold crack
			B5.2	Hot tear, hot crack
	B6	Metal-die interaction	B6.1	Erosion
			B6.2	Soldering
			B6.3	Thermal fatigue mark
			B6.4	Ejection mark
			B6.5	Corrosion of the die

Table 6 Classification of geometrical defects and imperfections

1st level	**2nd level**		**3rd level**	
C Geometrical defects and imperfections	C1	Lack of material	C1.1	Incompleteness
	C2	Excess material	C2.1	Flash
	C3	Out of tolerance	C3.1	Deformation

In [43] a useful application of this defect classification is described.
It is used in a dual way: (i) as an analytic method to identify defects and imperfections on produced castings, (ii) combined with MAGMASOFT software, to classify simulated defects.
This second approach is aimed at correlating real and simulated defects and predicting the casting quality according to the process parameters.

2.3 Inspection techniques

Inspection and testing of castings include five main categories: casting finishing, dimensional accuracy, mechanical properties, chemical composition and casting soundness. For the development of this doctoral thesis, the casting soundness investigation techniques are particularly important.

Among the several non-destructive techniques (NDT) that can be applied, one of the most important, and mainly used in the HPDC foundries, is the radiographic inspection. Its aim is to detect internal defects such as air/shrinkage porosity or inclusions. The casting is exposed to radiation from a x-ray tube; it absorbs part of the radiation, whereas the remaining exposes the radiographic detector and is viewed on a video screen. Dense material withstands the radiation penetration, so the film is exposed to a lesser degree in those areas, giving the film a darker appearance. Any hole, crack or inclusion that is less dense than the casting alloy is revealed as a light area. When carried out correctly, the x-ray analysis is the best NDT for detecting internal defects and radiograph serves as a permanent record for the casting quality that can be reviewed by multiple personnel.

Computerized tomography and micro-tomography (CT) are being increasingly used to develop 3D computer imagery to inspect a casting's soundness. It is a promising method to evaluate the casting integrity; as demonstrated by Pejryd et al. [44] the CT method can cover much larger volumes inspection than, for example, optical methods. It also holds the potential of quantification of defects in a way not achievable by optical inspection. However, it still has limitations for use on large components, due to resolution issues.

2.4 Mechanical behavior prediction: state of the art

The influence of defects on both static and cyclic behavior of high-pressure die cast aluminium alloys has been studied by several researchers [45-48]. In literature, many approaches for static and fatigue strength prediction of HPDC Magnesium and Aluminum alloys components have been proposed [47, 49-57]. Generally, two different groups based on (i) constitutive models or (ii) statistical and stochastic approaches are used.

2.4.1 Constitutive models

The first model presented by Caceres [58] was an attempt to rationalize the previous results obtained by Surappa et al. [59], according to which the decrease in the elongation to fracture could be related to the projected area of the pores in the fracture surfaces.
According to Caceres, the tensile ductility is controlled by the local level of porosity. By assuming the fracture occurs in the region of maximum strain, the overall strain to fracture can be calculated for different levels of porosity. According to the proposed model, even a small amount of localized porosity has a significant effect on the tensile ductility and produces, as well, a measurable loss in tensile strength. The predictions of this model showed good agreement with Surappa et al.'s results.

In a subsequent revision of the model [60], it was demonstrated that ductility and tensile strength show little or no correlation with the bulk porosity content, especially in the case of samples containing dross and oxide films. In contrast, a monotonic decrease of the mechanical properties with an increasing area fraction of defects in the fracture surface was observed. According to Caceres et al., whether the defect is single or multiple, cylindrical, near-spherical or two-dimensional does not seem to be significant.

The constitutive model introduced by Lee [61], takes into account the strain rate sensitivity term, even in the case of tensile deformation at room temperature. It allows a constitutive prediction based on the strain rate sensitivity and the strain-hardening exponent. According to the model, UTS and elongation exhibit a strong dependence upon the variation in microporosity, with a linear and inverse parabolic relationship, respectively. The constitutive prediction is based on the fractographic porosity, i.e. the projected area of micro-voids on the fractured surface, rather than on the volumetric porosity by the measurement of bulk density, as already suggested by Gokhale and Patel [62].

2.4.2 Statistical/stochastic models

Besides the constitutive approaches, another way to address the phenomenon of fracture is by means of the statistical models.

According to Griffith [63], the difference between the ideal and the actual mechanical behavior of a casting is attributable directly to the presence of defects weakening the structure.

Therefore, the statistical distribution of fracture-related mechanical properties can be linked to the defect distribution.

The most important empirical distribution introduced by Weibull and, since then, applied to ceramics and metals, is based on the theory of the 'weakest link' elaborated on the basis of Pierce's theory [64]. The cumulative probability function of the Weibull distribution is expressed as follows:

$$P = 1 - e^{\left[-\left(\frac{\chi-\lambda}{\eta}\right)^{\beta}\right]} \quad (1)$$

where P is the probability of failure at a given stress χ or lower. λ is the threshold parameter below which no specimen is expected to fail, η is the scale parameter and β is the shape parameter, alternatively referred to as the Weibull modulus [65].

The one presented is the three-parameter configuration of the Weibull distribution. Generally, for Aluminum castings, the two-parameter form is preferred since it is easier to estimate the parameters and can be expressed with the threshold value λ taken as zero.

Many researchers adopted this statistical method to study the influence of casting defects on the mechanical properties of Magnesium and Aluminum components [52, 56, 57, 66].

3 MICROSTRUCTURE

The microstructure of the Al-Si alloys consists of a primary phase, called α-phase, and a eutectic mixture of Al-Si. The α-phase is an Al solid solution that crystallizes in the form of non-faceted dendrites on the basis of the crystallographic lattice of Aluminum. The morphology of Si particle is plate-like and its amount determines the amount of eutectic mixture in the alloy.
The presence of elements such as Cu, Mg and Fe leads to the formation of various intermetallic compounds in the microstructure like Al_2Cu, β-Al_5FeSi and α-$Al_{12}(Fe,Mn)_3Si_2$.

Compared to other processing technologies, the solidification and consequently the microstructure in the HPDC process is quite complex due to factors such as liquid and semi-solid melt processing, flow and heat transfer phenomena [67,68]. This is why the relationship between microstructure and solidification mode has not been fully understood in HPDC.
It is clear that increasing cooling rate refines all microstructural features: reduces grain size, decreases SDAS, changes the morphology of the eutectic Si from flake-like to a more fibrous one and tends to reduce the size of all intermetallic compounds regardless of their type. However, in HPDCs, eutectic Si particles often tend to remain unaffected despite such an increased cooling rate. In Fig. 10 the typical microstructure of a high pressure die casting is shown.

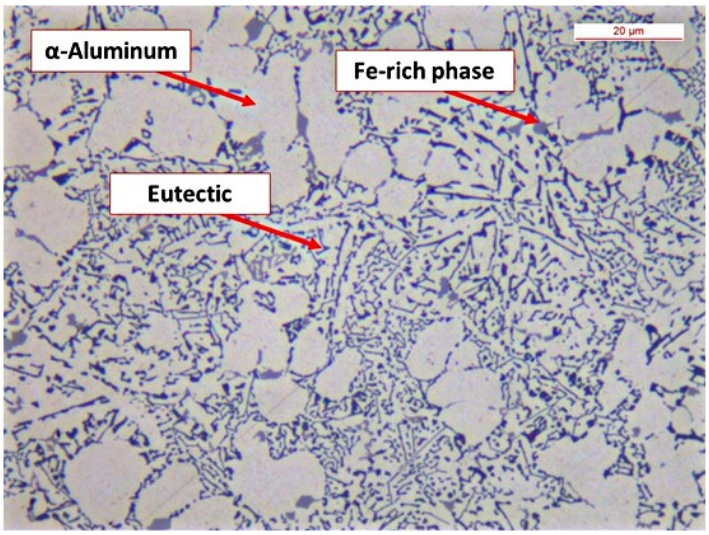

Fig. 10 Typical HPDC microstructure

3.1 Microstructural evolution by heat treatment

Upon addition of trace quantities of certain elements, such as Na or Sr, to a hypoeutectic AlSi alloy, the structure of the eutectic Si phase transforms from a plate-like (flake) to a fine fibrous (coral) structure [69,70]. This morphological change of the eutectic structure plays an important role in improving the mechanical properties of the components that are cast from these alloys.

Also, heat treatment can lead to changes in the silicon crystals' morphology. In as-cast unmodified components, there can be areas characterized by Si crystals that show a coarse morphology or others where Si particles display a finer but interconnected arrangement.
The implementation of short time heat treatments can modify this morphology; small Si crystals may fragment and the edges of the coarser particles may become more rounded [71].
Thus the mechanical properties are highly influenced not only by the defect content but also by the microstructure of the material and in turn, by heat treatments and their duration.

3.1.1 Heat treatment of HPDCs

The most used conventional heat treatments for Aluminum alloy castings are T6 and/or T7 and T5.
T6 and/or T7 require three stages:

1. solution treatment at a relatively high temperature below the melting point for times often exceeding 5 hours to dissolve the alloying elements and homogenize and modify the microstructure;
2. quenching in hot or cold water to retain all the alloying elements in the supersaturated solid solution;
3. artificial aging for a period of time and at a temperature suitable for achieving precipitation strengthening.

The T5 heat treatment, on the other hand, consists only of an artificial aging stage, as previously described.

High pressure die-cast components cannot normally be heat treated at high temperatures. Because of the extreme turbulence of the process, HPDCs always show a certain amount of defects, mainly porosity that can expand during solution treatment resulting in unacceptable surface blisters. This is the reason why HPDCs normally undergo only artificial aging (T5) without the preliminary solid solution stage. However, in HPDC process, the components are slowly cooled at a low temperature (below 200°C), before their removal from the die to quench. This slow cooling significantly diminishes the aging potential since the hardening solute solubility decreases drastically with the decrease in temperature [72].

Lumley et al. [73-76] dedicated great efforts to the study and development of heat treatments on HPDCs without causing blisters or dimensional instabilities. They demonstrated that lower solution-treatment temperatures and shorter times than those normally used for Al-Si based

alloys could effectively produce a good age hardening response without surface blistering. They also showed that significant mechanical responses were possible even reducing the solution temperature to values as low as 714 K (440°C) and to less than 15 min of total heat treatment.

It is well-established that the mechanical properties are strongly influenced not only by the amount of defects but also by the characteristics of the eutectic Si particles in Al-Si based alloys. Indeed, they can be adequately improved, through heat treatments, since Si crystals undergo substantial changes in size and shape during heat treatment and they normally require a solution-treatment time up to 16 hours to achieve complete homogenization within Al grains and spheroidization. However, the use of shorter temperatures and much shorter times has proven to be effective.

For this reason, besides the use of common chemical modifiers, i.e. Sr and Na, specific heat treatments are also applied to change the eutectic Si morphology from a coarse, flake-like form to a fine fibrous one [76,77].

4 OPEN ISSUES

A process as complex as High Pressure Die Casting has drawn a lot of research attention in recent years. Many steps forward have been done to improve the process reliability, however, many open issues are still present.
The developed research represents an effort to fill these gaps in order to obtain better and more stable components.
This doctoral thesis aims at addressing the following open issues:

1. Defect generation is still an actual problem in HPDC; there are many variables involved in the process that can seriously influence the casting quality. Understanding which is the most compelling and how they affect the outcome is a crucial matter.
2. Because of generated defects, HPDCs cannot be considered monolithic materials. The possibility to obtain valuable information about the material, its properties and potential applications must be reconsidered in view of their intrinsic characteristics, i.e. defect content and microstructure. On one hand, HPDCs' specific microstructure, which is different from any other production process, must be taken into account; on the other, the presence of defects and imperfections, seldom completely avoidable or eliminable, is another fundamental aspect.
3. To this end, deeper knowledge of the correlations between casting quality, mainly in terms of defect content, and mechanical properties, both static and cyclic, is necessary.
4. Heat treatment in HPDC represents, on one hand, an important mean to improve the mechanical response of the components acting on the microstructure; on the other, it still shows some limits due to the inner defects that tend to nullify the benefit.

RESEARCH APPROACH

This chapter opens with the presentation of the aim of the Ph.D. thesis and the environment in which the research can be applied. The chapter continues dealing with the methodology adopted to develop the research.

1 AIM AND SCOPE

High Pressure Die Casting is a production process applied in several industrial fields; approximately half of the world production of light metal castings is obtained by this technology. However, because of its complexity, it shows a very high scrap rate (i.e. it is not uncommon to have 5-10% of scarp) mainly due to different kinds of defects, in almost all cases exposed during or after the final operations [30,42].

The aim of this work is to understand which are the correlations between defect content, microstructure and casting mechanical response (both static and fatigue) and to comprehend how the latter can be improved. Numerical and experimental investigations have been carried out on Al-Si commercial HPDCs.

A penalization criterion was proposed; it adopts information coming from fractographic analysis and simulated stress distribution bands to describe the mechanical behavior of the castings. The immediate outcome can be its adoption in order to understand how to redesign a critical component, moreover, with the wider diffusion of industrial high-resolution Computed Tomography (CT) techniques, the proposed criterion can be used also for predictive analyses.

Unconventional heat treatments were also carried out; the enhancement of both static and cyclic mechanical properties was achieved even using temperatures and soaking times shorter than those commonly applied in industry.

2 RESEARCH PERSPECTIVE

The present work has originated from real industrial problems within the HPDC foundries. It started within the EU MUSIC project and the challenge to transform a production-rate-dominated manufacturing field into a quality/efficiency-driven and integration-oriented one. During the research development, a specific focus was always devoted to the possible industrial application in order to narrow down the gap between academic research and industry.

Prior to each research phase, a literature survey was carried out to acquire a broader knowledge of the process, its limits and challenges. The survey, together with the cooperation with Italian foundries and refiners, highlighted the enormous potential of the process, the great interest afforded by researchers but also the remarkable limits of a technology that often shows a great untapped potential.

At the very beginning of this work, in the frame of the EU MUSIC project, an investigation procedure was developed which led to the definition of preliminary correlations between process parameters, defect content and static mechanical properties obtained analyzing both reference castings and commercialized industrial demonstrators. The further definition of a Penalty Index based on FE model and fractographic investigation gave satisfactory predictions of both static strength and fatigue life of castings containing defects. It is expected that the main drawback of the developed criterion, i.e. its “post-mortem” application, can be overcome thanks to the wider diffusion of industrial high-resolution Computed Tomography (CT). Finally, stabilization heat treatments at 624 K (350C) were developed in order to improve the mechanical properties without causing surface blistering or component distortion.

The results obtained were analyzed and compared with data available in literature and they were also discussed with industrial partners to validate their applicability.
The present research comprises three major interconnected topics:

1. The effect of process parameters on the casting quality, in terms of porosity and oxide contents and mechanical response. This led to the identification of the process parameters mainly responsible for defect generation and therefore for the consequent casting mechanical behavior.
2. An in-depth analysis of the effect of the defect content to the casting mechanical behavior. The outcome was the development of a penalization criterion that simultaneously could take into account defects on the fracture surface and the in-service mechanical behaviour simulated through an FE software.
3. An in-depth analysis of the effect of microstructure, i.e. eutectic Si morphology, on the castings' mechanical response and its improvement through the setup of unconventional heat treatments.
   The focus was also put on the fine Si precipitation within the Al matrix and the effect of common alloying elements, such as Cu and Fe, on the eutectic Si.

3 MATERIALS AND EXPERIMENTAL

3.1 Materials

Four secondary Al-Si based alloys were taken into account: AlSi9Cu3(Fe), AlSi11Cu2(Fe), AlSi12Cu1(Fe) and AlSi12(b) (EN-AC46000, EN-AC46100, EN-AC47100, EN-AC44100) according to UNI EN1706 [78]. They were selected in agreement with the industrial partners involved in the development of this work and adopted to produce reference and commercial diecastings. The alloy chemical compositions, measured by optical emission spectroscopy, are listed in Tables 7-10.

Table 7 Chemical composition of alloy AlSi9Cu3(Fe) (wt%).

Alloy	Si	Fe	Cu	Mg	Mn	Ni	Ti	Zn	Al
AlSi9Cu3(Fe)	8-11	0.6-1.3	2-4	0.05-0.55	0.55	0.55	0.25	1.2	Bal.
Tested alloy	10.4	0.8	3	0.42	0.3	0.05	0.05	0.9	Bal.

Table 8 Chemical composition of alloy AlSi11Cu2(Fe) (wt%).

Alloy	Si	Fe	Cu	Mg	Mn	Ni	Ti	Zn	Al
AlSi11Cu2(Fe)	10-12	1.1	1.5-2.5	0.3	0.55	0.45	0.25	1.7	Bal.
Tested alloy	10.7	0.81	1.65	0.22	0.22	0.06	0.07	1.44	Bal.

Table 9 Chemical composition of alloy AlSi12Cu1(Fe) (wt%).

Alloy	Si	Fe	Cu	Mg	Mn	Ni	Ti	Zn	Al
AlSi12Cu1(Fe)	10.5-13.5	1.3	0.7-1.2	0.35	0.55	0.30	0.20	0.55	Bal.
Tested alloy	11.6	0.85	0.85	0.08	0.20	0.05	0.05	0.45	Bal.

Table 10 Chemical composition of alloy AlSi12(b) (wt%).

Alloy	Si	Fe	Cu	Mg	Mn	Ni	Ti	Zn	Al
AlSi12 (b)	10.5-13.5	0.65	0.15	0.10	0.55	0.10	0.20	0.15	Bal
Tested alloy	13	0.46	0.08	0.02	0.29	0.01	0.03	0.12	Bal.

3.2 Castings and their processing

The alloys were adopted to produce three different HPDCs: a reference casting and two commercial components. In this section a thorough casting description is given for each component; details of the production processes are also pointed out.

3.2.1 The Reference Casting

In the frame of European MUSIC (Multi-layers control & cognitive System to drive metal and plastic production line for Injected Components, No. 314145) project [79], a Reference Die was elaborated and designed with the aim of exacerbating the generation of different kinds of defects in some regions of the casting; the AlSi9Cu3(Fe) was adopted to produce this component. The concept behind its design was to allow an easy assessment of different kinds of defect and, through controlled variations of the process parameters, obtain different levels of severity of each defect. The defect classification introduced in section 2.1 of Chapter 1 was fundamental during the design phase of the die and different designs with various inserts led to the final concept shown in Fig. 11, the so-called *horse-shoe* shape casting.

Fig. 11 *Horse-shoe* reference casting

As shown in Fig. 11, six main parts can be observed: (1) three thin-walled specimens representing the thickness typically used in HPDC, (2) three bosses with mass concentration aimed at generating shrinkage porosity (one of them was equipped with a squeeze pin to monitor its effect), (3) a thick-walled area close to the venting channel and three holes on each side of the *horse-shoe* aimed at creating die soldering and increased turbulence respectively, (4) a small extension with the purpose of generating melt flows and vortexes leading, in turn, to cold laps, (5) the whole casting geometry aimed at generating distortion and (6) a runner system intended to cause turbulence in the melt flow, as Dai et al. [80] suggested in their work.

The castings were manufactured using a cold chamber die-casting machine with a locking force of 750 ton, a shot chamber length of 0.482 m and a diameter of 0.08 m. The molten metal inside the furnace, was kept at 978 K (705°C) and the pouring temperature was 933K (660°C); the melt was periodically manually skimmed. During the process, the thermoregulation control unit was set up at 518K (245°C) in the moving side circuit of the die and at 508K (235°C) in the fixed side one.

The experimental campaign was carried out on the basis of a developed Design of Experiment (DOE). It consisted of 32 arrays, i.e. process parameter changes, totalizing an amount of approximately 150 castings produced. The nominal process parameter intervals were:

- I phase plunger velocity range from 0.2 to 0.8 m/s
- II phase plunger velocity range from 1.5 to 4 m/s
- The switching point position was set from a minimum of 300 mm to a maximum of 350 mm
- The intensification pressure ranged from 500 to 1000 bar.

At least three castings for each combination of process parameters were produced.

3.2.1.1 Installed equipment: the sensor network

Among the several equipments installed on the HPDC machine and adopted during the casting trial, an intelligent sensors network (ISN) represents the most innovative device. It allowed a continuous control of the process itself, recording the evolution of in cavity temperatures, pressures and plunger speed and displacement.

Three sensor types were installed in the die cavity: a *Metal Front Pressure Sensor* measuring the pressure of the melt on the die surface during the whole filling and solidification phases, a *Metal Front Temperature sensor* measuring the temperature of the molten metal on the die surface during the whole cycle and a *Metal Front Contact sensor* providing a digital signal when it got in contact with the melt, achieving a real-time evolution of incoming metal position [81].

3.2.2 The Gear Box Housing

Within the EU MUSIC project, a gear box housing was chosen as industrial demonstrator (see Fig. 12). In this case, the AlSi11Cu2(Fe) alloy was chosen to produce the castings.

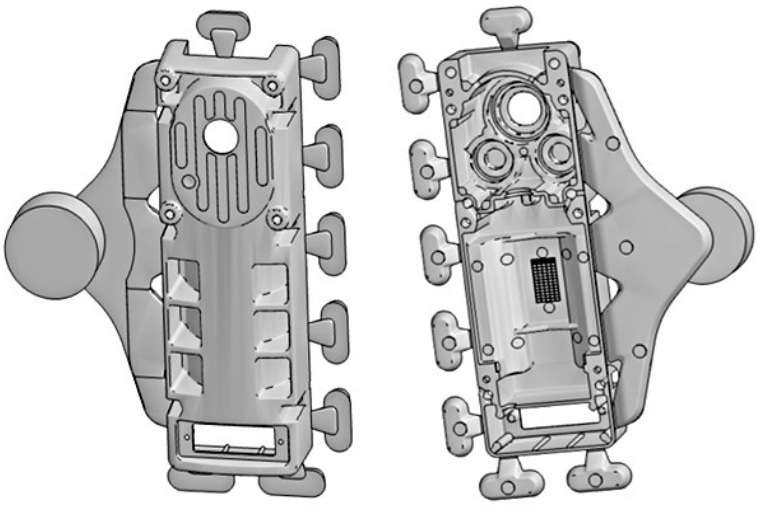

Fig. 12 Gear motor housing

The components were manufactured using a cold chamber die-casting machine; the molten metal inside the furnace was progressively increased from 943K (670°C) to 973K (700°C). The experimental campaign was carried out in accordance with a DOE made up of 29 arrays for a total of approximately 200 HPDCs produced. The nominal process parameter intervals were:

- I phase plunger velocity was kept constant for the entire casting trial
- II phase plunger velocity range from 2.1 to 4.4 m/s
- The switching point position was set from a minimum of 212 mm to a maximum of 260 mm
- The intensification pressure ranged from 502 to 958 bar

3.2.3 The sleeve

The AlSi12Cu1(Fe) and AlSi12(b) alloys were adopted to produce sleeves for photographic devices. The casting includes four appendixes: two are fastened to the tripod leg and two can be opened and closed in order to allow the lengthening of the telescopic leg. The moving parts of the component are labeled as A- and B-side (see Fig. 13); the focus was put on the B-side since it was the most critical one.

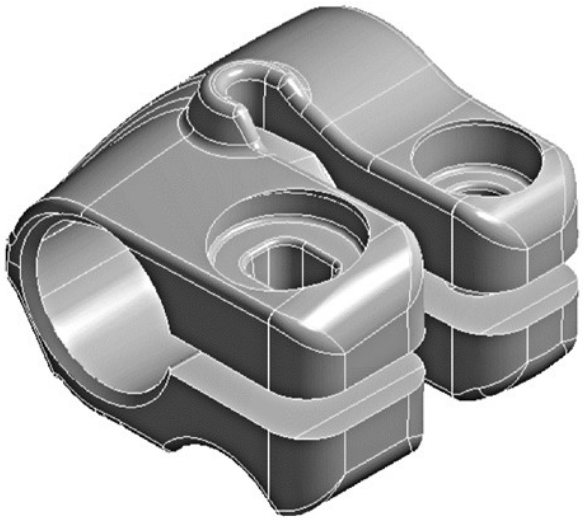

Fig. 13 The sleeve

Net-to-shape castings were produced using a multi-cavity die in a horizontal cold chamber HPDC machine whose process parameters were optimized and constant.

3.2.3.1 Heat treatment of AlSi12Cu1(Fe) and AlSi12(b) castings

The as-cast AlSi12Cu1(Fe) alloy components were heat treated at a stabilization temperature equal to 624 K (350°C), with soaking times of 1, 2, 4 and 8 hours in order to improve their static and fatigue mechanical behaviors. The duration of the various heat treatments represents the actual time of heat treatment (i.e. time to heat up is not included).

As a remarkable improvement of mechanical properties in the AlSi12Cu1(Fe) castings was observed already after 1 h at 624 K (350°C), the AlSi12(b) castings were also heat treated at the same stabilization time and temperature in order to study the effects on this alloy which showed a better tensile and fatigue response in the as-cast condition.

3.3 ND investigation technique

All the castings were visually inspected in order to highlight possible surface defects or imperfections.

Radiographic investigations were carried out, according to UNI EN 12681:2006 [82], in order to detect possible inner defects, mainly macro- and/or micro-porosities due to gas/air entrapment or shrinkage. In Figs. 14a-c the inspected areas for each casting are displayed.

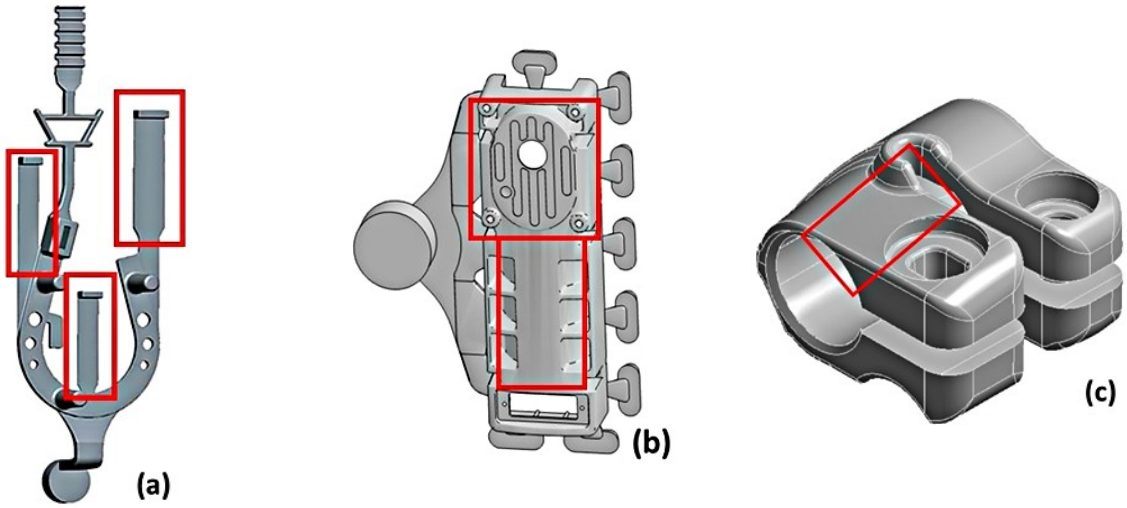

Fig. 14 X-Ray inspection zones: (a) *Horse-shoe* reference casting, (b) Gear motor housing, (c) sleeve

Several images for each area were captured, varying current and voltage depending on the analyzed thicknesses. The detected grey level was kept constant only for parts with the same thickness in order to make the results comparable.

The x-ray images were investigated using an image analysis software in order to define a casting qualitative classification based on the highlighted porosities.

3.3.1 FE simulation model and strain gage analysis

As regards the sleeve casting, a numerical model was carried out by means of Ansys® Workbench 14.5 in order to calculate the stress and strain distributions induced by service loads on the component.

Moreover, in order to determine the deformation induced by the service loads on the component, a strain gage analysis was also performed. Two strain gages were placed on the B-side of the component; the surfaces of interest were cleaned with a grinder and smoothed out to remove the debris remaining from the grinding. A solvent specifically designed to prepare surfaces for bonding was used. Once the surface was clean, it was roughened to improve the bonding power to increase the active surface area. The applied strain gages were metallic foil

gages arranged in a grid pattern, HBM 0.6/120 LY41. A tightening torque of 1.8 Nm was applied in order to clamp the casting to the support.

Elastic and elastic-plastic properties of AlSi12(b) at room temperature were evaluated by means of preliminary static tensile tests on standard specimens, according to ASTM E08-04 [83]. The material was assumed to be isotropic, and the true stress-strain curve obtained from tensile tests was implemented in the numerical model; Young modulus (E), Poisson's ratio (ν) and material density (ρ) are listed in Table 11.

Table 11 Material characteristics

E (MPa)	ν	ρ (kg/dm^3)
71,000	0.33	2.66

In order to accurately capture the 3D stress distribution, a higher mesh density was applied on the hole contact surfaces and close to the critical point shown in Fig. 15a. After few convergence tests, the optimized mesh showed a total of 59,586 tetrahedral elements. It is worth observing that the portion of the tripod on which the component had to be fastened during service was also modeled (see Fig. 15b).

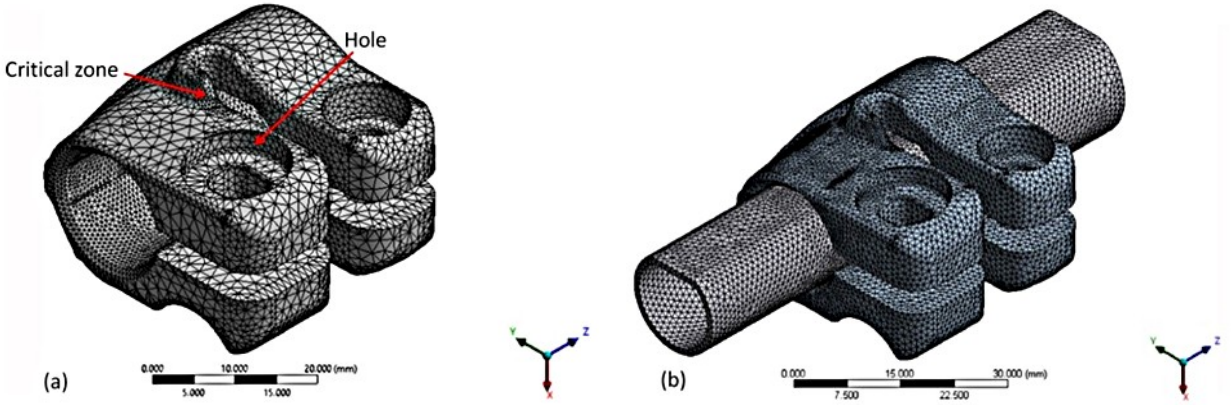

Fig. 15 (a) Mesh density (b) component and tripod leg meshing

Due to the presence of an initial gap between casting and support and their subsequent contact after the load application, a *symmetric frictionless* contact type was defined between the initial surface of the component and the external surface of the support. The *Augmented Lagrange* was chosen as solver algorithm; it is a penalty-based approach described by Eq. (2):

$$p = k_n x_n + \lambda \tag{2}$$

Where k_n is the contact stiffness, x_n is the resulting penetration which, during the Newton-Rapson iterations, is checked against an automatically-calculated maximum allowable

penetration tolerance ε_n and p is the contact pressure. If $x_n \geq \varepsilon_n$ then λ is increased and a message is printed indicating the number of contact points that have excessive penetration.

3.4 Sample preparation and metallographic observations

Samples for metallographic investigations were cut from each casting, depending on the most interesting area; in Figs. 16a-c the cutting zones are shown.

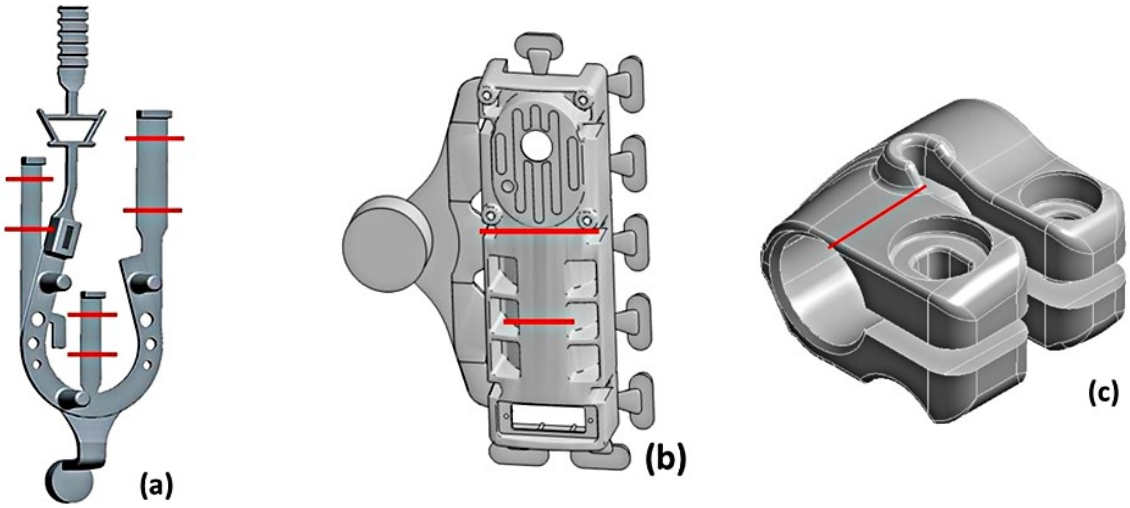

Fig. 16 Metallographic section positions (a) *Horse-shoe* reference casting, (b) Gear motor housing, (c) sleeve

They were mechanically prepared to a 3-µm finish with diamond paste and, finally, polished with a commercial 0.04-µm silica colloidal suspension.
Some samples were also deeply etched in a concentrated NaOH solution, as reported by Timelli et al. [84], to remove Aluminum and reveal the 3D morphology of eutectic Si crystals.
Samples for TEM observations were taken from thin slices; discs with 3-mm diameter were cut and then mechanically ground to 20-30 µm, followed by low-angle ion milling. TEM investigations were carried out using a JEM 2000 EX II microscope (JEOL©), operating at 200 keV.

3.5 Mechanical testing

Static and cyclic mechanical tests were carried out on as-cast and heat treated samples. The static tests were performed on a computer-controlled MTS Criterion C43 machine with a load cell capacity of 50 kN; whereas the fatigue tests were carried out on a servo-hydraulic MTS 858 Mini Bionix test system with a load cell capacity of 25 kN.
The mechanical samples obtained from each diecasting geometry are described below:

- *Reference Casting* – Three-point-bending tests were carried out, according to ASTM E290-97a [85], on samples drawn from two of the three thin-walled areas of the casting, labeled as B and F in Fig. 17. Each appendix was divided into two halves, *upper* and *lower* specimens respectively. All the specimens were 40 mm wide, 75 mm long and 2 mm thick. The crosshead speed applied was 4 mm/min.

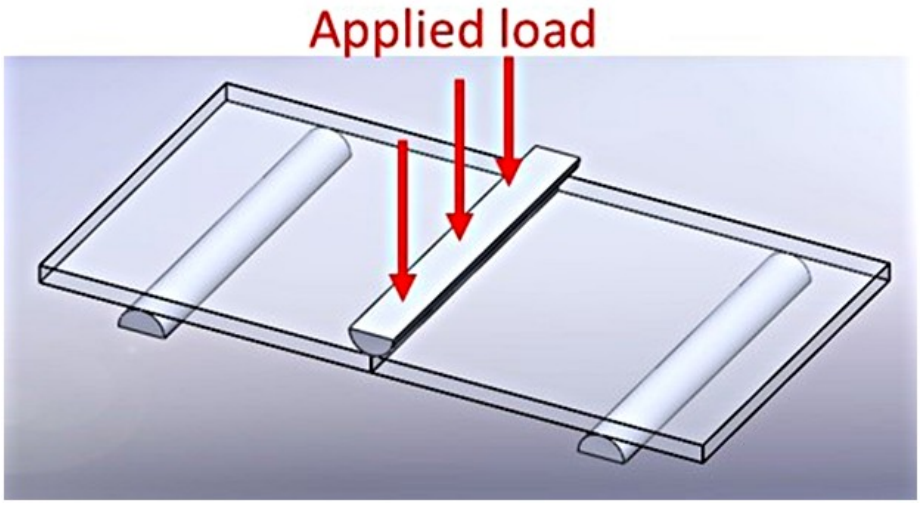

Fig. 17 Three-point bending test

- *Gear box housing* – Tensile and three-point-bending test samples were drawn from different areas of the component (see Fig. 18a,b). Tensile tests were carried out, according to [83], applying a crosshead speed equal to 2 mm/min; the three-point bending tests were conducted according to [85] with a crosshead speed of 4 mm/min.

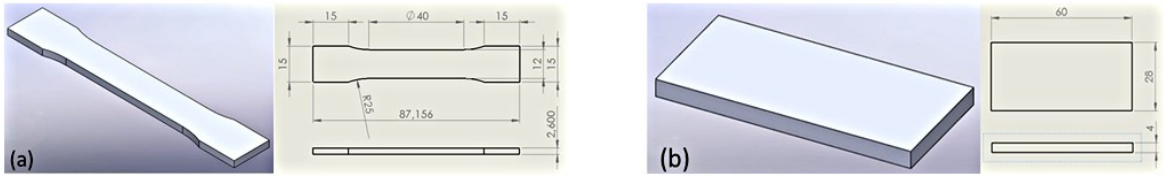

Fig. 18 (a) Tensile test specimen, (b) three-point bending test specimen

- *Sleeve* – Static and fatigue mechanical tests were carried out on the whole castings; the component was clamped by means of the fixed appendixes on a framework (see Fig. 19) specifically designed; the tightening torque was equal to 1.8 Nm. The load was then applied *via* the crosshead on the position shown in Fig. 19, so as to reproduce the real in-service force.
  The crosshead speed for the static tests was 2 mm/min.
  The load-controlled fatigue tests were carried out at room temperature and a constant frequency of 5 Hz; the nominal load ratio, R, was kept constant and equal to 0.1. Two load ranges were adopted (1125 N and 1350 N).

Fig. 19 Ongoing mechanical test carried out on the sleeve casting

3.5.1 Hardness test

Brinell hardness measurements were performed on ground and polished samples; the tests were carried out using a load of 62.5kgf and a dwell time of 15 seconds. Each data point represents the average of three or more hardness tests. Due to the differing levels of porosity within samples and the inherent variability of the tests, results clearly affected by the presence of porosity were discarded and the measurement repeated.

As regards the sleeve casting, the test was carried out on samples in as-cast condition and after stabilization heat treatment. The hardness outcomes were adopted to reveal trends in changes in the alloy due to time increase during heat treatment rather than as values representative of the bulk material.

3.6 Analysis techniques

3.6.1 Microscopy investigations

Microstructural observations were carried out using an OM (Leica® DMLA) and a field emission gun-environmental scanning electron microscope (FEG-ESEM, FEI® QUANTA 250) equipped with an energy-dispersive spectrometer (EDS, EDAX®). OM and SEM micrographs were processed by image analysis software and various microstructural parameters were investigated and measured, such as Si particle size and roundness (ρ). For a deeper evaluation of the eutectic Si morphology, structure and orientation, electron back-scattered diffraction (EBSD, EDAX®) investigations were performed on the sample surfaces. All the EBSD maps acquired had confidence index (CI) standardization followed by exclusion of points with CI lower than 0.1.

3.6.2 Fractographic investigation

The fracture surfaces of all tested specimens were analyzed using a scanning electron microscope. The fractographic images were then inspected using an image analysis software; porosities and oxides, on the fracture surfaces, were quantified in terms of their projected areas as shown in Fig. 20.

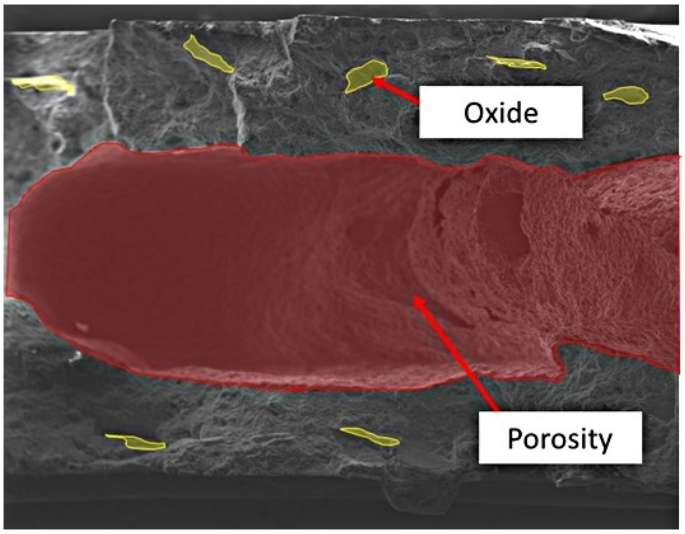

Fig. 20 Example of fractographic image with highlighted defects – porosity and oxides

3.7 Cu and Fe effect on eutectic Si morphology

3.7.1 Materials

Secondary AlSi12(b) alloy was used as baseline material. The chemical composition of the alloy was measured by optical emission spectroscopy on separately poured samples and presented in Table 12.

Table 12 Chemical composition of the ingot in AlSi12(b) [wt%].

Alloy	Si	Fe	Cu	Mg	Mn	Ni	Ti	Zn	Al
AlSi12 (b)	10.5-13.5	0.65	0.15	0.10	0.55	0.10	0.20	0.15	Bal
Tested alloy	13.2	0.46	0.06	0.11	0.35	0.01	0.07	0.18	Bal.

Three tests were conducted adding Fe, Mn, Cu and Zn in order to reach the levels of AlSi12Cu1(Fe) alloy (see Table 9), as shown in Table 13.

Table 13 Alloying element addition procedure

Test	Base material	Additions	
		Element	$[wt\%]_{final}$
1	AlSi12(b)	• Fe	0.7 - 0.8
		• Mn	0.29
		• Zn	0.46
1a	Alloy 1	• Cu	0.92
2	AlSi12(b)	• Cu	0.94

Chemical composition analyses were performed with optical emission spectroscopy; they are shown in Tables 14-16.

Table 14 Chemical composition of Alloy 1 [wt%].

Alloy	Si	Fe	Cu	Mg	Mn	Ni	Ti	Zn	Al
AlSi12Cu1(Fe)	10.5-13.5	1.3	0.7-1.2	0.35	0.55	0.30	0.20	0.55	Bal.
Alloy 1	13	**0.7**	0.15	0.12	**0.29**	0.01	0.08	**0.42**	Bal.

Table 15 Chemical composition of Alloy 1a [wt%].

Alloy	Si	Fe	Cu	Mg	Mn	Ni	Ti	Zn	Al
AlSi12Cu1(Fe)	10.5-13.5	1.3	0.7-1.2	0.35	0.55	0.30	0.20	0.55	Bal.
Alloy 1	13	**0.79**	**0.92**	0.11	0.30	0.02	0.08	**0.44**	Bal.

Table 16 Chemical composition of Alloy 2 [wt%].

Alloy	Si	Fe	Cu	Mg	Mn	Ni	Ti	Zn	Al
AlSi12Cu1(Fe)	10.5-13.5	1.3	0.7-1.2	0.35	0.55	0.30	0.20	0.55	Bal.
Alloy 1	13.2	0.46	**0.94**	0.11	0.35	0.01	0.07	0.18	Bal.

A SiC crucible was used to melt about 1 kg material inside a resistance-heated furnace at 1023 K (750°C). After homogenization at 1023 K (750°C) for at least 30 min, the melt was stirred and the surface skimmed to remove the dross. The molten metal was poured into a boron nitride-coated cylindrical steel cup (outer diameter 45 mm, height 60 mm, uniform wall thickness of 3 mm), preheated at 723 K (450°C).

3.7.2 Thermal Analysis

A K-type thermocouple (Ø 1 mm) was used for the thermal analysis experiments; it was fixed at the lid of the cup and covered with tightly fitting steel tubes, it was inserted into the melt 30 mm below the surface of the specimen.

The temperature and time were collected by means of a data acquisition system with a sampling rate of 0.5 s^{-1}, analog-to-digital converted accuracy of 0.1°C, and connected to a personal computer. The system was allowed to cool in air.

A minimum of two thermal analyses was performed for each experimental alloy. The thermocouples were calibrated against the melting point of pure Aluminum, assuming a melting point of 933 K (660°C). For each set of temperature/time relations, the cooling curves and the corresponding derivative curves were plotted to determine the characteristic temperatures related to the formation of phases based on the first derivative cooling curve approach [86,87].

In Table 17 the thermal analysis parameters used in the present work are described, as defined by Rakhmonov et al. [88].

Table 17 Definition of the characteristic temperatures obtained from thermal analysis

Symbol	Description
T_{nuc}	Nucleation temperature of a phase
T_{min}	Minimum temperature of a phase
T_{growth}	Growth temperature of a phase
$T_{solidus}$	Solidus temperature

3.7.3 In-lab casting production: mold design and casting trials

A casting was designed using Solidworks software in order to produce in-lab castings with microstructure comparable to those of HPDCs. The resulting design and the real system are shown in Fig. 21a,b.

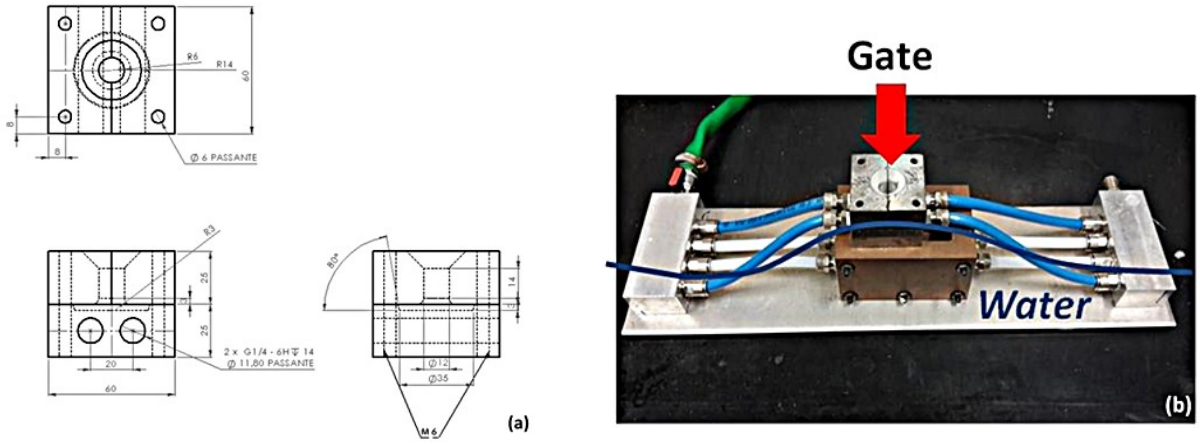

Fig. 21 (a) Mold design and (b) casting system for lab tests

A water cooling system was used in order to obtain cooling rates similar to those of HPDC process and two K-type thermocouples were placed radially in the cross-section of the feeding channel, in order to pour the molten Aluminum at the same mold temperature, i.e. 468 K (195°C).

Intensification pressure could not be applied. At least two tests were performed for each experimental alloy.

3.7.4 Microstructural characterization

Samples for microstructural characterizations were sectioned from the produced castings. They were mounted, ground and polished using standard polishing techniques.
Optical microscope (OM) was used to compare the obtained microstructure with that of a diecasting sample with similar thickness and to characterize type and morphology of the phases precipitated during solidification as well as the obtained eutectic Si morphology.

RESULTS AND DISCUSSION

This chapter summarizes the main results of a three-year work. More details are reported in the appended papers. This chapter is divided into three interconnected parts: correlations between process and casting quality, effect of defects on the casting mechanical properties and effect of microstructure on the mechanical response and its modification through heat treatment.

1 CORRELATIONS PROCESS–CASTING QUALITY

In this segment, the main findings of the correlation between HPDC process parameters and the casting quality are introduced. The presented work was developed within the EU MUSIC project, a four-year program aimed at improving the process reliability, reducing casting weights and production costs and implementing an intelligent system to optimize casting design and manufacturing. The significance of this preliminary part stands in the design and manufacturing of the Reference Die and in the employment of the innovative devices installed on the machine to optimize and monitor the process.

It is in this preliminary part that defects caused by metal-die interaction, air/gas entrapment, shrinkage or Al oxide formation are introduced as the main causes of casting failure.
As documented in the literature [35,43,84], these kinds of defects are related to HPDC injection parameters, besides to the alloy chemical composition and melt treatment.

1.1 MUSIC Reference Die: preliminary correlations [89]

Each sensor installed on the HPDC machine, and previously described [81], recorded 20,000 values at each cycle (i.e. one value every 0.5 ms). In order to allow an easy data elaboration, the definition of key parameters is fundamental.

- *Temperature profiles* - maximum temperature value [°C] and corresponding time [ms] for each casting. In Figs. 22a,b examples of temperature profiles and corresponding key parameters are shown.
- *Pressure profiles* – pressure trends [bar] for each casting. In Figs. 22c examples are shown.
- *Plunger displacement and velocity curves* – A significant change in the slope of the velocity curve corresponds to the switching point: position [mm] and time [ms] of this point are considered.

  The first phase plunger velocity is obtained considering the constant values standing before the switching point position, whereas the second phase plunger velocity is approximated by the maximum velocity value standing after the switching position. Examples of the profiles are shown in Figs. 22d,e.

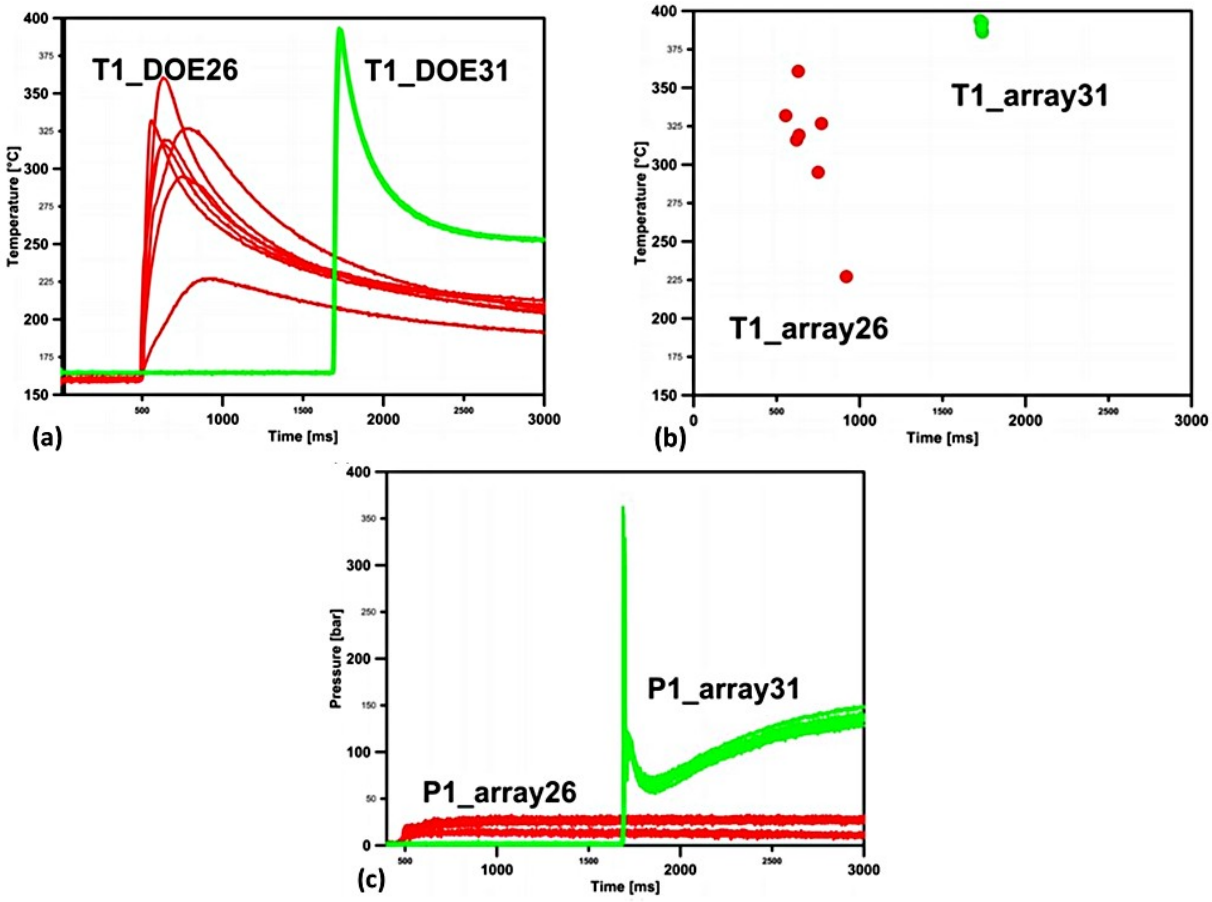

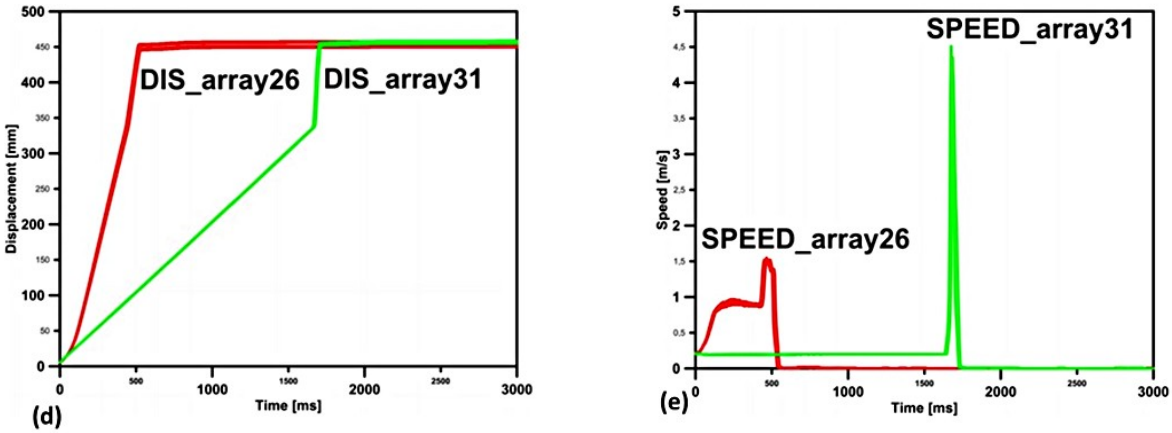

Fig. 22 (a) Temperature profiles, (b) maximum temperatures, (c) pressure profiles, (d) displacement trends, (e) speed profiles

The extracted data represent a linkage between process, i.e. the independent variable, and casting quality, i.e. the dependent variable.

Concerning the casting quality, two classifications are obtained: a qualitative one based on the visual inspection of each diecasting and a quantitative one based on the radiographic investigation and the following image analysis.

As regards the qualitative classification, the following qualitative levels are assigned:

- *Level 1* is attributed to castings without defects,
- *Level 2* is assigned in case of roughness change on the surface caused by metal-die interaction, or slightly visible melt flows,
- *Level 3* is assigned to castings showing a great roughness change or if contaminants, cold shots or clearly visible melt flows are present on the surface,
- *Level 4* is attributed to incomplete, cracked or blistered castings.

The porosity percentage assessment conducted on radiographic images by means of the image analysis software allowed a quantitative classification. However, it is possible to determine a percentage of porosity only when this is detectable.

In Table 18 the qualitative and partly quantitative classification is shown; a brief description is given below.

Table 18 Qualitative and partly quantitative classification based on x-ray investigation

CLASS	QUALITATIVE DESCRIPTION	POROSITY [%]
1	Absence of defects	
2	Slightly visible melt flows	
3	Clearly visible melt flows	
4	Melt flows and detectable porosity (Low level)	0 – 0.8
5	Micro and macro detectable porosity (Medium level)	0.8 – 1.5
6	Distributed micro and macro detectable porosity (High level)	>1.5
7	Scrap – Crack or incomplete filling	

Levels 1 to 3 refer to castings with porosities hard to detect by means of the x-ray device; level 7, on the contrary, is attributed to incomplete, cracked or blistered castings that need no x-ray investigation to be discarded.
Levels 4 to 6 are simply referred to as *Good*, *Acceptable* or *Bad* castings.

The described classifications allow an easier correlation between casting quality and the main process variables, i.e. injection velocities and in-cavity temperatures and pressures.
As shown in Figure 23a, the molten metal should reach the utmost parts of the die cavity (i.e. the end of the stepped wedge of the reference casting) with relatively high measured temperature and pressure avoiding, in this way, surface defects, cracks and incomplete filling.
The same temperature and pressure values are correlated to the casting porosity content; the higher the temperature and pressure, the lower the porosity content (see Fig. 23b).

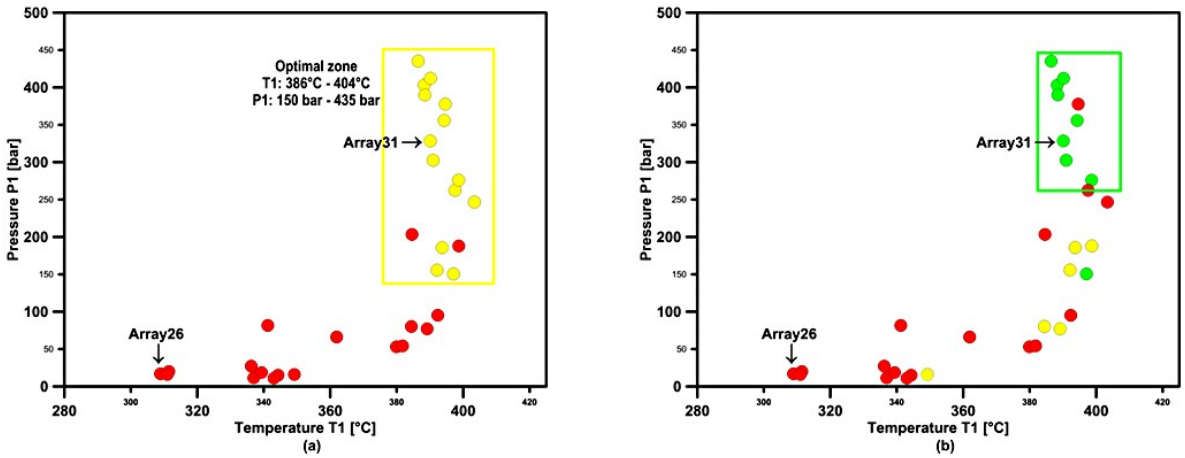

Fig. 23 (a) T1 temperature sensor *vs* P1 pressure sensor: the values in the box correspond to sound castings according to visual inspection; (b) T1 *vs* P1: the values in the box correspond to castings with low porosity content; red, yellow and green colors are related to *Bad*, *Acceptable* and *Sound* castings.

Plunger velocities, overpressure and switch point are also fundamental. Indeed, a too low second phase piston velocity can result in a compact metal front, but a longer cycle time is required which may cause incomplete casting (considering the first phase unvaried); conversely,

a too high velocity can produce higher flash amount or spraying behavior with consequent formation of cold joints and air porosities.
Moreover, since the piston speed is also related to the filling time, the correct compromise must be obtained; indeed, despite higher flash amounts or spraying problems, a faster piston also leads to shorter filling times and higher heat levels of the melt in the die, as can be seen in Figs. 24a,b.

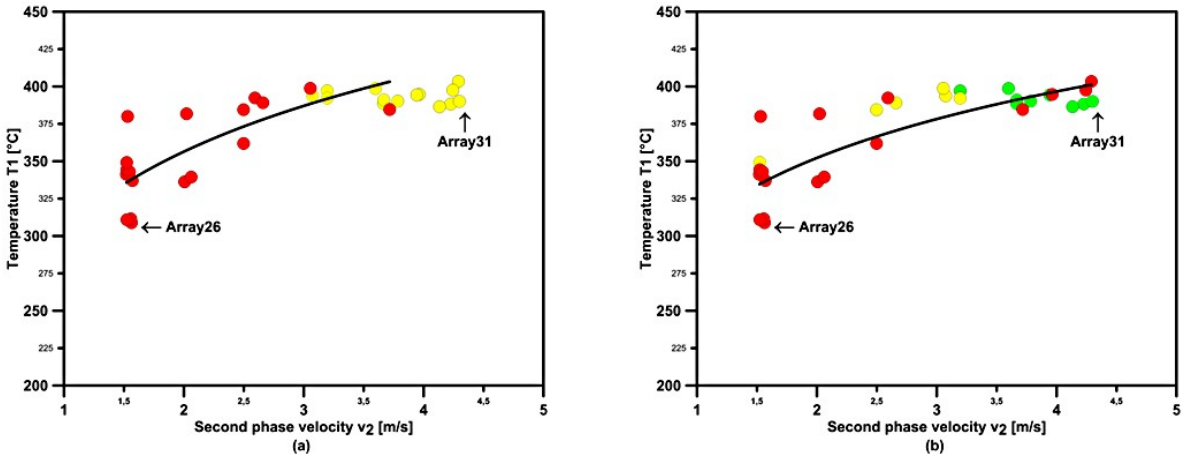

Fig. 24 T1 sensor temperature as a function of second phase plunger velocity with reference to (a) visual inspection and (b) porosity content; red, yellow and green are related to *Bad, Acceptable* and *Good* casting respectively. Data present a logarithmic relationship

To further validate the described correlations, the process parameters and quality investigation results of the worst and best configurations of process variables are reported in Table 19.

Table 19 Comparison between worst and best process parameters settings - horseshoe casting (Nominal values written in brackets)

	v1 [m/s]	**v2 [m/s]**	**switch [mm]**	**T1 [°C]**	**P1 [bar]**	**Vis. Insp. Level**	**Porosity XR [%]**
Worst array	0.9 (0.8)	1.5 (1.5)	329 (330)	311	16	4	13.5
Best array	0.2 (0.2)	4.3 (4)	332 (335)	390	329	3	0.5

In Figs. 25a,b MAGMASOFT simulations of the two settings are represented: temperatures at the end of the filling phase of the best casting are higher than those of the worst one.

(a) (b)

Fig. 25 Simulations of the temperature distribution of the castings obtained by (a) worst and (b) best process parameters configurations.

1.2 From the Reference Casting to the industrial demonstrators [90]

The main contribution of the work developed within the EU MUSIC project [79] was the introduction of an overview on the preliminary correlations between process, casting defects and static mechanical properties obtained analyzing both Reference Castings characterized by a defect generator geometry and already commercialized industrial demonstrators.
The Gear Box Housing, Italian demonstrator chosen in the frame of the EU MUSIC project, was used as the component to apply, at industrial scale, the outcomes obtained from the Reference Die analyses and to define possible criteria to predict the defect formation while simulating the die cavity filling through Magmasoft software.

The correlations obtained studying the Reference Casting are more well-defined than those obtained analyzing the industrial demonstrator. The reason is that the former was designed and precisely aimed at generating defects that could be easily controlled, detected and assessed; moreover, the two castings show a different in-gate configuration. A branched gating system like that of the Gear Box gives more opportunities to direct the metal flow which results in more randomly distributed defects and thus in a higher scatter of mechanical results. Hence, the industrial demonstrator, with its more complex shape, results in less predictability and repetitiveness of defect positions, leading again to a higher quality scatter as shown in Fig. 26a,b.

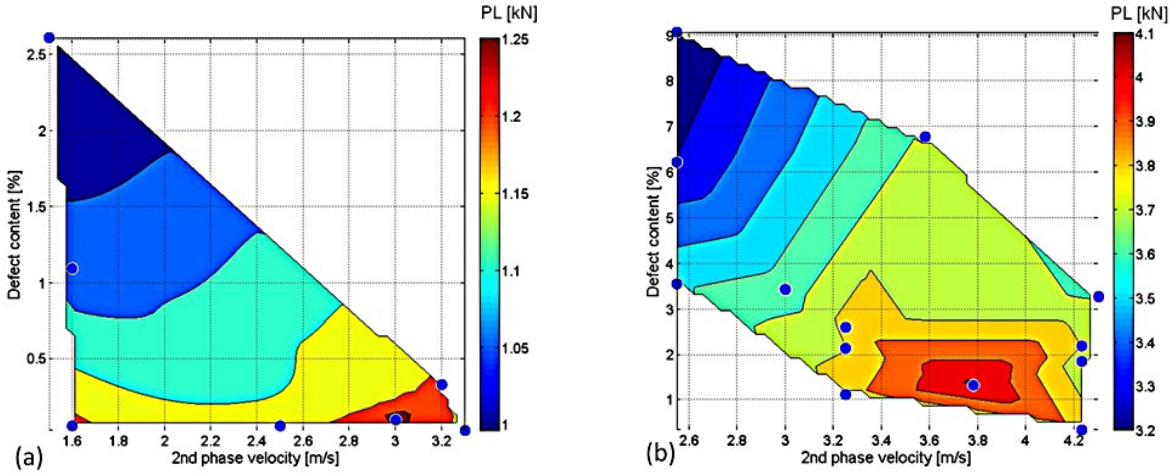

Fig. 26 Preliminary correlations between defect content on the fracture surfaces and mechanical properties: (a) *Horse-shoe* casting, (b) Gear Box Housing.

Modefrontier software was also used to understand how the main process parameters, i.e. overpressure, switch point position, first and second phase plunger velocities, may influence the casting quality.

In order to better assess the defect content, 14 zones of the Gear Box were separately inspected as shown in Fig. 27.

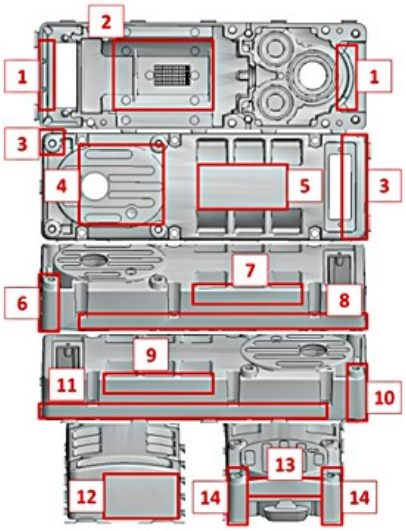

Fig. 27 Gear box inspected zones

Among the various defect types, the most interesting in terms of correlation with process parameters are porosity and cold joints. Figs. 28a-d displays the results in terms of cold joint contents: zones 1 and 5 are the most interesting as, changing second phase velocity and switch point position, consequences on the casting quality are visible.

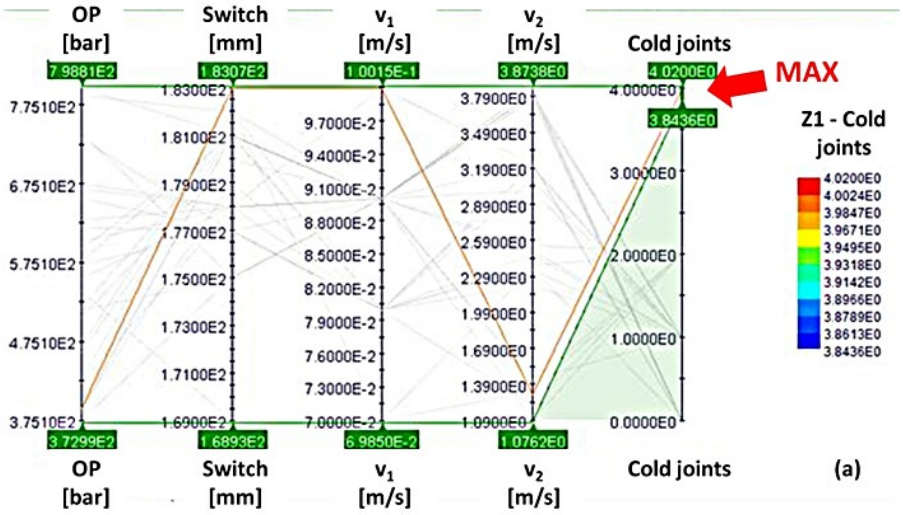

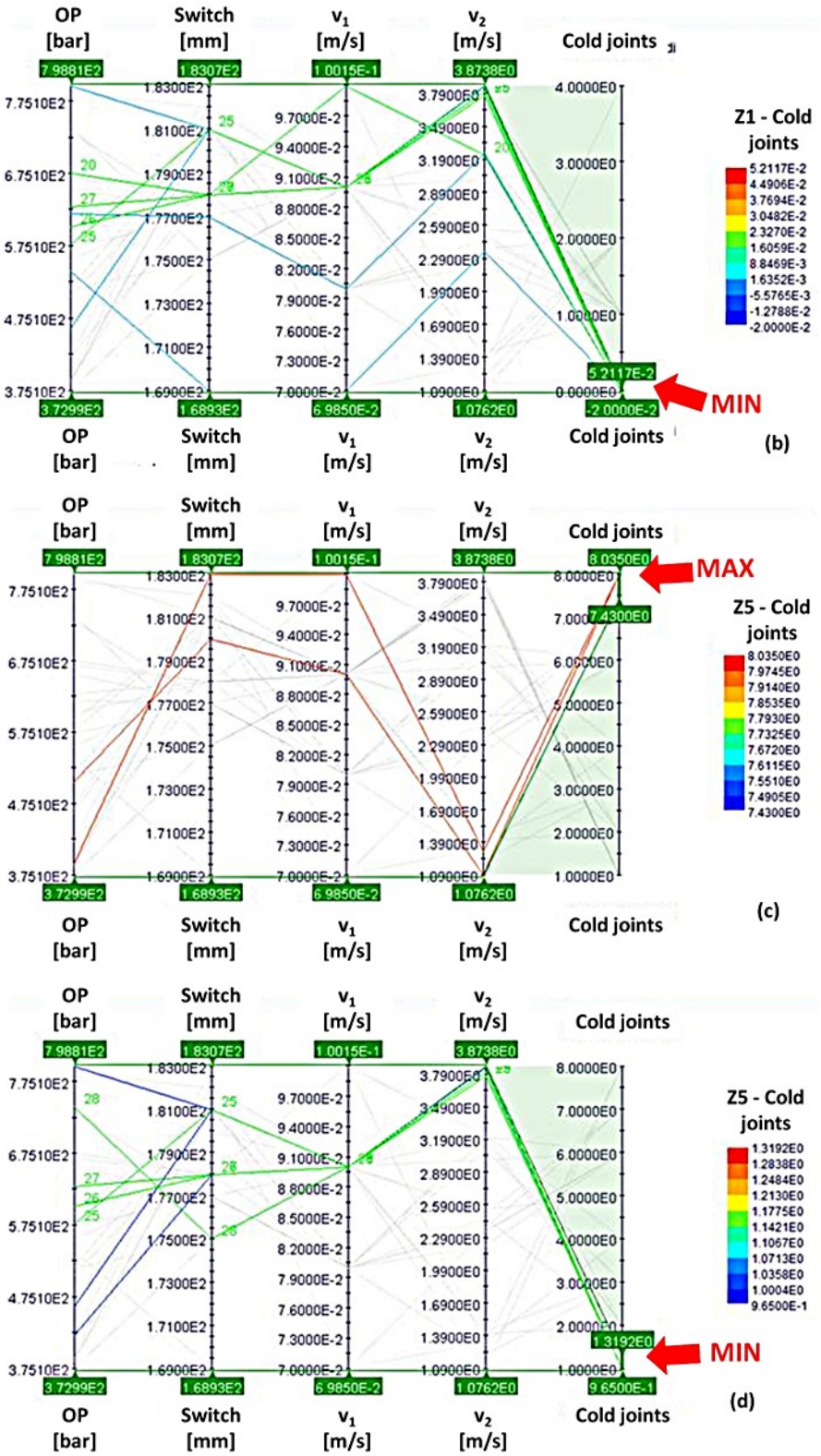

Fig. 28 Modefrontier parallel charts - effect of process parameters on cold joints

The parallel charts of Figs. 28, confirm what previously stated; the filling phase is quicker and a higher metal temperature is maintained which, in turn, result in a reduction of cold joints. A higher overpressure (Figs. 28b,d) contributes to decreasing defect formation as well.
On the contrary, a longer first phase duration causes a decrease of the molten metal temperature, resulting in a higher amount of defects.

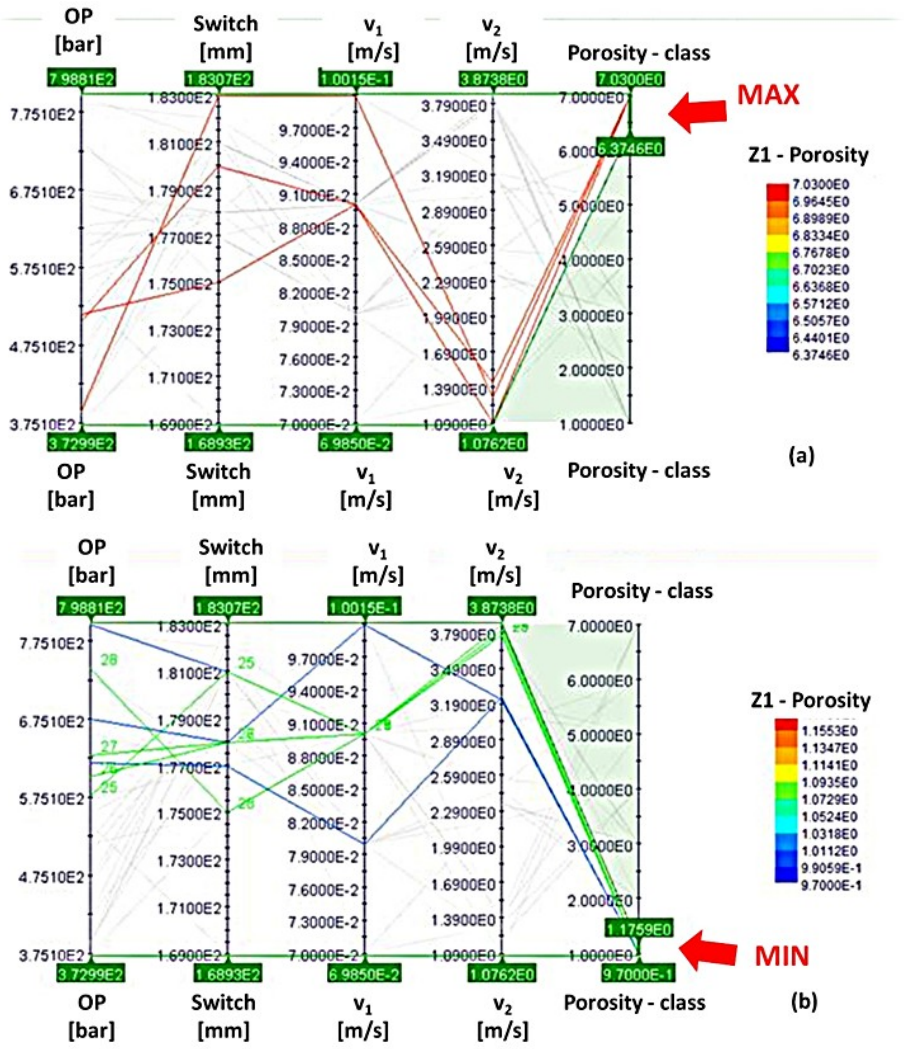

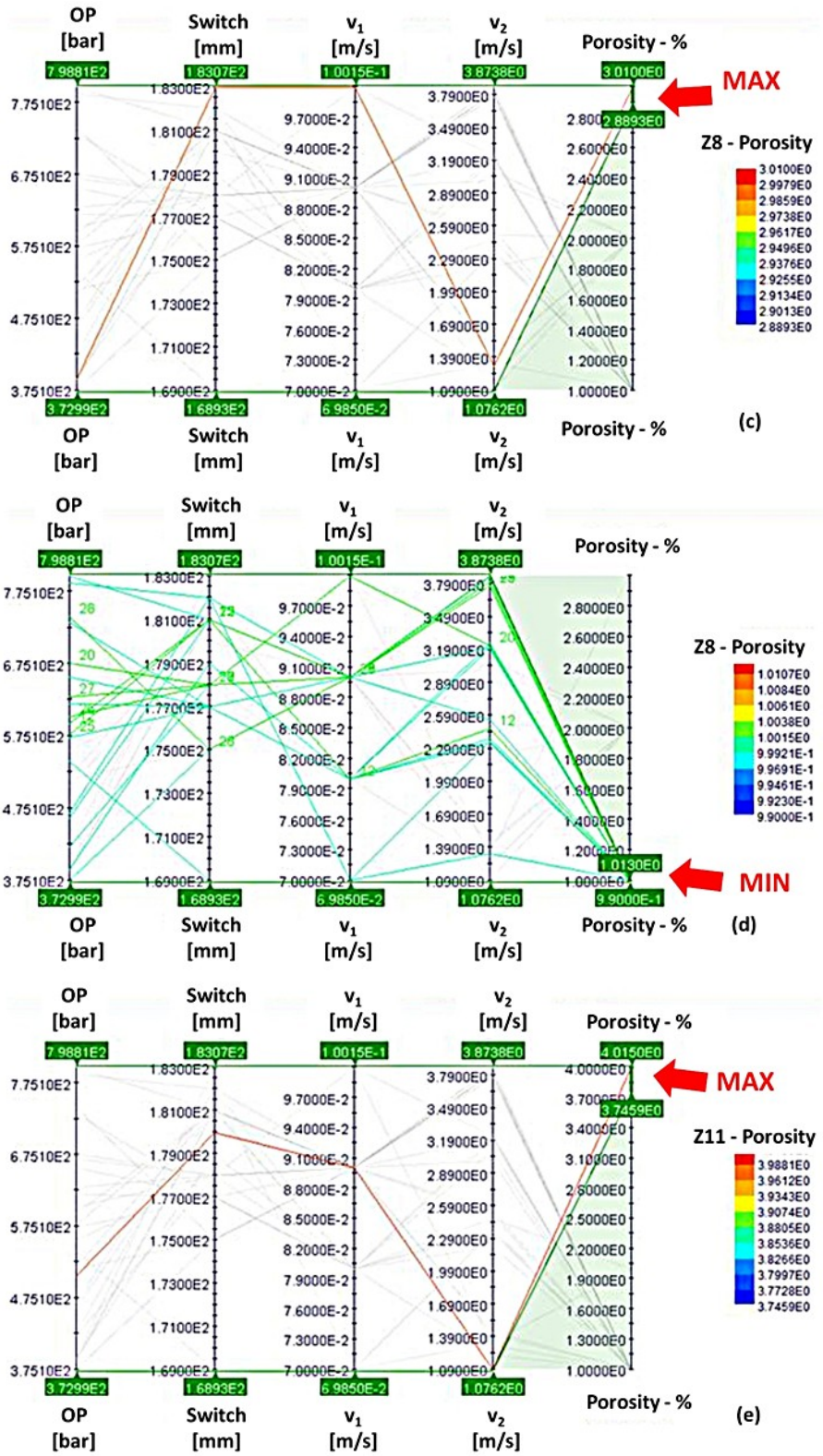
OP [bar]
Switch [mm]
v1 [m/s]
v2 [m/s]
Porosity - %
MAX
Z8 - Porosity
(c)
MIN
(d)
Z11 - Porosity
(e)

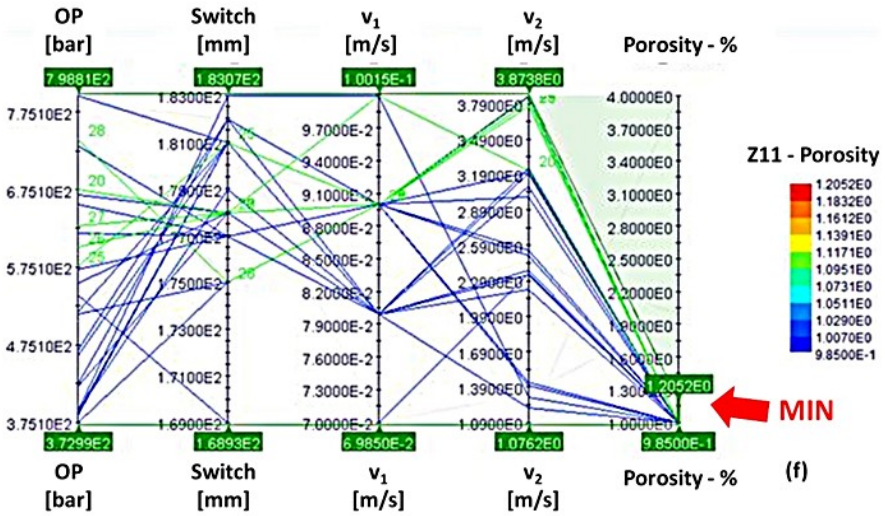

Fig. 29 Modefrontier parallel charts - effect of process parameters on porosity content

Zones 1, 8 and 11 are the most interesting in terms of porosity content; zone 1 shows the highest amount of porosity detected, zones 8 and 11 are located opposite to each other, the former on the gate side, the latter opposite to it (see Fig. 27). Once again overpressure and second phase velocity are the most influencing process parameters leading to higher or lower defect amount depending on their intensities.

Thanks to the analyses shown (mainly Figs. 28 and 29), Magmasoft criteria can be developed to predict cold joints and porosity formation depending on the process parameter levels set on the machine. According to the characteristics of each detected defect, certain Magmasoft parameters are more interesting than others; therefore they should be taken into account in order to elaborate the most appropriate predicting criteria.

It is the author's opinion that the presented results can be considered as starting point for further research in order to improve the die filling simulation results and lead to even more reliable defect predictions.

2 DEFECTS AND MECHANICAL BEHAVIOR [91]

2.1 Preliminary correlations: the limits of x-rays

2.1.1 Numerical results

Besides the gear box, another industrial demonstrator, easier to handle in lab-scale, was chosen by the author to develop further research work.

The preliminary FE simulation model, developed for the sleeve, was fundamental to understand how defects and casting geometry contribute to the casting in-service behavior.

The maximum Von Mises stresses were found to be approximately 208 and 261 MPa, corresponding to applied forces equal to 1000 and 1400 N, respectively, as shown in Figs. 30a,b. The choice of these two force values was made in agreement with those normally used to fix the casting to the photographic device were it is used.

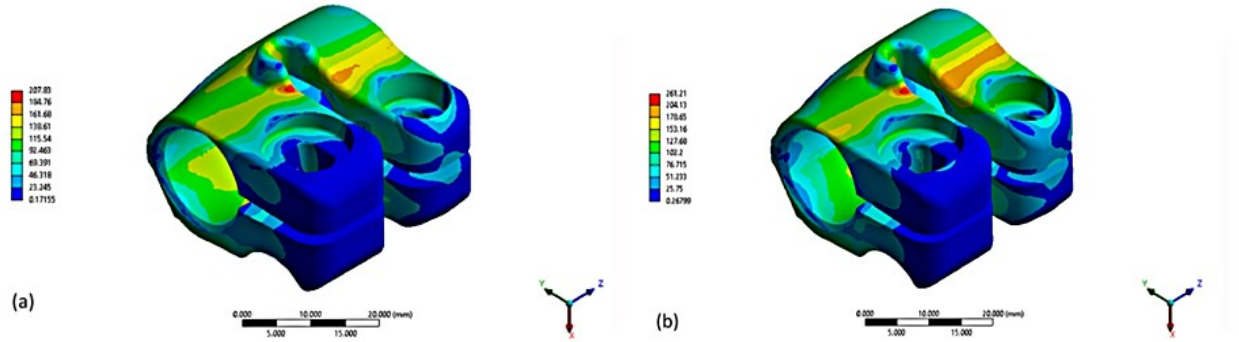

Fig. 30 Equivalent Von Mises stress distributions with an applied force of (a) 1000 N and (b) 1400 N.

In both load-cases, the peak value exceeds the material yield stress (i.e. 125 and 165 MPa according to standard UNI 4514 and preliminary tensile tests) leading to permanent deformation and casting failure during its service.

The reliability of the developed model was verified by comparing the $\mu\varepsilon$ values registered through the strain gages and those calculated by the simulation. Results are summarized in Table 20.

It can be noted that there is a good match between experimental and simulated results since the disagreement between the obtained values can be considered negligible.

Table 20 Comparison strain gage-FE results

Strain gage	Experimental $\mu\varepsilon$	FE $\mu\varepsilon$	Error (Pct)
1	4800	4810	0.2
2	4500	4420	1.8

2.1.2 NDT, mechanical and fractographic investigation

As explained in the previous sections, different methods are used to detect casting defects and assess their quality. Visual inspection, magnetic particle and dye penetrant testing, radiographic analysis, ultrasonic and eddy current testing are the major six non-destructive investigation techniques (NDT).
Among them, the x-ray investigation technique is the most important. It is used within all HPDC foundries as, it is worth mentioning that, even high integrity castings are expected to contain defects; it is thus important to be able to predict their effect on the mechanical properties of the component.

A casting qualitative classification, according to ASTM E0505-01 [92], was carried out on the basis of the x-ray investigation also for this component, as described in Section 1.1 of Chapter 3. According to the classification introduced within the EU MUSIC project and displayed in Table 18, the castings were divided into three classes (see Fig. 31):

(a) *good* castings presented almost no defects close to the geometric critical point,

(b) *acceptable* castings showed small or negligible defects,

(c) *bad* castings were characterized by a significant amount of defects detected within the area of interest.

A first and fundamental limit of the radiographic investigation is that it can only detect porosities due to entrapped gas/air, shrinkage or local filling problems. Indeed, intermetallic compounds and oxide films are often difficult, if not impossible, to be detected since they are characterized by very small dimensions, sometimes negligible, and a density closed to that of the surrounding material. In Table 21 the total amount of inspected castings and their qualitative classifications are reported.

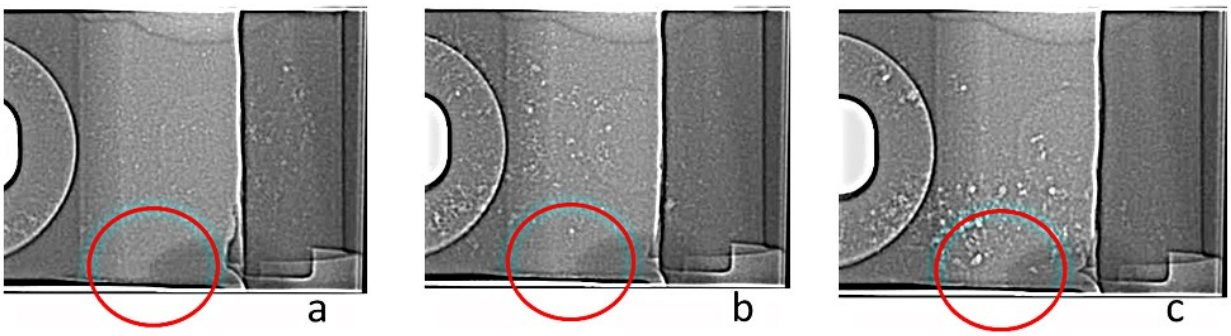

Fig. 31 Qualitative classification according to X-ray inspection: (a) *good*, (b) *acceptable* and (c) *bad* casting.

Table 21 X-ray qualitative classification results

Analyzed samples	Good	Acceptable	Bad
69	35 pct	51 pct	14 pct

As described at the beginning of Chapter 2, the castings were also mechanically tested. The maximum load at break [kN] and the corresponding displacement [mm] ranged from 3.34 to 5.43

kN and from 1.21 and 1.64 mm respectively. Figs. 32a,b shows how the casting quality prediction based only on the x-ray investigation is misleading. There is not always good correlation between the castings showing the best quality concerning the x-ray qualitative classification, and those showing the best mechanical behavior and *vice versa* [89].

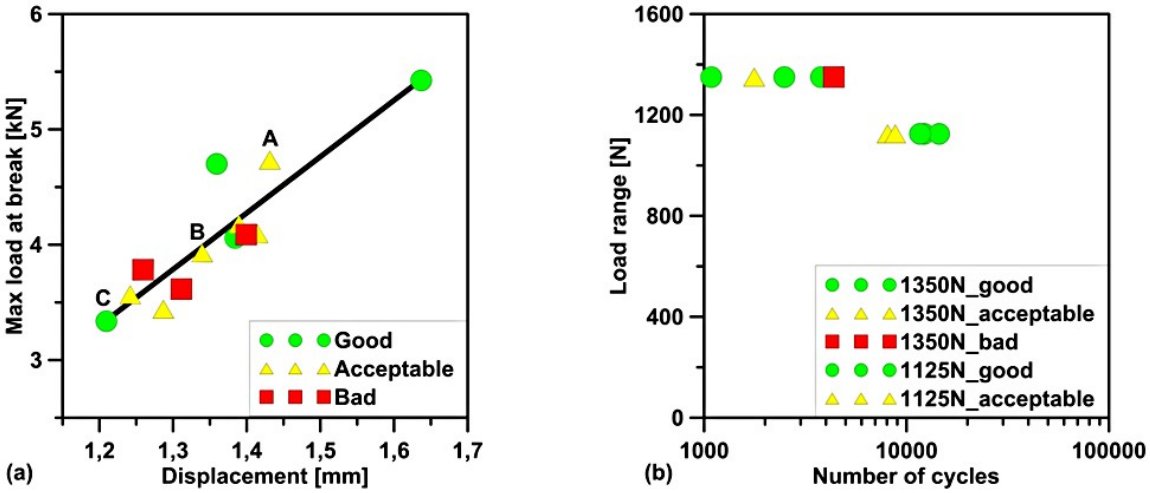

Fig. 32 Mechanical results of (a) static and (b) fatigue tests with reference to the x-ray qualitative classification

Likewise, the disagreement between radiographic and fatigue properties is due to the fact that, even though radiographic is one of the oldest and most widely used methods of non-destructive testing, oxides are more difficult to be observed than porosities which, on the contrary, were adopted as qualitative discriminating element. X-ray analysis uses radiation energy to penetrate the casting and assess variations in thickness or density, generating a 2D shadowgraph of a 3D object; therefore, information in depth and volume can only be obtained observing the object with several orientations, when possible. This is why the X-ray equipment is not the most precise device to reveal the presence of all the defects and their relative orientation and position towards the most stressed casting point.

Campbell stated that a large pore in a low-stressed area of the casting may be far less detrimental than a small bifilm near the sharp corner subjected to a high tensile stress [29], and this is what can be observed in Figs. 33a,b.

Negative contribution to the casting mechanical properties is given also by oxide orientation; depending on whether they are parallel or perpendicular to the fracture surface, they can be more or less detrimental to the casting mechanical behavior. As a matter of fact, oxide films act similarly to cracks in terms of stress concentration and load-bearing area reduction; they easily propagate if critically oriented with respect to the applied load (pure Mode I of crack opening) [93].

In Figs. 33a-c, the critical area is identified with a red square. It can be seen that:

- casting C shows *good* quality characteristics according to the x-ray analysis, but *bad* mechanical properties;
- casting A reaches an *acceptable* quality level, but *good* mechanical resistance. It actually shows a big oxide film located far from the critical area and not parallel to the fracture surface.

- casting B shows both *acceptable* quality characteristics and mechanical response. Moreover, the oxide film detected in casting B, even though detected within the red square, has a less harmful effect on the mechanical properties compared to that observed in casting C because of its orientation less favorable to crack propagation.

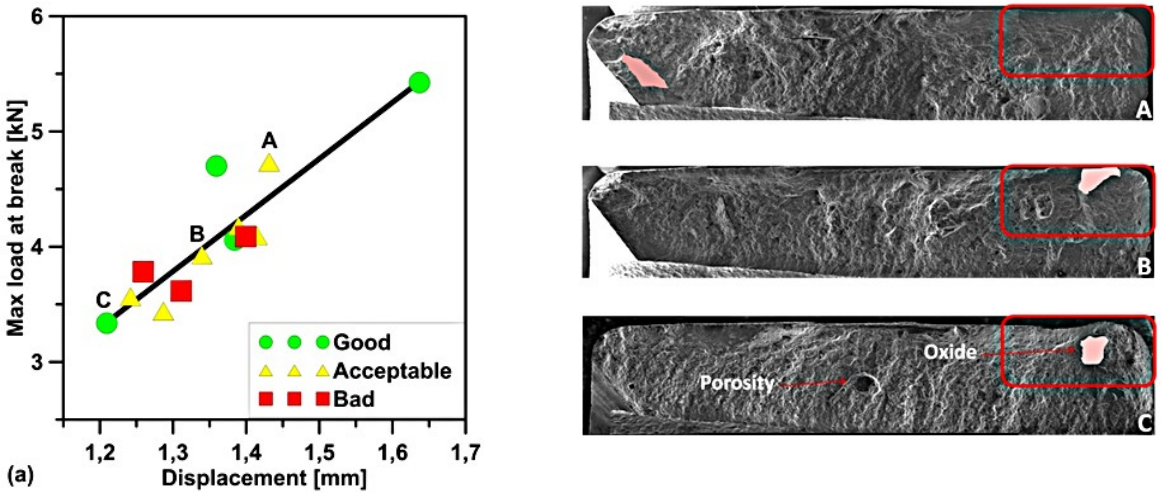

Fig. 33 (a) Misleading casting quality prediction only based on the x-ray investigation; (b) fracture surfaces (oxide films are marked in red).

2.2 Penalization criterion

As shown in Section 2.1.2, the casting's mechanical behavior is strongly influenced by oxide and porosity dimension [52,53], shape, orientation and position towards the critical region; thus a penalization criterion was elaborated in order to take simultaneously into account all these features.

The criterion is based on the developed FE model, used to give each defect a precise weight according to the position, and the fractographic investigation, necessary to detect the flaws that caused the component failure.

In this case, as described in Section 2.1.1 of Chapter 3, the simulated model showed 9 zones or bands, inferred from the FE normal stress distribution, each one characterized by a stress interval (see Fig. 34a).

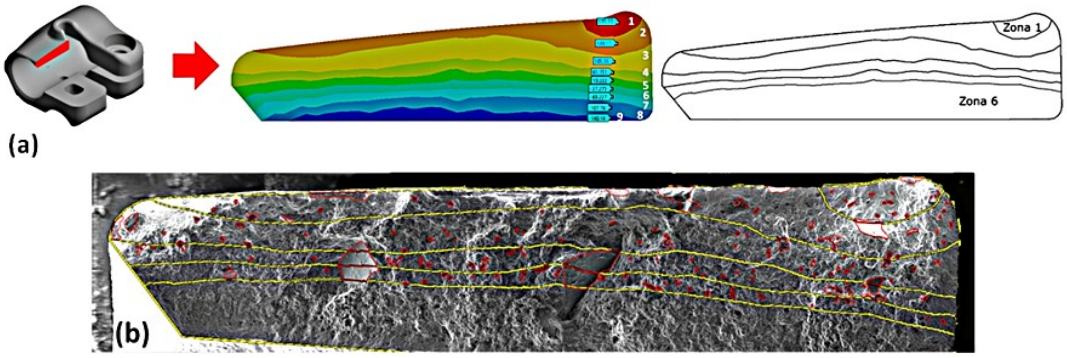

Fig. 34 (a) Normal stress distribution mask, (b) defect detection through mask superimposition

Notably, because of the geometrical stress concentration effect, the bands closer to the critical corner showed the highest stress values, due to the particular in-service behavior of the component. Such values gradually decrease moving towards the compression zone (bands 6 to 9).

The five bands subjected to tensile stress were the only ones taken into account (active bands) since only the defects located within those regions were supposed to degenerate and lead to the component failure, not only during static failure but also during cyclic loading. As already stated by Skallerud et al. [54] and Lados [55], during fatigue life of cast Aluminum alloys the region where the fracture initiates is much more important than the propagation one.

The superimposition of the stress band distribution mask and the actual fracture surface (Fig. 34b) allowed the calculation of a so-called Penalty Index (PI) as defined in Eq. (3).

$$PI = \sum_{z=1}^{N} \left[\frac{A_D}{(A_{SB})_z} * (W)_z \right]. \quad (3)$$

Projected area, orientation and position of all defects were taken into account simultaneously; z refers to the stress band (1 to 5 as already mentioned); N is the number of active bands (N = 5);

A_D is the projected area of each defect detected on the fracture surface by means of an image analysis software; A_{SB} refers to the area of the z^{th} stress band and W is the weight attributed to each stress band and determined according to Eq. (4).

$$W_z = \frac{(\sigma)_z}{(\sigma)_5}. \quad (4)$$

In Eq. (4) the σ is the average normal stress of each *zth* band (1 to 5, active bands). The calculated values are plotted in Table 22.

Table 22 Weight values for the Penalty Index calculation

	Zone 1	**Zone 2**	**Zone 3**	**Zone 4**	**Zone 5**
Average stress value (MPa)	182	142	102	61	20
W	9.1	7.1	5.1	3.05	1

In Tables 23 and 24, the static and fatigue strength results, expressed in terms of Maximum load at break and Cycles to failure, respectively, are listed together with the Penalty Index values.

Table 23 Penalty Index results of A (worst) and B (best) castings according to static testing

Casting	**Peak Load [kN]**	**PI parameters**	**Zone 1**	**Zone 2**	**Zone 3**	**Zone 4**	**Zone 5**	**PI**
A worst	3.44	A_D (mm^2)	0.496	0.555	0.258	0.192	0.049	3.844
		A_{SB} (mm^2)	1.48	8.35	10.64	5.94	4.87	
		W	9.35	7.25	5	3	1	
B best	4.73	A_D (mm^2)	0	0.043	0.294	0.092	0.313	0.286
		A_{SB} (mm^2)	1.48	8.35	10.64	5.94	4.87	
		W	9.35	7.25	5	3	1	

Table 24 Penalty Index results of C (worst) and D (best) castings according to fatigue testing

Casting	**Peak Load [kN]**	**PI parameters**	**Zone 1**	**Zone 2**	**Zone 3**	**Zone 4**	**Zone 5**	**PI**
C worst	1084	A_D (mm^2)	0.050	0.626	0.999	0.721	0.400	1.816
		A_{SB} (mm^2)	1.46	8.21	10.33	5.79	4.61	
		W	9.35	7.25	5	3	1	
D best	4380	A_D (mm^2)	0	0.198	0.297	0.264	0.153	0.489
		A_{SB} (mm^2)	1.46	8.21	10.33	5.79	4.61	
		W	9.35	7.25	5	3	1	

The proposed penalization criterion provides good results; sounder castings (i.e. B and D) show better mechanical properties and lower PI values because of their lower defect content or dangerousness.

Figs. 35a,b summarize the correlations obtained; best and worst castings are pointed out. It is confirmed that both oxides and porosities control the casting mechanical behavior which is well described by the Penalty Index.

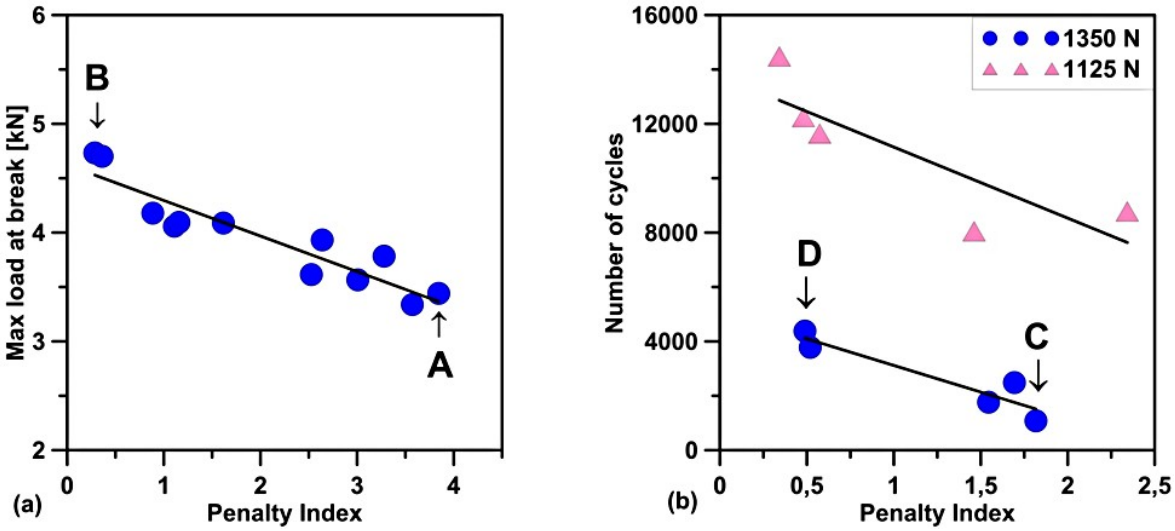

Fig. 35 Correlations between the Penalty Index and (a) static and (b) fatigue mechanical properties

Even if X-ray investigation is widely used in controlling the quality of the castings, it was shown that it is often not sufficient to assess the real quality of the components. As a matter of fact, the x-ray device was not able to detect all kinds of defects (i.e. oxide films) which are very detrimental for the mechanical properties of the castings.

In this regard, the proposed penalization criterion is able to quantify the effect of defects on the mechanical properties of the castings. The main drawback is that is a "post-mortem" approach and it can be implemented only after the component testing. Anyway, it is expected that thanks to the wider diffusion of industrial high-resolution Computed Tomography (CT) techniques, the proposed criterion can be adopted also for predictive analyses.

3 IMPROVING THE MECHANICAL RESPONSE THROUGH HEAT TREATMENT [94]

As highlighted by the analyses conducted on the as-cast components, a stress concentration was found near the region characterized by a severe thickness variation (see Fig. 30a,b), leading to permanent deformation and component failure during its service.

In Fig. 37a,b, the mechanical properties of the tested as-cast components are shown and compared in terms of static and fatigue behavior; in Table 25 the average mechanical results with the corresponding standard deviations are listed.

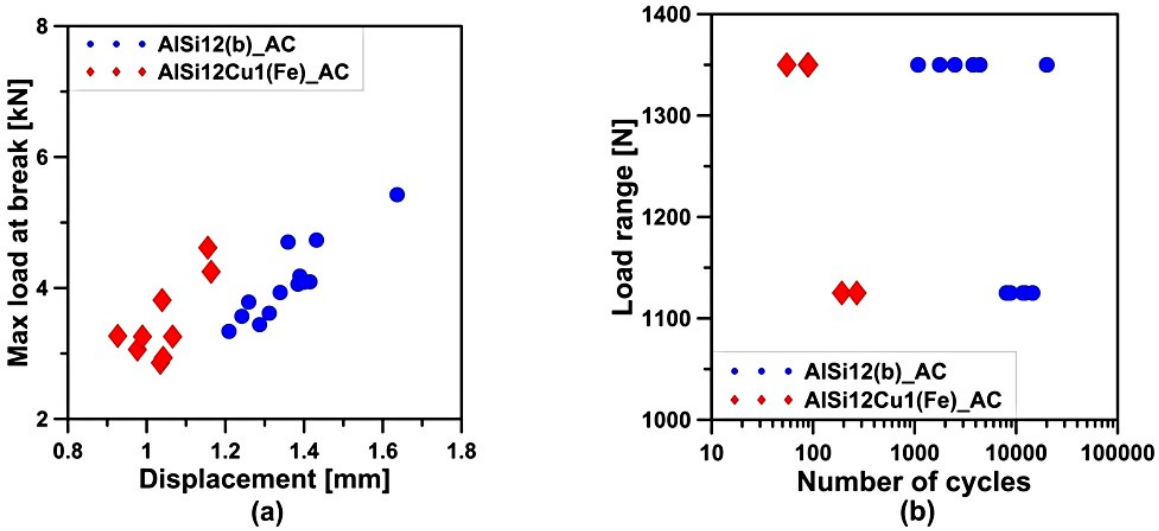

Fig. 37 Mechanical results of (a) static and (b) fatigue test in as-cast conditions.

Table 25 Average mechanical properties of as-cast AlSi12(b) and AlSi12Cu1(Fe) alloy components

Alloy	Max load at break [kN]	Displacement [mm]	Load range [N]	Number of cycles	HB
AlSi12(b)	4.07 ± 0.59	1.36 ± 0.11	1350	5583 ± 3585	76 ± 1
			1125	11041 ± 2629	
AlSi12Cu1(Fe)	3.48 ± 0.61	1.04 ± 0.08	1350	70 ± 20	77 ± 1
			1125	231 ± 54	

As shown, AlSi12(b) displays a better mechanical response than AlSi12Cu1(Fe) alloy. The reason is that it is characterized by a lower Fe content; Fe is the most detrimental impurity of Al-Si alloys since it forms brittle and complex intermetallic compounds [5-7]. In addition, in the AlSi12(b) alloy the amount of Mn, that is the most common alloying element introduced to suppress the development of needle particles by promoting the formation of a thermodynamically stable α-phase, is sufficient to keep the Fe:Mn ratio lower than 2 which is the value recommended to encourage the α-phase precipitation [95]. To be precise, the Fe:Mn ratio

in the AlSi12(b) alloy reaches 1.8, whereas in the AlSi12Cu1(Fe) alloy it achieves 2.36.Hence, the heat treatments described in Section 3.2.3.1 of Chapter 2, were conducted only on AlSi12Cu1(Fe) HPDCs, with the aim of improving their mechanical response without excessively affecting the costs. In Figs. 38a,b the mechanical responses of the AlSi12Cu1(Fe) alloys castings after heat treatment are displayed and compared to the as-cast properties of both AlSi12Cu1(Fe) and AlSi12(b) alloys. In Table 26 the average mechanical results and the corresponding standard deviations are listed.

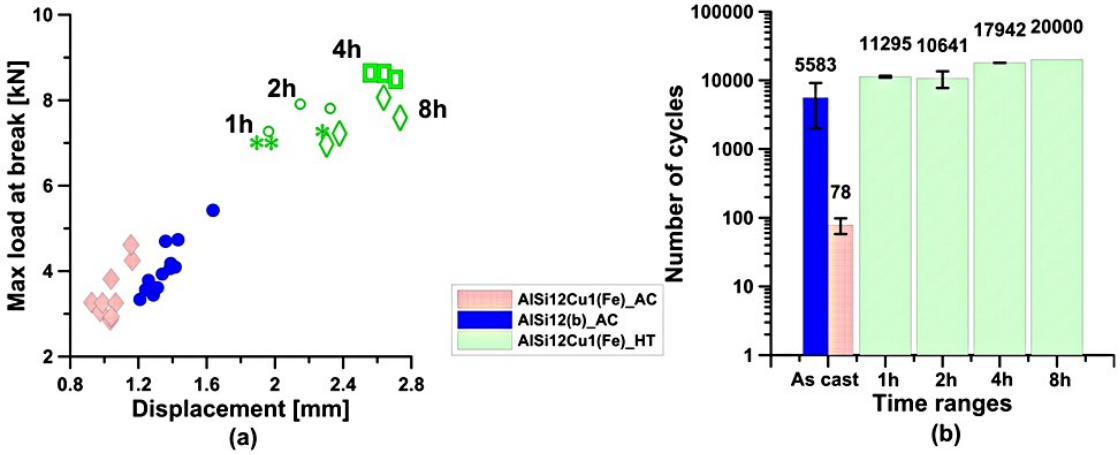

Fig. 38 Mechanical results of (a) static and (b) fatigue test in as cast and heat treated conditions

Table 26 Average mechanical properties of AlSi12Cu1(Fe) alloy components after heat treatment

HT duration	Max load at break [kN]	Displacement [mm]	Load range [N]	Number of cycles	HB
1h	7.09 ± 0.15	2.05 ± 0.20	1350	11295 ± 2636	69 ± 0.6
2h	7.66 ± 0.34	2.14 ± 0.18	1350	10641 ± 374	66 ± 0.6
4h	8.58 ± 0.08	2.64 ± 0.08	1350	17942 ± 2910	64 ± 0.6
8h	7.46 ± 0.48	2.51 ± 0.21	1350	20000 ± 0	60 ± 2.1

After heat treatment, the mechanical properties are significantly improved both in terms of static and cyclic responses.

3.1 Microstructural evolution

The mechanical improvement due to heat treatment can be related primarily to changes in the Si crystal morphology in the eutectic areas [71]. Moreover, the formation of Si precipitates within the α-Al matrix and the interruption of Si continuity within eutectic colonies also affect the mechanical improvement.

The higher static and fatigue mechanical improvement of the heat treated AlSi12Cu1(Fe) alloy compared to the heat-treated AlSi12(b) alloy has many reasons. Solidification conditions, nucleant characteristics and alloy chemistry strongly influence the microstructure of the Al-Si

eutectic grains. The heat treatment does not only affect the mechanical properties in terms of maximum load at break and number of cycles but also the hardness, as can be seen in fig. 39a,b and in Table 26.

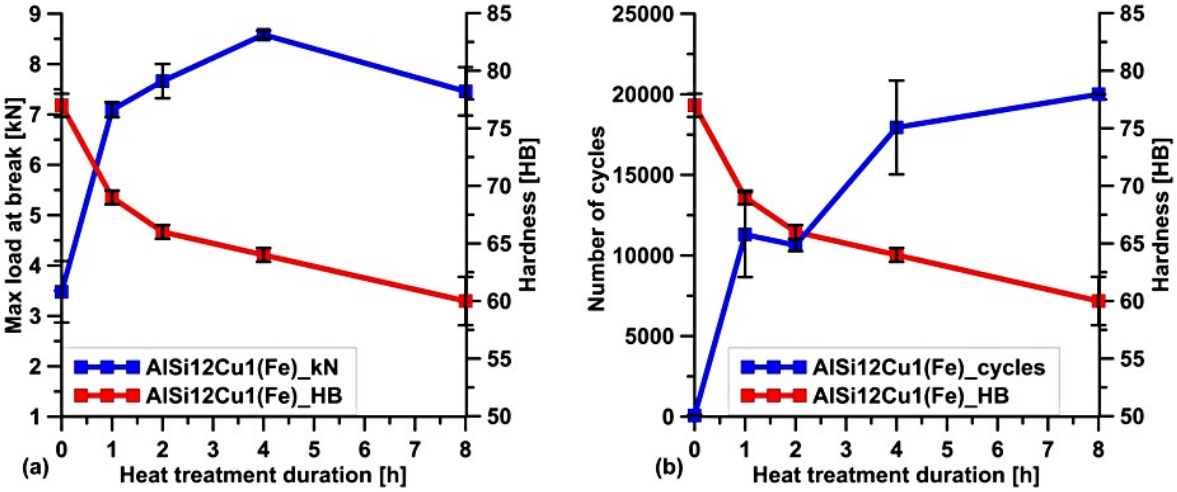

Fig. 39 Hardness and (a) maximum load at break, (b) number of cycles of AlSi12Cu1(Fe) alloy, as function of increased heat treating times.

Since the mechanical improvement is already visible after 1 hour of heat treatment and in order to avoid permanent deformations after heat treatment that may prevent further employment, the shortest heat treatment duration was chosen as the best solution.
As aforementioned, the static and cyclic mechanical properties of the AlSi12(b) alloy heat-treated at 624 K (350°C) for 1 h were measured for comparison with the as-cast conditions; they are shown in Fig. 40a,b.

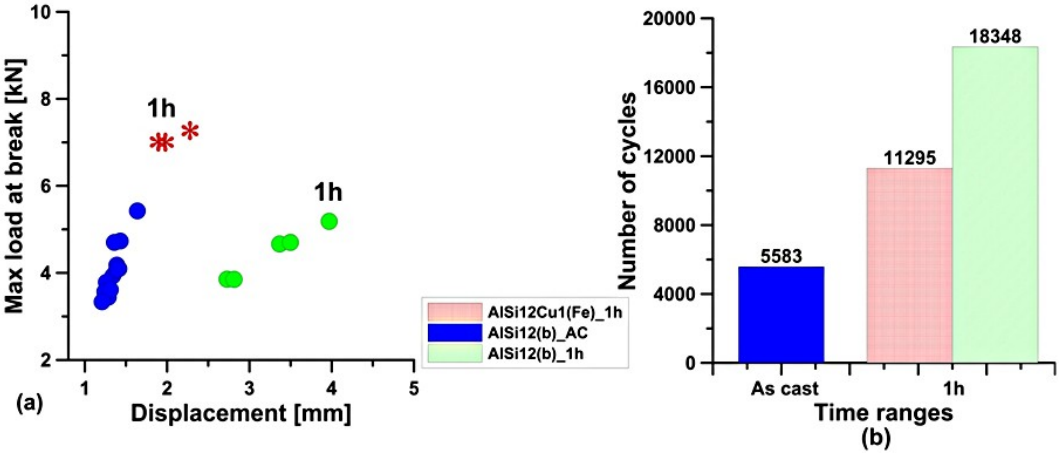

Fig. 40 Mechanical results of (a) static and (b) fatigue tests conducted on AlSi12(b) alloy after 1 hour of heat treatment at 624 K. The AlSi12(b) as-cast results are also displayed.

AlSi12(b) mechanical response is shown in Fig. 40 confirms the effectiveness of the heat treatment. Two concepts are worth mentioning, first of all, as already stated, the cyclic mechanical improvement of the AlSi12Cu1(Fe) alloy, after heat treatment, is noteworthy. Only after 1 hour soaking time at 624 K (350°C), its fatigue mechanical behavior is 145 times better compared to the as-cast condition; on the contrary, the AlSi12(b) alloy shows a fatigue mechanical response three times higher than the starting as-cast condition.
Secondly, AlSi12(b) components show a noticeable enhancement of their ductility rather than an improvement of the maximum load at break; on the contrary, AlSi12Cu1(Fe) HPDCs show a shift of the maximum load at break. These different behaviors of the two alloys can be attributed, on one hand, to a similar modification that eutectic Si crystals undergo, i.e. the Si "network" fragmentizes and coarser crystals smooth their edges during heat treatment and, on the other, to their slightly different chemical compositions. In particular, AlSi12Cu1(Fe) alloy shows higher amounts of strengthening alloying elements, such as Cu and Mg (see Table 9 in Chapter 2), that contribute to a peak load improvement. Moreover, these common ternary alloying elements, i.e. Cu, Mg and Fe, may influence the nucleation and growth dynamics of the eutectic and thus the final microstructure [96].

3.2 Effect of Cu and Fe on eutectic Si morphology

Unlike typical modifying elements as Sr, Na and Sb, little research has been devoted to understanding the effect on the Al-Si microstructure of common alloying elements. These elements, such as Cu, Mg and Fe, may influence the nucleation and growth dynamics of the eutectic and thus the final microstructure, as stated by Darlapudi et al. [97].

Figs. 41a,c show micrographs of the castings obtained melting AlSi12(b) ingot with no additions during the in-lab tests described in Section 3.7 of Chapter 2, and Figs. 41b,d display micrographs of the same alloy processed through High Pressure Die Casting.

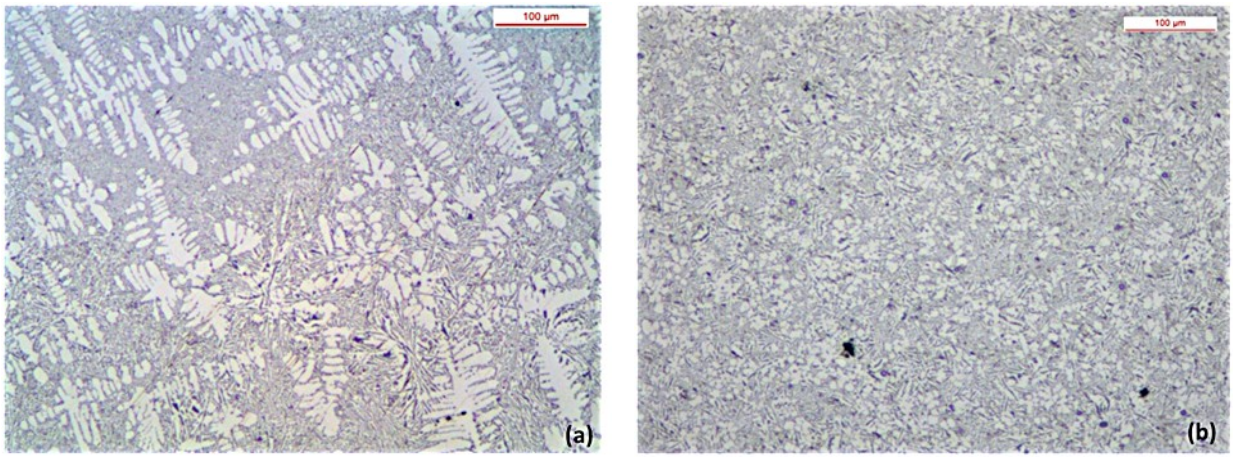

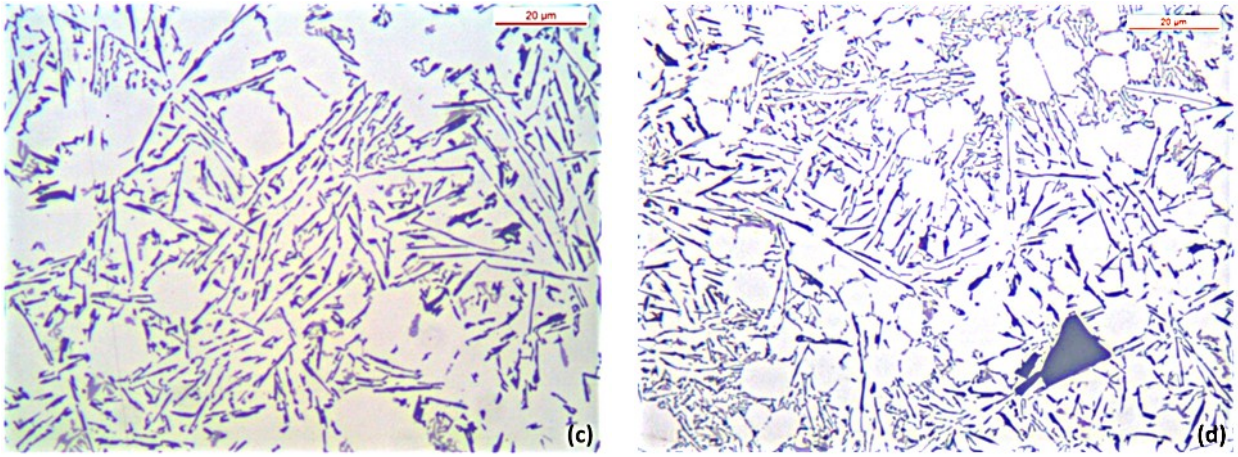

Fig. 41 Microstructure observed from (a), (c) in-lab tests and (b), (d) HPDC process of AlSi12(b) alloy; same thicknesses.

As can be seen from Fig. 41a, unlike HPDCs, in-lab samples show a partially dendritic structure; the main cause is that overpressure could not be applied during lab tests.
However, at higher magnifications, the two micrographs show similar eutectic Si morphologies; lab tests were therefore considered representative of HPDC solidification velocities.

3.2.1 Thermal analysis

After alloying element additions, changes took place in the solidification paths of the three alloys, as shown in Figs. 42. The typical cooling curves and the corresponding first derivatives are displayed.

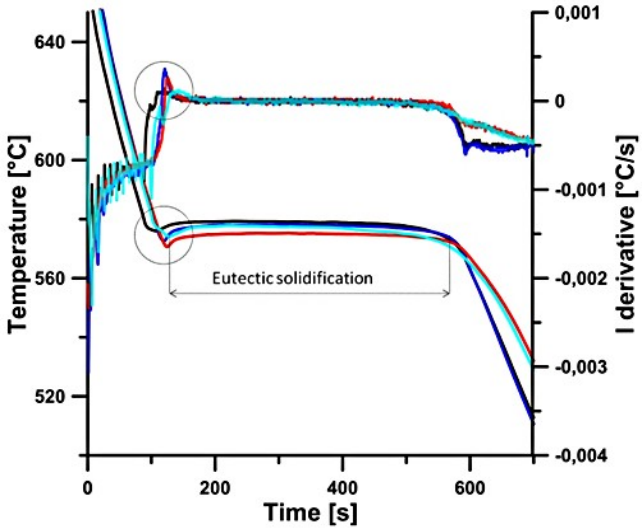

Fig. 42 Thermal analyses - cooling curves and first derivatives

The derivative curves show a main peak associated with the formation of Al-Si eutectic (circled in Fig. 42); after the addition of Cu, in Alloys 1a and 2 changes in the solidification

paths can be observed due to Cu-rich phase formation (Al_2Cu). The characteristic temperatures obtained from the cooling curves and corresponding first derivatives are listed in Table 27. The addition of common alloying elements such as Fe and Cu influenced eutectic temperatures in the three alloys.

Table 27 Characteristic temperatures determined through the first derivatives

Temperature [°C]	**AlSi12(b)**	**Alloy 1**	**Alloy 1a**	**Alloy 2**
Nucleation temperature	593.5	583	587.5	587
Minimum temperature	576	573.3	571.4	574.2
Growth temperature	578.9	577.8	575.2	577.4
Solidus temperature	555.5	544.6	532	531

The effect of these temperature changes is confirmed in the micrographs shown in Figs. 43a-d.

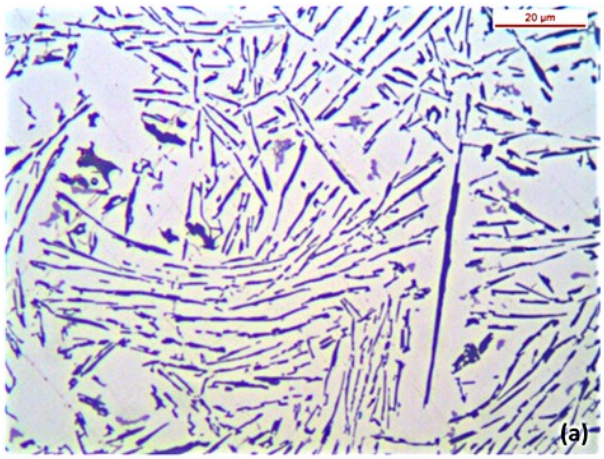

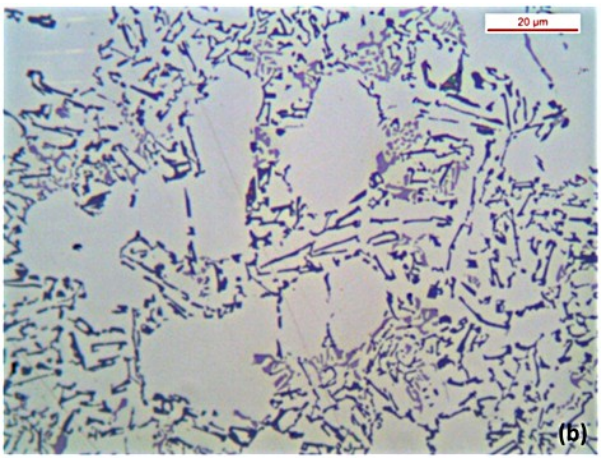

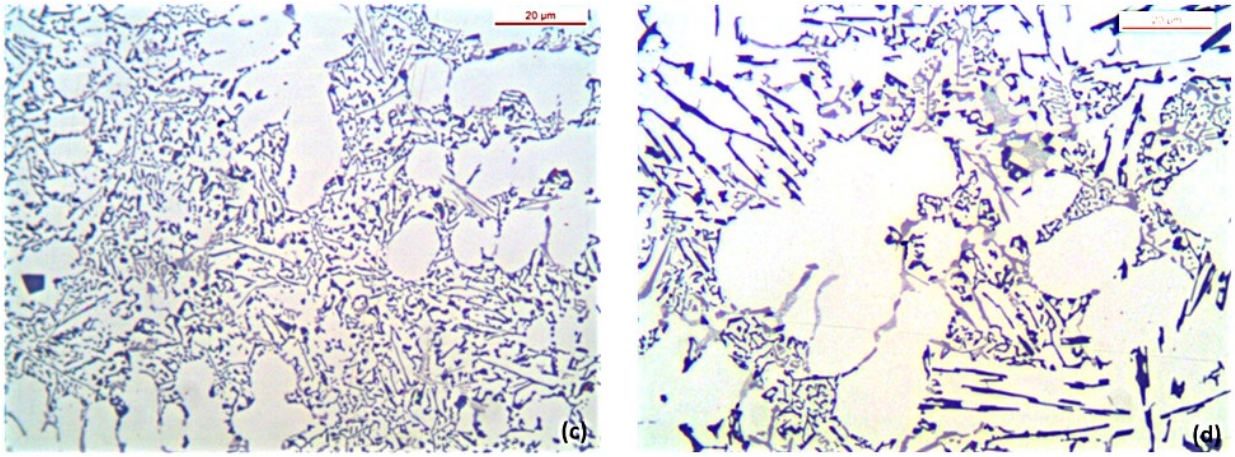

Fig. 43 Micrographs of (a) AlSi12(b) alloy, (b) alloy 1, (c) alloy 1a and (d) alloy 2

From the thermal analyses and the microstructure investigations, it is clear that common alloying elements such as Fe and Cu affect the eutectic Si morphology even if the intensification pressure, typical of HPDC process, is not applied. The author believes that the process has a strong effect on castings' microstructure, but it is not the only variable affecting their microstructure.

There is a good chance that not only Cu and Fe affect the eutectic Si morphology separately, but also their interaction (depending on their ratio) has consequences on the microstructure. Alloy 1a (Fig. 43c) shows the most evident refining effect on the Si morphology; on the other hand, Alloy 2, with a lower Fe content (Fig. 43d), still shows unaffected eutectic Si areas.

Further research is necessary, in particular, HPDC casting trials with different alloying element contents would be beneficial for a more effective research work.

3.3 How heat treatment affects microstructure

3.3.1 Eutectic Si morphology evolution

As shown in Fig. 44, heat treatments tend to break the eutectic Si particles into smaller ones or, for shorter times, tend to smooth and round their edges. As already observed by Pedersen and Arnberg [71], in as-cast conditions, the Si crystals are coarse or thin but interconnected; on the other hand, even a short heat treatment can cause the fragmentation of small Si crystals and the curvature of their edges.

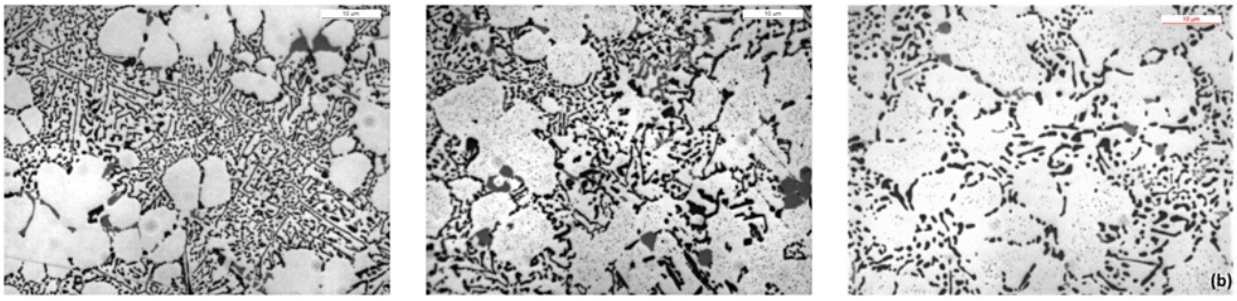

Fig. 44 Evolution of the eutectic Si morphology of AlSi12Cu1(Fe) alloy: (a) as-cast condition, (b) after 1h and (c) after 4 hours at 624 K.

In Fig. 45a,b the as-cast Si structure, after deep-etching, is shown. It can be observed that the areas of the structure that appear like a sort of eutectic Si "network" are indeed more or less connected to each other. This interconnection is confirmed by Figs. 46a,b in which a SEM micrograph and the corresponding EBSD grain-orientation maps, are shown.

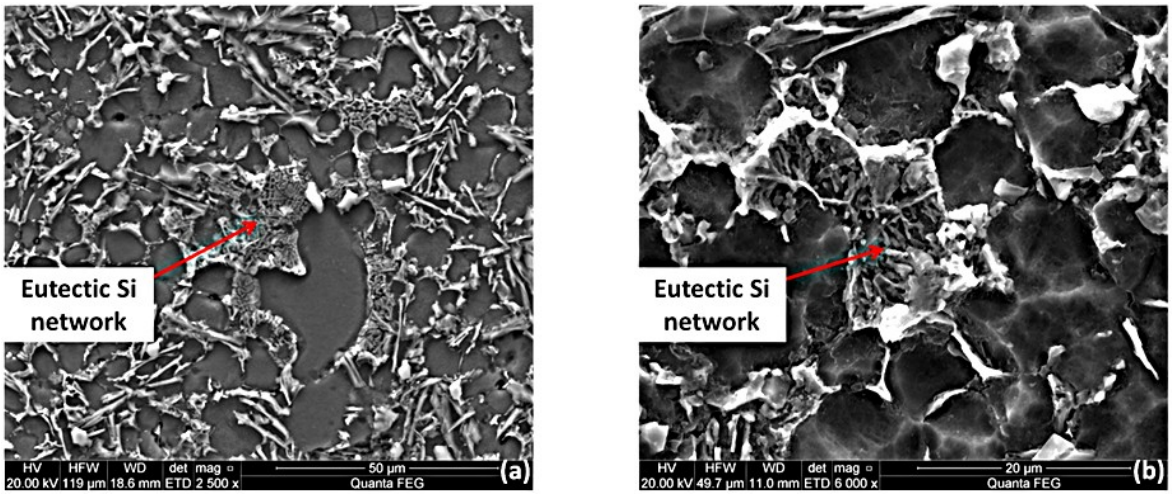

Fig. 45 Si crystals in the eutectic region of AlSi12Cu1(Fe) alloy. Images obtained with secondary electrons: (a) 2500x, (b) 6000x. The material has been deep etched.

From the Inverse Pole Figure (IPF) in Fig. 46b, it appears that the Si particles of the eutectic "network" areas of AlSi12Cu1(Fe) alloy form colonies that show preferential crystal orientations that are therefore reasonable to be considered connected.

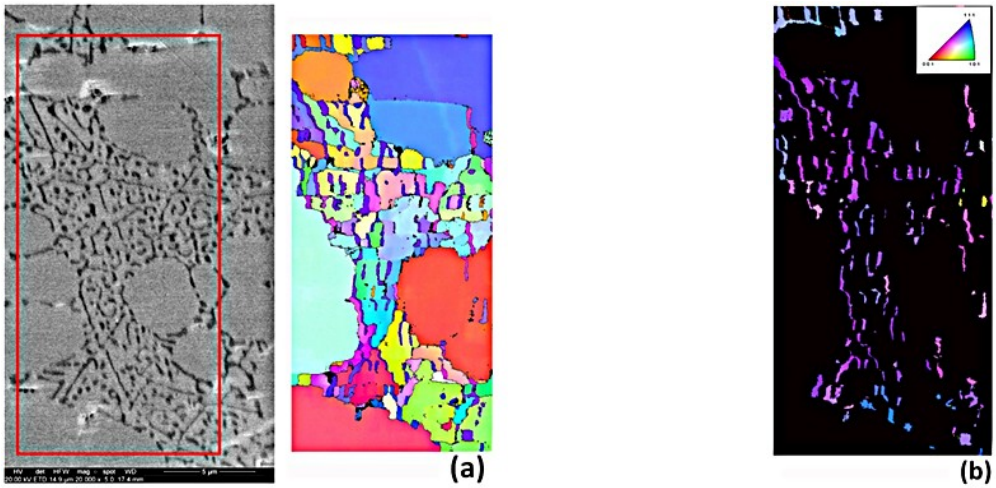

Fig. 46 (a) SEM micrograph of the eutectic Si "network" and corresponding IPF map; (b) IPF map of the Si phase.

As already observed by Manente and Timelli [98], increasing the heat treating time the interparticle distance increases; since Rayleigh instability occurs, Si crystals undergo necking and are broken down into fragments. The instability generated and the reduction in the total interface energy lead to eutectic Si spheroidization and coarsening. As stated by Greenwood [99], coarsening and spheroidization, evaluated through roundness assessment, are diffusion-controlled processes so they are directly proportional to heat treating time (temperature is kept constant in this study).

The ductility of the components strongly depends on Si crystals' size and morphology. The as-cast structure, characterized by coarse Si plates or an interconnected "network" leads to a rapid reduction of the load-bearing area during the component use and the crack can propagate rapidly through the structure. On the contrary, as confirmed in the literature by Pedersen and Arnberg [71], when the size of the Si crystals is reduced and the fragmentation has taken place, the casting failure is less instantaneous as the crack has to propagate through the ductile Aluminum matrix.

In order to confirm the effect of heat treatment duration on Si smoothing and fragmentation, the roundness (ρ) of eutectic Si crystals was calculated as follows:

$$\rho = \frac{p^2}{4\pi A} \tag{5}$$

where P is the perimeter and A is the area of each particle. According to Eq. (5), the minimum value of ρ is 1 corresponding to a circle shape. The mean roundness values for the experimental AlSi12Cu1(Fe) alloy, reported in Table 28, point out a morphological variation after heat treatment which can be correlated to the hardness decrease as shown in Fig. 47. Indeed, the rounder the Si crystals, the lower their stress intensification effect, the higher the component ductility and thus its in-service duration.

Table 28 Mean roundness values of eutectic Si particles for AlSi12Cu1(Fe) alloy in as-cast condition and after 1 and 4 hours of heat treatment

Time range [h]	ρ	Standard deviation
As cast	8.7	0.6
1	7.2	0.4
4	4.3	0.5
8	3.4	0.1

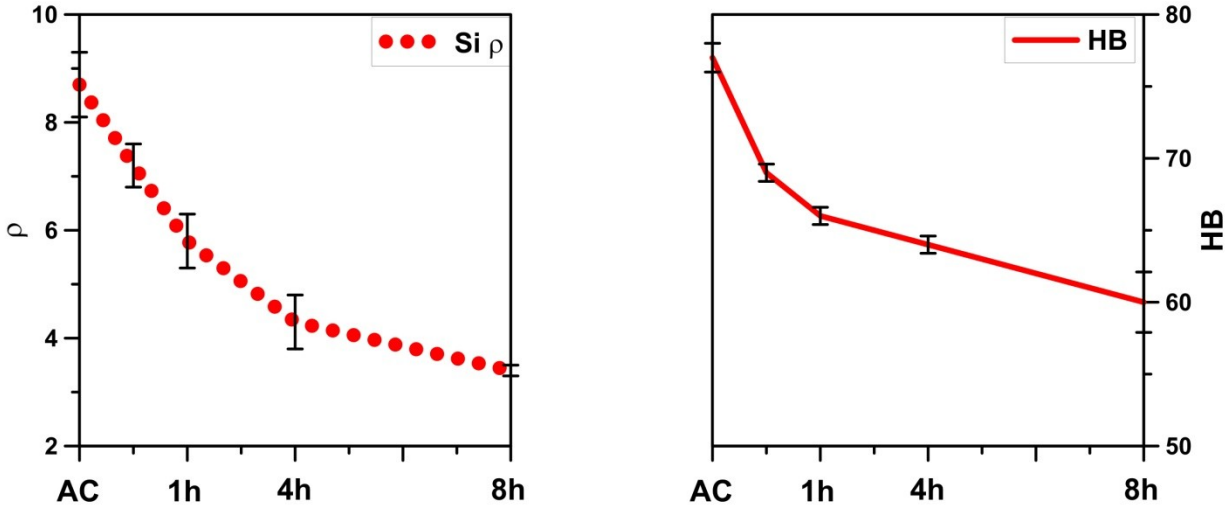

Fig. 47 (a) Si particle roundness and (b) hardness trends for AlSi12Cu1(Fe) alloy

3.3.2 Si precipitates within α-Al matrix

The precipitation of a Si phase within the α-Al matrix after heat treatment was also observed. This phenomenon seems to be less widely investigated in the literature.
Several researchers studied the precipitation behavior of Mg-containing precipitates from solid solution mainly in 3xxx and 6xxx wrought alloys during heating and homogenization processes [71,100-104]. Li and Arnberg, [101] focused on a DC-cast AA3003 alloy and highlighted the formation of very fine precipitates with sizes of several nanometers, only after heating the alloy at 573 K (300°C). They also noticed a size evolution of the precipitates controlled by nucleation, growth, coarsening and dissolution. Chen et al. [103] investigated the mechanism of precipitation of a Si-containing phase and its hardening effect for an AlSi7Mg alloy. They concluded that the supersaturated Si concentration in the matrix leads to the precipitation of Si particles after the completion of solidification; it was also observed that increasing the heat treating time, they become fewer and coarser.

The evolution of size and number per area of these precipitates after 1 and 8 hours of stabilization heat treatment is shown in Figs. 48a,b, respectively. Because of diffusion

phenomena, a size growth takes place together with a reduction of the precipitate density; this causes the loss of strengthening elements from the as-cast solid solution with the α-Al.

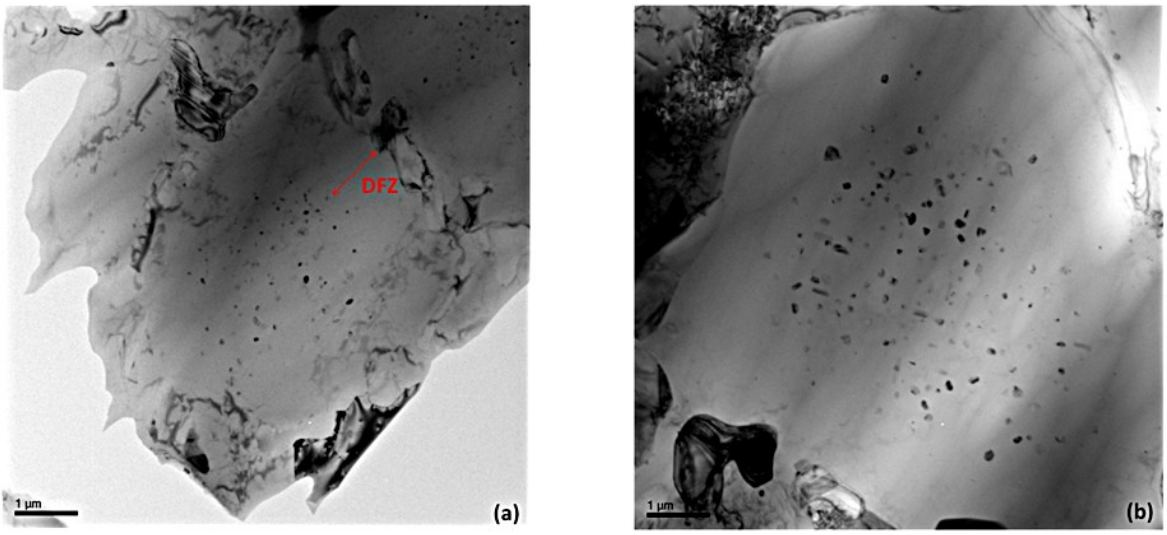

Fig. 48 Al grain with evident Si precipitates after (a) 1 h and (b) 8 h of heat treatment

As shown in Fig. 49a and 49b, most of the precipitates formed in the vicinity of dislocations probably because (i) heterogeneous nucleation at dislocations can reduce the nucleation energy barrier of precipitates [103,104] (ii) solid state diffusion (in this case of Si atoms) is made easier by the presence of dislocations. Dislocations, as well as vacancies, grain boundaries, stacking faults, inclusions and free surfaces are suitable nucleation sites since they increase the free energy of the material and contribute to reducing the total strain energy of the embryo. Nucleation on dislocations may also be promoted by solute segregation which can rise the composition of the matrix to nearer that of the precipitate [96,104].

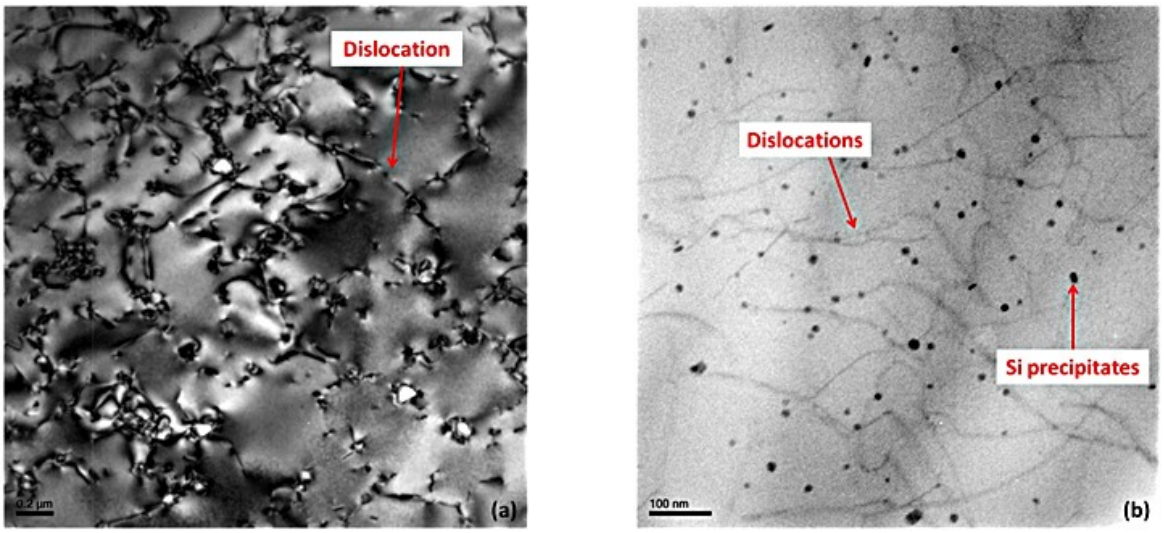

Fig. 49 Si precipitates in the vicinity of dislocations after (a) 1 h and (b) 8 h of heat treatment.

However, an in-depth analysis is necessary to understand their influence on the mechanical response of the analyzed diecastings and how their evolution with heat treating time can affect the casting properties.

CONCLUDING REMARKS

This chapter summarizes the main conclusions which were drawn from the study

HPDC is a versatile and highly productive process, it allows the production of complex engineering metal parts. Casting quality depends on many parameters had to check; there are many sequential actions in the three phases of the process that may affect the casting quality, its integrity and its mechanical response.

Even though high pressure die casting process has drawn, and it is still drawing, a lot of research attention, no standard is given to choose the best solution according to processes, methods, alloys and design.

The significance of this work stands in the attempt to improve HPDC reliability, correlating the data acquired during the process with defect content, microstructure features and mechanical properties.

Process - casting quality

The presence of defects leads to a reduction of the casting quality and increases the scatter of the mechanical results. HPDCs cannot be considered monolithic materials, they always show intrinsic defects that compromise the component mechanical properties and make them difficult to be heat treated.

The Reference casting, specifically designed and manufactured within the EU MUSIC project, allows an accurate study of the effects of process parameters on the quality of the castings since it causes different defect levels through controlled variations of the process parameters. The production of the *horse-shoe* reference castings, varying the process parameters according to a DOE methodology, helps in searching for correlations between process and quality of the casting. Precisely, second phase plunger velocity, temperature and pressure inside the die cavity show significant influence on surface and internal quality of the castings. The best results in terms of internal and surface quality are obtained when high second phase plunger velocity is applied and relatively high temperature and pressure are detected by the sensor network installed on the machine.

The effectiveness of the correlations obtained analyzing the reference casting can be extended to a real industrial demonstrator: the gear box housing. In both cases the defect content negatively influences the casting mechanical behavior and filling and intensification pressure are the most influential phases in HPDC.

Defects - mechanical properties

The presence of defects leads to reduced properties and a lack of repeatability of casting quality.

The penalization criterion elaborated to evaluate the defect influence on the mechanical properties of the castings gives satisfactory predictions of both static strength and fatigue life of castings containing defects. Indeed, the casting mechanical behavior cannot be predicted only on the basis of the porosity content detected through the radiographic device. Oxides are difficult to be observed since they are characterized by tiny dimensions and a material density close to that of the Aluminum.

Defects have a detrimental effect both on static and fatigue life and it can be directly correlated to their projected area and their relative position towards the zone subjected to a high tensile stress.

Microstructure - mechanical behavior

Increased solidification velocities like those obtained through HPDC, refine all the microstructural constituents. However, small additions of ternary alloying elements, i.e. Cu, Fe and Mn, result in a modification on the morphology of eutectic Si particles. A change in the Al-Si eutectic morphology is associated with an increase of these elements, however, a deeper study is fundamental to understand how their ratio can influence the microstructure since exceeding certain reciprocal amounts seems irrelevant to this refining effect.

This changed Si morphology plays an important role in the fracture and its propagation velocity.

Heat treatment setup

High pressure die cast components can be successfully heat treated without causing blistering or distortion, by stabilization heat treatment for short times and at lower temperatures.

The HPDCs, when heat treated at 624 K (350 °C) for 1 to 8 hours, show a change of the eutectic Si morphology with consequent change of the mechanical response. The improved ductility is determined by the change of both size and shape of Si crystals; it fragments and smoothes its edges.

The author's proposal of 1 h heat treatment can be considered satisfactory to obtain good mechanical results, avoid undesirable drawbacks and limit extra costs.

FUTURE DEVELOPMENTS

The findings presented in this doctoral thesis are the result of a three-year research work carried out thanks to the achievements within the EU MUSIC project and the cooperation with Italian foundries and companies operating in the Aluminum diecasting field.

Based upon the presented results the following suggestions for future work are proposed.

Penalization criterion improvement

An improvement of the proposed penalization criterion is possible thanks to the support of Computer Tomography. The wider diffusion of Computed Tomography allows a better porosity assessment and the possibility to evaluate pores 3D development.

This can lead, on one hand, to a better defect morphology evaluation so that to be included in the Penalty Index calculation, on the other, to continuous improvements in the detecting accuracy and the perspective of a non-destructive detection of defects such as oxides or cold joints. In Fig. 50 a CT scan of the sleeve casting is shown.

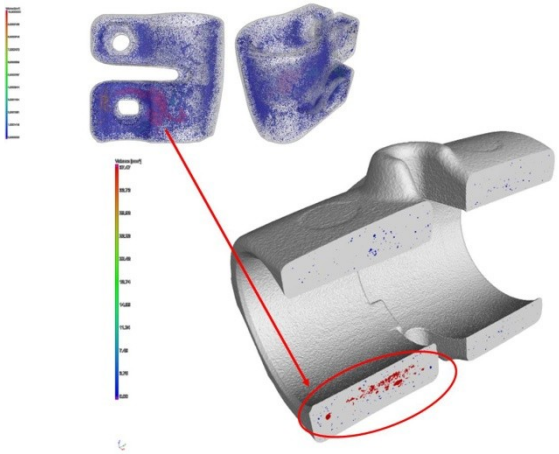

Fig. 50 CT scan of sleeve casting

Alloying elements ranges

The thesis demonstrated the importance and the consequences of the addition of common alloying elements such as Cu and Fe; however, a number of point at issue are still present. A deeper study of the effect of these elements and their ratio is necessary as well as the need for a more effective definition of the alloying element ranges.

In AlSi alloys, not only common alloying elements are fundamental and may influence the nucleation and growth dynamics of the eutectic but also impurities (very common in secondary Aluminum alloys) may or may not influence the quality of the alloy, depending on their amounts.

Heat treatment setup

Finally, thanks to the described work on the heat treatment of HPDCs, the author believes that it is fundamental for the future, a customization of the heat treatments depending on the alloying elements and the final use of the components.

The heat treatment of diecastings is possible, but a precise definition of the parameters is also crucial.

REFERENCES

[1] PRESS DPT. GIFA 2015: *Proc. 13th Int. Foundry Trade Fair,* Dusseldorf (2015), Germany, Art. n. 1.
[2] NADCA: *2016 State of die casting industry*, Arlington Heights (2017), IL, USA.
[3] Otarawanna S., Dahle A.K.: *Casting of Aluminum alloys*, chapter 6, Fundamentals of aluminium metallurgy, Woodhead Publishing, 2011, pp. 141-154.
[4] AFS: *Aluminum alloys*, Engineered casting solutions, 2006, pp. 30-34.
[5] Ferraro S., Fabrizi A., Timelli G.: *Evolution of sludge particles in secondary die-cast Aluminum alloys as function of Fe, Mn and Cr contents*, Mater. Chem. Phys., 153 (2015), pp. 168-179.
[6] Zhu H., Zhang X., Couper M.J., Dahle A.K.: *Effect of primary intermetallic particles on surface microstructure and appearance of Aluminum extrusions*, Mater. Chem. Phys., 113 (2009), pp. 401-406.
[7] Yang C.-Y., Lee S.–L., Lee C.-K., Lin J.-C.: *Effects of Be and Fe on the mechanical and corrosion behaviors of A357 alloys*, Mater. Chem. Phys., 93 (2005), pp. 412-419.
[8] Ji S., Yang W., Gao F., Watson D., Fan Z.: *Effect of iron in Al-Mg-Si-Mn ductile diecast alloys*, Light Metals, (2013), pp. 317-321.
[9] Domkin K., Hattel J.H., Thorborg J.: *Modelling of high temperature- and diffusion-controlled die soldering in Aluminum high pressure die casting*, J. Mater. Proc. Tech., 209 (2009), pp. 4051-4061.
[10] Shankar S., Apelian D.: *Die soldering: mechanism of the interface reaction between molten Aluminum alloy and tool steel*, 33 (2002), pp. 465-476.
[11] Conserva M.: *Stacast project, an update*, P&TF, Edimet, 2013.
[12] Mathers G.: *The welding of Aluminum and its alloys*, Woodhead Publishing (2002), pp. 236.
[13] Adamane A.R., Arnberg L., Fiorese E., Timelli G., Bonollo F.: *Influence of injection parameters on the porosity and tensile properties of high-pressure die cast AlSi alloys: a review*, Int. J. Metalcasting, 9 (2015), pp. 43-53
[14] Sahoo M., Smith R.: *Mechanical properties of unidirectionally solidifed AlSi autectic alloys*, Metal Science, 9 (1975), pp. 217-222.
[15] Dorum C., Laukli H.I., Hopperstad O.S., Langseth M.: *Structural behavior of AlSi Die-castings: experiments and numerical simulations*, European J. of Mechanics - A/Solids, 28 (2009), pp. 1-13.
[16] OEA: *Aluminum recycling in Europe: the road to high quality products*, (2006).
[17] Das S.K., Green J.A.S., Kaufman J.G.: *The development of recycle-friendly automotive Aluminum alloys*, JOM, (2007), pp. 47-51.
[18] Das S.K., Green J.A.S., Kaufmaan J.G.: *Aluminum industry and climate change – assessment and responses*, JOM, 62(2), (2010), pp. 27-31.
[19] Rombach G.: *Integrated assessment of primary and secondary Aluminum production*, Material for the future: Aluminum production and process, DMG Business Media Limited, Surrey UK, 1998.
[20] Centro di ricerca di economia industriale e finanza "Guido Carli": *The impact of EU policies on the competitiveness of the EU Aluminum industry: a focus on non-integrated downstream users*, Rome IT, 2015.

[21] International Aluminum Institute, 2017.
[22] Information on: *http://www.custompartner.com/wu/die-casting*
[23] Butler W.A., Timelli G., Battaglia E., Bonollo F.: *Die Casting (Permanent Mold)*, Materials Science and Materials Engineering, Elsevier (2016), pp. 1-10.
[24] Casarotto F., Franke J., Franke R.: *6 – High pressure die cast (HPDC) Aluminum alloys for automotive applications*, Woodhead Publishing, Rheinfelden Alloys Gmbh & Co. KG, Germany 2012.
[25] Bacaicoa I., Wicke M., Luetie M., Zeismann F., Brueckner-Foit A., Geisert A., Fehlbier M.: *Characterization of casting defects in a Fe-rich Al-Si-Cu alloy by microtomography and finite element analysis*, Engineering Fracture Mechanics (2017).
[26] Yi J.Z., Gao Y.X., Lee P.D., Lindley T.C.: *Effect of Fe content on fatigue crack initiation and propagation in a cast Aluminum-Silicon alloy (A356-T6)*, Mater. Sci.Eng., 286 (2004), pp. 397-407.
[27] Lumley R.: *Fundamentals of Aluminum metallurgy*, Woodhead Publishing in Materials, 2011, pp. 843.
[28] Information on http://www.ducker.com/news-insights/ducker-worldwide-study-aluminum-content-cars-public-summary
[29] Campbell J.: *Castings*, 2nd ed., Butterworth-Heinemann, Bodmin, 2003, pp. 352.
[30] Bonollo F., Gramegna N., Timelli G.: *High Pressure Die Casting: Contradictions and Challenges*, JOM, 67 (2015), pp. 901-908.
[31] Rai J.K., Lajimi A.M., Xirouchakis P.: *An intelligent system for predicting HPDC process variable in interactive environment*, J. Mater. Proc. Tech., 203 (2008), pp. 72-79.
[32] Kong L.X., She F.H., Gao W.M., Nahavandi S., Hodgson P.D.: *Integrated optimization system for high pressure die casting processes*, 201 (2008), pp. 629-634.
[33] Fiorese E., Bonollo F., Timelli G., Arnberg L., Gariboldi E.: *New classification of defects and imperfections for Aluminum alloy castings*, Int. J. Met. Cast., 9 (2015), pp. 55-66.
[34] EN12258-1:2012 *European standard for products made from Aluminum and Aluminum alloys*, 2012.
[35] Information on: *http://www.stacast-project.org*
[36] Gariboldi E., Bonollo F., Parona P.: *Handbook of Defects in High Pressure Die Casting*, 2nd ed., AIM, Milano, 2010.
[37] CEN/TR 16749:2014 *Aluminum and Aluminum alloys – classification of defects and imperfections in high pressure, low pressure and gravity die cast products*, 2014, pp. 1-41.
[38] Herman E.A.: *Diecasting dies: designing*, NADCA Publ. No ECDS 506, 1985.
[39] Dour G., Dargusch M.S., Davidson C.J., Nef A.: *Development of a non-intrusive heat transfer coefficient gauge and its application to high pressure die casting. Effect of the process parameters*, J. Mater. Proc. Tech, 169 (2005), pp. 223-233.
[40] Cocks D.L., *A proposed simple qualitative classification for die-casting defects*, Proc. Die-Casting Conference, Montreaux, pp. 19/1-19/15, 1996.
[41] Campbell J., Hadring R.A.: *Casting technology*, TALAT 2.0 CD-ROM, EAA, Brussels, 2000.
[42] Walkington W.G.: *Die Casting Defects – Causes and Solutions*, NADCA, 1997.
[43] Paolin S.: Master Thesis, DTG - University of Padova, Vicenza, 2017.
[44] Pajryd L., Beno T., Carmignato S.: *Computed tomography as a tool for examining surface integrity in drilled holes in CFRP composites*, Proc. CIRP, 13 (2014), pp. 43-48.

[45] Battaglia E., Bonollo F., Tonello I., Fiorese E.: *Correlations between defect content, mechanical properties and fractographic investigation of AlSi9Cu3(Fe) alloy reference castings*, Materials Science Forum, 879 (2017), pp. 193-198.
[46] Sanna F., Fabrizi A., Ferraro S., Timelli G., Ferro P., Bonollo F.: *Metall Ital.*, 105 (2013), pp. 13-24.
[47] Wang Q.G., Apelian D., Lados D.: *Fatigue behavior of A365-T6 Aluminum cast alloys. Part I. Effect of casting defects*, J. Light Metals, 1 (2001), pp. 73-84.
[48] Lados D.A., Apelian.: *Relationships between microstructure and fatigue crack propagation paths in Al-Si-Mg cast alloys*, Eng. Fracture Mech., 75 (2008), pp. 821-832.
[49] Avalle M., Belingardi G., Cavatorta M.P., Doglione R.: *Casting defects and fatigue strength of a die cast Aluminum alloy: a comparison between standard specimens and production components*, Int. J. Fatigue, 24 (2002), pp. 1-9.
[50] Gokhale A.M., Patel G.R.: *Origins of variability in the fracture-related mechanical properties of a tilt-pour-permanent-mold cast Al-alloy*, Scripta Mater., 52 (2005), pp. 237-241.
[51] Timelli G., Bonollo F.: *Quality mapping of Aluminum alloy diecastings*, Metal. Sci. Tech., 26 (2008), pp. 2-8.
[52] Timelli G.: *Constitutive and stochastic models to predict the effect of casting defects on the mechanical properties of high pressure die cast AlSi9Cu3(Fe) alloys*, Metal. Sci Tech, 28 (2010), pp. 9-17.
[53] Caceres C.H., Selling B.I.: *Casting defects and the tensile proeprties of an Al-Si-Mg alloy*, Mat.. Sci Eng. A, 220 (1996), pp. 109-116.
[54] Skallerud B., Iveland T., Harkegard.: *Fatigue life assessment of Aluminum alloys with casting defects*, Eng. Frac. Mech., 44 (1993), pp. 857-874.
[55] Lados D.: PhD Thesis, WPI, Worcester USA, 2004.
[56] Tiryakioglu M., Campbell J.: *Weibull analysis of mechanical data for castings: a guide to the interpretation of probability plots*, Met. Mat. Trans. A, 41 (2010), pp. 3121-3129.
[57] Tiryakiouglu M.: *Weibull analysis of mechanical data for castings II: Weibull mixtures and their interpretation*, Met. Mat. Trans. A, 46 (2015), pp. 270-280.
[58] Caceres C.H.: *On the effect of macroporosity on the tensile properties of the Al-7%Si-0.4%Mg casting alloy*, Scripta Met. Mater, 32 (1995), pp. 1851-1856.
[59] Surappa M.K., Blank E., Jaquet J.C.: *Effect of macro-porosity on the strength and ductility of cast Al-7Si-0.3Mg alloy*, Scripta Metal., 20 (1986), pp. 1281-1286.
[60] Caceres C.H., Selling B.I.: *Casting defects and the tensile properties of an Al-Si-Mg alloy*, Mat. Sci. Eng. A, 220 (1996), pp. 109-116.
[61] Lee C.D.: *Effects of microporosity on tensile properties of A356 Aluminum alloy*, Mat. Sci. Eng. A, 464 (2007), pp. 249-254.
[62] Gokhale A.M., Patel G.R.: Aluminum *2002,* KD Subodh, H.S. Michael ed., Proc. TMS 2002 Automotive alloys and Aluminum sheet symposium, Warrandale, pp. 65-73, 2002.
[63] Griffith A.A.: *The phenomena of rupture and flow in solids*, Phil. Trans. Royal Soc. London, Series A, 221 (1921), pp. 163-198.
[64] Pierce F.T.: *Tensile tests for cotton yarns vs "the weakest link"*, J. Textile Inst., 17 (1926), pp. T355-T368.
[65] Weibull W.: *A statistical distribution function of wide applicability*, J. Appl. Mech., 18 (1951), pp. 293-297.
[66] Dai X., Yang X., Campbell J., Wood J.: *Influence of oxide film defects generated in filling on mechanical strength of Aluminum alloy castings*, Mater. Sci. Tech, 20 (2004), pp. 505-513.

[67] Yamagata H., Kasprzak W., Aniolek M., Kurita H., Sokolowski J.H.: *The effect of average cooling rates on the microstructure of the Al-20%Si high pressure die casting alloy used for monolithic cylinder blocks*, J. Mat. Proc. Tech., 203 (2008), pp. 333-341.
[68] Cho J.I., Kim C.W.: *The relationship between dendrite arm spacing and cooling rate of Al-Si casting alloys in high pressure die casting*, Int. J. Metalcasting, 8 (2014), pp. 49-55.
[69] Makhlouf M.M., Guthy H.V.: *The Aluminum-silicon eutectic reaction: mechanisms and crystallography*, J Light Met., 1 (2001), pp. 199-218.
[70] Shankar S., Riddle Y.W., Makhlouf M.M.: *Nucleation mechanism of the eutectic phases in Aluminum-silicon hypoeutectic alloys*, Acta Materialia, 52 (2004), pp. 4447-4460.
[71] Pedersen L., Arnberg L.: *The effect of solution heat treatment and quenching rates on mechanical properties and microstructures in AlSiMg foundry alloys*, Met. Mat. Trans. A, 32 (2001), pp. 525-532.
[72] Wang Q., Yang W.: *Methods of enhancing mechanical properties of Aluminum alloy high pressure die castings*, US8,636,855 B2, 2014.
[73] Lumley R.N., O'Donnell R.G., Gunasegaram D.R., Givord M.: International patent application PCT/2005/001909.
[74] Lumley R.N., O'Donnell R.G., Gunasegaram D.R., Givord M.: *Heat treatment of high pressure die castings*, Met. Mat. Trans. A, 38 (2007), pp. 2564-2574.
[75] Lumley R.N., Polmear I.J., Groot H., Ferrier J.: *Thermal characteristics of heat-treated Aluminum high pressure die castings*, Scripta Materialia, 58 (2008), pp. 1006-1009.
[76] Lumley R.N., Gunasegaram D.R., Gershenzon M., O'Donnell R.G.: *Effect of alloying elements on heat treatment response of Aluminum high pressure die castings*, Int. Heat Treat. and Surf. Eng., 4 (2010), pp. 25-32.
[77] Ibrahim M.F., Elgallad E.M., Valtierra S., Doty H.W. and Samuel F.H.: *Metallurgical parameters controlling the eutectic silicon characteristics in Be-treated Al-Si-Mg alloys*, Materials, 2016, Vol. 9, pp. 1-17.
[78] UNI EN1706: *Aluminum and Aluminum alloys – Casting – Chemical composition and mechanical properties*, European Committee for Standardization, Brussels, 2010.
[79] Information on *http://www.music.eucood.com/intro/body.pe*
[80] Dai X., Yang X., Campbell J., Wood J.: *Effects of runner system design on the mechanical strength of Al-7Si-Mg alloy castings*, Mater. Sci Eng., 354 (2003), pp. 315-235.
[81] Information on http://www.electronics-gmbh.de/
[82] UNI EN12681:2006, *Founding – Radiographic examination,* European Committee for Standardization, Brussels, 2006.
[83] ASTM E08-04: *Standard test methods for tension testing of metallic materials*, ASTM International.
[84] Timelli G., Fabrizi A., Capuzzi S., Bonollo F., Ferraro S.: *The role of Cr additions on Fe-rich compounds on microstructural features and impact toughness of AlSi9Cu3(Fe) diecasting alloys*, Mat. Sci. Eng. A, 603 (2014), pp. 58-68.
[85] ASTM E290-97a: *Standard test method for bend testing of materials for ductility*, ASTM International.
[86] Djurdjevic M.B., Vicario I., Huber G.: *Review of thermal analysis applications in Aluminum casting plants*, Ree. Metal., 50 (2014).
[87] Rakhmonov J., Timelli G., Bonollo F.: *Characterization of the solidification path and microstructure of secondary Al-7Si-3Cu-0.3Mg alloy with Zr, V and Ni additions*, Mat. Characterization, 128 (2017), pp. 100-108.

[88] Rakhmonov J., Timelli G., Bonollo F.: *Influence of melt superheat, Sr modifier, and Al-5Ti-1B grain refiner on microstructural evolution of secondary Al-Si-Cu alloys*, Met. Mat. Trans. A, 47 (2016), pp. 5510-5521.
[89] Battaglia E., Bonollo F., Timelli G., Fiorese E., Kral G.: *Correlation between process, microstructure and properties in High Pressure Die Casting Aluminum-Silicon alloys*, Adv. Mat and Proc. Tech., 3 (2017), pp. 111-124.
[90] Battaglia E., Bonollo F., Fiorese E., Kral G.: *Overview of the correlations between process parameters, microstructure and mechanical properties of Reference castings and industrial demonstrators*, Key Eng Mat, 710 (2016), pp. 35-40.
[91] Battaglia E., Bonollo F., Ferro P.: *Experimental damage criterion for static and fatigue life assessment of commercial Aluminum alloy die castings*, Met Mat Trans A, 48 (2017), pp. 2574-2583.
[92] ASTM E0505-01: *Standard Reference Radiographs for Inspection of Aluminum and Magnesium Die Castings*, ASTM International, 2001.
[93] Battaglia E., Bonollo F., Ferro P., Cenghialta A., Mazzacavallo G.: *Performance analysis of an Aluminum alloy for the production of commercial High Pressure Die Castings*, Metall. Ital., 108 (2016), pp. 61-64.
[94] Battaglia E., Bonollo F., Ferro P., Fabrizi A.: *Effect of heat treatment on commercial AlSi12Cu1(Fe) and AlSi12(b) Aluminum alloy diecastings*, under review Met Mat Trans A
[95] Campbell J.: *Complete Casting Handbook*, 2nd ed., Elsevier, Oxford, 2015.
[96] Ji S. Yang W., Gao F., Watson D., Fan Z.: *Effect of iron on the microstructure and mechanical property of Al-Mg-Si-Mn and Al-Mg-Si diecast alloys*, Mater Sci Eng A, 564 (2013), pp. 130-139.
[97] Darlapudi A., McDonald S. D., Terzi S., Prasad A., Felberbaum M., StJohn D.H.: *The influence of ternary alloying elements on the Al-Si eutectic microstructure and the Si morphology*, J of Crystal Growth, 433 (2016), pp. 63-73.
[98] Manente A., Timelli G.: *Optimizing the heat treatment process of cast Aluminum alloys*, Recent trends in processing and degradation of Aluminum alloys, www.intechopen.com
[99] Greenwood G.W.: *The growth of dispersed precipitates in solutions*, Acta Metallurgica, 4 (1956), pp. 243-248.
[100] Hu R., Ogura T., Tezuka H., Sato T., Liu Q.: *Dispersoid formation and recrystallization behavior in an Al-Mg-Si-Mn alloy*, J. Mater. Sci. Tech., 26 (2010), pp. 237-243.
[101] Li Y.J., Arnberg L.: *Quantitative study on the precipitation behavior of dispersoids in DC-cast AA3003 alloy during heating and homogenization*, Acta Materialia, 51 (2003), pp. 3415-3428.
[102] Du Q., Poole W.J., Wells M.A., Parson N.C.: *Microstructure evolution during homogenization of Al-Mn-Fe-Si alloys: Modeling and experimental results*, 61 (2013), pp. 4961-4973.
[103] Chen R., Xu Q., Jia Z., Liu B.: *Precipitation behavior and hardening effect of Si-containing dispersoids in Al-7Si-Mg alloy during solution treatment*, Mater. Des., 90 (2016), pp. 1059-1068.
[104] Muggerud A.W.F., Mortsell E.A., Li Y., Holmestad R.: *Dispersoid strenghtening in AA3xxx alloys with varying Mn and Si content during annealing at low temperatures*, Mater. Sci. Eng. A, 567 (2013), pp. 21-28.

APPENDED PAPERS

The following supplements constitute the basis of the thesis.

Supplement I E. Battaglia, F. Bonollo, G. Timelli, E. Fiorese, G. Kral: "Correlation between process, microstructure and properties in high pressure die casting Aluminum-Silicon alloys" Advances in Materials and Processing Technology (2016): 1-14.

Work developed within the EU MUSIC project

Supplement II E. Battaglia, E. Bonollo, I.Tonello, E. Fiorese: "Correlations between defect content, mechanical properties and fractographic investigation of AlSi9Cu3(Fe) alloy reference castings" Material Science Forum (2017): 193-198.

Work developed within the EU MUSIC project

Supplement III E. Battaglia, F. Bonollo, E. Fiorese, G. Kral: "Overview of the correlations between process parameters, microstructure and mechanical properties of reference castings and industrial demonstrators" Key Engineering Materials (2016): 35-40.

Work developed within the EU MUSIC project

Supplement IV E. Battaglia, F. Bonollo, P. Ferro: "Experimental damage criterion for static and fatigue life assessment of commercial Aluminum alloy die castings" Metallurgical and Materials Transactions A (2017): 2574-2583.

Supplement V E. Battaglia, F. Bonollo, P. Ferro, A. Fabrizi: "Effect of heat treatment on commercial AlSi12Cu1(Fe) and AlSi12(b) Aluminum alloy diecastings" Submitted for publication to Metallurgical and Materials Transactions A (2017).

Supplement VI E. Battaglia, F. Bonollo, A. Fabrizi: "Effect of Cu and Fe on the eutectic Si morphology of AlSi12(b) and AlSi12Cu1(Fe) alloy diecastings"
It is currently being drafted

SUPPLEMENT I

Correlation between process, microstructure and properties in high pressure die casting Aluminum-Silicon alloys

E. Battaglia, F. Bonollo, G. Timelli, E. Fiorese, G. Kral; Advances in Materials and Processing Technology, 2016, pp.1-14

Advances in Materials Processing Technology 2016
Taylor & Francis online

CORRELATION BETWEEN PROCESS, MICROSTRUCTURE AND PROPERTIES IN HIGH PRESSURE DIE CASTING ALUMINIUM-SILICON ALLOYS

E. Battaglia, F. Bonollo, G. Timelli , E. Fiorese and G. Kral
DTG – University of Padova, Stradella S. Nicola 3, Vicenza, Italy

ABSTRACT

Nowadays automotive industry and, in general, transportation one increasingly needs light components in order to reduce total weights and therefore limit harmful emissions and fuel consumption. The die casting process, on one hand, is a versatile and highly productive process but, on the other, the elevated amount of defects found in the castings sometimes compromises the characteristics of the final product. This paper presents the results of the analyses carried out using a Reference Die, referred to as *horse shoe*-shaped die, specifically designed to generate as many kinds of defects as possible, at different levels of severity. A Design of Experiments method has been applied for analyzing the influence of the main process parameters on the casting quality and an innovative sensor network installed on the machine allowed a continuous control of the process itself. Visual inspection, X-ray investigations and micrograph analyses have been carried out in order to assess the casting quality. Correlations
between process parameters and casting quality have been deduced analyzing the data collected through the equipment installed on the die casting machine: in-cavity sensor network, plunger speed and displacement sensors. Results show the effectiveness of the *horse shoe*-shaped casting in highlighting the correlations between process
and quality and the strong influence of second phase plunger velocity, temperature and pressure on defect formation.

1. Introduction

High Pressure Die Casting (HPDC) is a versatile and highly productive process: currently about half of the world production of light metal castings is obtained by this kind of process.
HPDC process allows the production of complex engineering metal parts by forcing molten metal under high pressure into reusable steel dies, where it is held by a powerful press until the metal solidifies. Casting quality depends on many parameters hard to check; there are many sequential actions in the three phases of the process that may affect the casting quality, i.e. injection of molten metal, solidification, casting extraction and lubrication system.[1,2]
The combination of these aspects and many others, such as die temperature, mould filling capacity of the molten metal, cooling rate and geometrical complexity of the casting have effects on the integrity of the component. If these parameters are not adequately controlled,

various defects are expected to be generated; therefore in HPDC, due to the complexity of the process, casting scrap rates lie in the range of parts per hundred while, in other production lines, they are measured in parts per million.[1–4]

Even if in literature some corrections guidelines are given to die casting operators, supervisors and engineers to common die casting defects,[5] no standard is given to choose the best solution according to processes, methods, alloys and design. As revealed by a recent survey carried out among European foundries, the most frequent defects in castings manufactured by HPDC are shown in Figure 1.[6]

On the other hand, as revealed by the above-mentioned survey,[6] HPDC is fundamental for medium and small companies, thanks to its higher productivity than other kinds of process, and the HPDC worldwide production rate is expected to substantially increase by 2025.[7]

In the development of this work, a recent defect classification for HPDC components, introduced in[8] has been taken into account. This classification distinguishes between internal, surface and geometrical defects, and investigates the causes of defects. Moreover, several permanent mould designs, still documented in literature, have been analysed. In particular, two designs are the most widely diffused in foundries. The Stahl mould developed by K.R. Whaler from Stahl Specialty Company, which is based on a design of Grandier-Vazeille and Jacob, was adopted as reference test-bar mould design by the International Organisation for Standardization.[9] The other design is the Step mould, which is not internationally standardized.

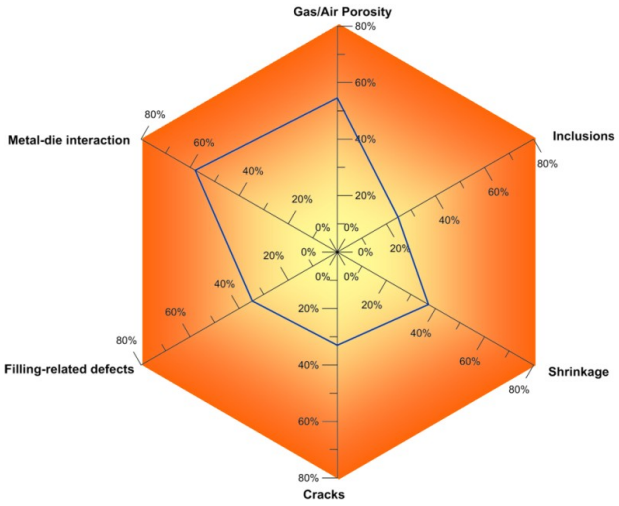

Figure 1. Frequency of defects in die castings, as estimated by European HPDC foundries.

The significance of this work stands in the conception and realization of a Reference Die aimed to generate different kinds of defects at different levels of severity depending on the process parameters adopted and to employ innovative devices installed on the machine to optimize and monitor the process, recording basic process data as piston velocity and displacement, as well as pressure and temperature inside the die-cavity. One of the most important aspects of the proposed reference casting is the possibility to gather in one single

design different thicknesses, geometries and modified features to generate many defect typologies. Furthermore, this work mainly focuses on metal-die interaction defects and air/gas or shrinkage porosity which can compromise both the mechanical and the aesthetic quality of the castings, these defects being the most frequent in Al–Si alloys (Figure 1). Moreover, as documented in literature and in particular in[6,9], these kinds of defect are related to the die casting injection parameters, besides the chemical composition of the alloy.

2. Experimental procedure

2.1 Horse shoe-shaped reference die

In the frame of European Music project,[10] a Reference Die was elaborated and designed with the aim of producing Reference Castings with typical HPDC defects. The concept behind the design of the Reference Die was that severity level for each kind of defect has to be easy to measure and different defect levels have to be achieved through controlled variations in process parameters. The defect classification introduced in [8] was fundamental during the design phase of the die and the different designs evaluated with various inserts led to the final concept shown in Figure 2, the so called *horse shoe*-shaped casting.

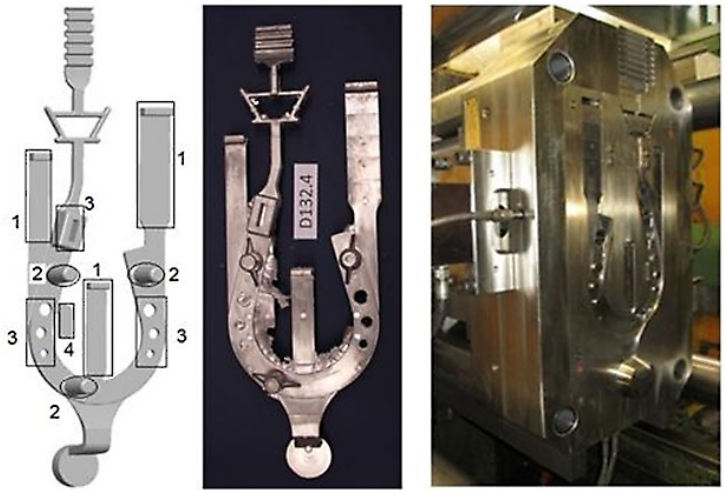

Figure 2. *Horse-shoe* shaped Reference Casting and Reference Die.

As shown in Figure 2, the *horse shoe*-shaped casting consists of (1) three specimens with thin walls representing the thickness typically used in HPDC, (2) three bosses with mass concentration aimed to generate shrinkage porosity (one of them was equipped with a squeezer pin to reduce shrinkage), (3) a thick-walled area close to the venting channel and three holes for both sides of the *horse shoe* created in order to cause die soldering, (4) a small extension aimed to generate cold laps caused by melt flows and vortexes, (5) the whole *horse shoe* aimed to generate distortion and (6) a runner system aimed to cause turbulence on the melt flow.[11]

2.2 Installed equipment

During the casting trial, several innovative equipment were adopted to allow a continuous control of the process itself, recording the evolution of some variables during each manufacturing cycle. Particularly, in-cavity sensor network was installed on the machine.

Figure 3 shows the location of the temperature (referred to as *T*i) and pressure (referred to as *P*i) in-cavity sensors.

The three typologies of sensors installed inside the die cavity were: the *Metal Front Pressure sensor,* which measured the pressure of the melt on the die surface during the whole filling and solidification process; the *Metal Front Temperature sensor*, which measured the temperature of the molten metal on the die surface during the whole cycle; and the *Metal Front Contact sensor*, which provided a digital signal when it got into contact with the melt, achieving a real-time evaluation of incoming metal position.

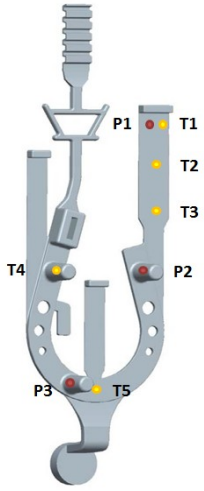

Figure 3. In-cavity sensor position during the *horse shoe*-shaped casting production.

In summary, the parameters obtained through the sensors installed on the machine for each casting were:

- Five in-cavity temperature profiles from T1 to T5,
- Three in-cavity pressure profiles from P1 to P3,
- Plunger displacement and velocity profiles.

2.3 Casting trials and quality control procedure

In the present work, the Aluminium alloy EN AB-46000 according to UNI EN 1706 [12] has been cast and the chemical composition, measured by optical emission spectroscopy on separately poured samples, is shown in Table 1. The castings were manufactured using a cold chamber die-casting machine with locking force 7500 kN, shot chamber length 0.482 m and diameter 0.080 m. Before producing the first casting, it was necessary to preheat the tool to reach

a uniform temperature of the inserts (minimum 160/180 °C). The molten metal inside the holding furnace was kept at 705 °C and the pouring temperature was 660 °C; the melt was periodically manually skimmed. Approximately 10–12 castings were scrapped after each start-up in order to reach a quasi-steady state temperature in the shot chamber and die. Casting extraction and application of the lubricant spray were done automatically. During the process, the thermoregulation control unit was set up at 245 °C in the moving side circuit of the die and at 235 °C in the fixed side one.

The Design of Experiment (DOE) consisted of 32 arrays, i.e. process parameter changes, totalising an amount of approximately 150 castings. The nominal process parameter intervals were:

- I phase plunger velocity ranged from 0.2 to 0.8 m/s;
- II phase plunger velocity varied between 1.5 and 4 m/s;
- the position of the piston at the switching point between the two phases was set from a minimum of 300 mm to a maximum of 350 mm;
- the intensification pressure ranged from 500 to 1000 bar.

At least three castings for each combination of process parameters were manufactured.

All the castings were visually inspected, focusing on six zones of main interest represented in Figure 4: (A) stepped wedge, (B) first appendix for bending test, (C) left holes, (D) right holes, (E) hollow thick area and (F) second appendix for bending test. A score from 1 to 4 was attributed to each area according to its surface quality level, whereas a different qualitative evaluation was assigned to the whole casting according to flash presence, distinguishing between low, medium and high level.

Radiographic inspection was carried out, according to UNI EN 12681:2006[13] on the stepped wedge of the castings in order to detect the presence of macro-porosities due to gas/air entrapment or shrinkage. The stepped wedge has five steps with decreasing thickness (from 3 to 1 mm), thus an image for each step varying current and voltage was captured. In Figure 5, two examples of X-ray images are shown: in both the images, the grey scale varies according to the thickness of the step under analysis.

Table 1. Chemical composition of the experimental alloy (wt.%); the composition limits of the EN AC-Al-Si9Cu3(Fe) alloy (EN AC-46000) are also reported according with EN 1706:2010 standard.

Alloy	Si	Fe	Cu	Mg	Sr	Zn	Cr	Ni	Ti	Pb	Mn	Al
ENAC 46000	8-11	0.6-1.3	2-4	0.05-0.55	-	1.2	0.15	0.55	0.25	0.35	0.55	Bal
Tested alloy	10.4	0.8	3	0.42	0.0001	0.9	0.04	0.05	0.05	0.06	0.3	Bal

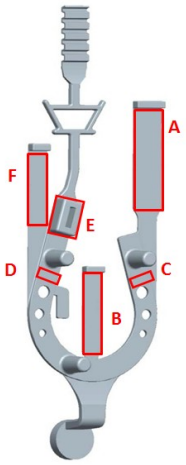

Figure 4. Six visually inspected zones of the *horse shoe*-shaped Casting: (A) stepped wedge, (B) first bending test appendix, (C) left holes, (D) right holes, (E) hollow thick area, (F) second bending test appendix.

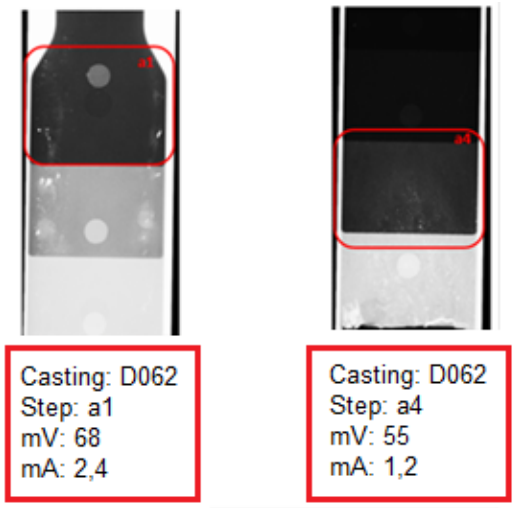

Figure 5. Example of X-ray images captured for two different steps (a1 and a4) of the stepped wedge with the corresponding current and voltage settings.

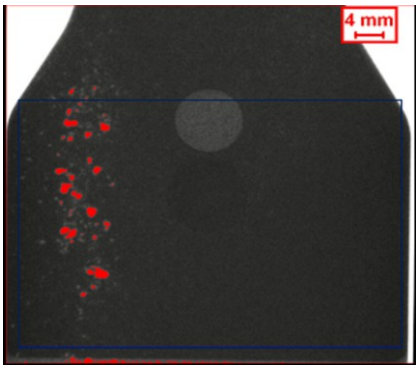

Figure 6. Image analysis with QWin software of the step a1.

The X-ray images of three steps were considered sufficient for the quality assessment and therefore they were imported in the optical microscope and analysed using an image analysis software (Leica QWin). The three steps have two temperatures and one pressure sensor, i.e. T1, T3 and P1, and they showed a higher amount of defects in most cases. The same measure frame was adopted for all the images imported, whereas the grey level detected was kept constant only for steps with the same thickness in order to make the results comparable. The porosity percentage for each stepped wedge was obtained from the image analysis. In Figure 6, an example of porosity detection is shown.

2.4 Data extraction from sensors

The temperature and pressure sensors recorded 20000 values at each HPDC cycle (one sample every 0.5 ms), and then decimation using a Visual Basic algorithm was performed to make data easier to process. The key parameters obtained through the manipulation of the temperature profiles were the maximum temperature value and the corresponding time for each casting. Examples of temperature profiles and key parameters derived from them are given in Figure 7(a) and (b), respectively. Similar key parameters were extracted from pressure profiles, i.e. the maximum pressure and the corresponding time. Example of pressure profiles are given in Figure 7(c). As for the plunger displacement and velocity curves (Figure 7(d) and (e)), this work focused on the extraction of information from the plunger velocity. The procedure of extracting some key parameters consisted in using a Visual Basic algorithm, which searches for a significant change in the slope of the velocity curve slope corresponding to the real switching position, and returns this value and its corresponding time. The real first phase velocity was equal to the constant values standing before the switching position. Finally, the second phase velocity was approximated by the maximum velocity value standing after the switching position.

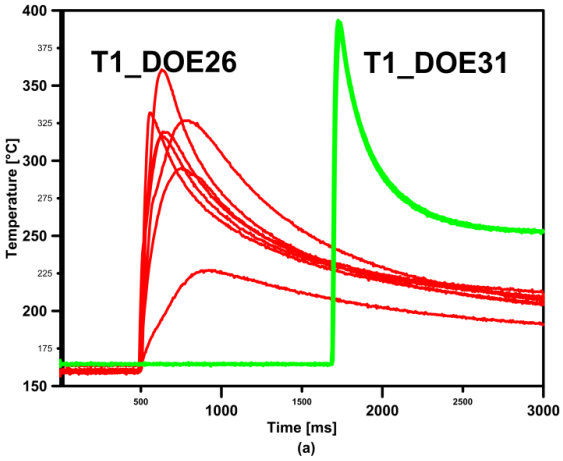

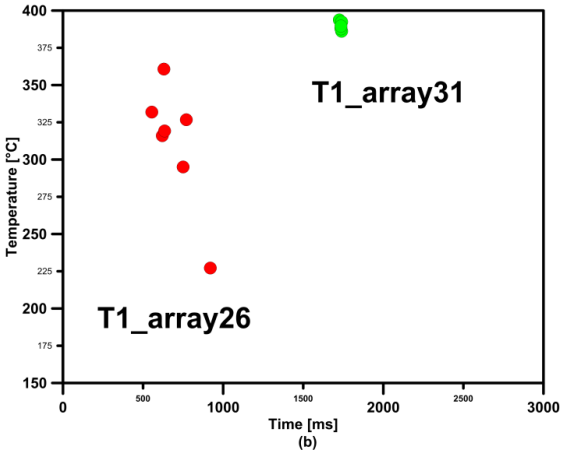

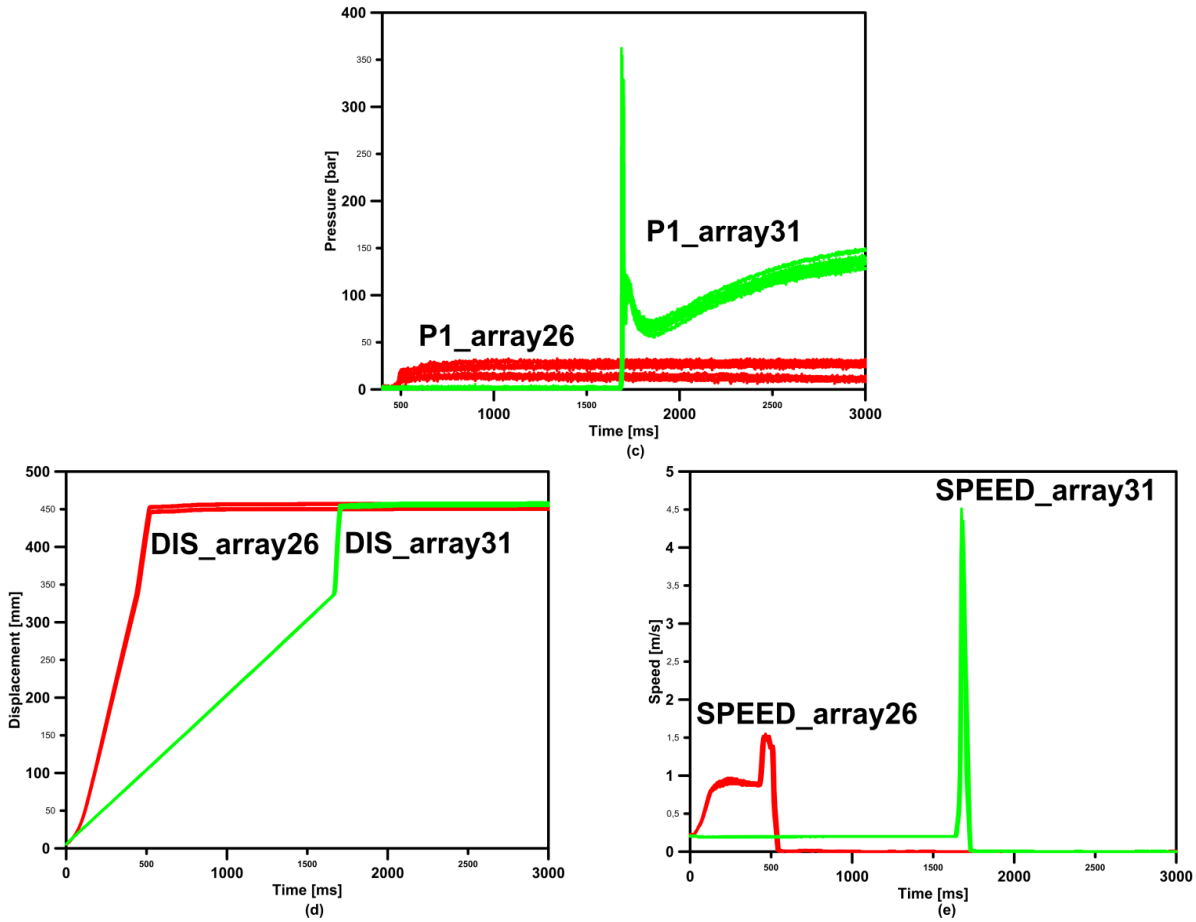

Figure 7. (a) Temperature profiles of the sensor T1; (b) maximum temperatures and corresponding times; (c) pressure profiles of the sensor P1; (d) plunger displacement curves; (e) plunger velocity curves. Worst and best configurations are compared, i.e. array26 and 31, respectively.

3. Results and discussion

3.1 Quality assessment

The aim of elaborating sensor data was to supply a linkage between the process, which represents the independent variable, and the casting quality, which represents the dependent variable.

Table 2. Qualitative classification based on visual inspection carried out on the six main zones of the castings. A qualitative level from 1 to 4 has been attributed to each part A–F.

	Zone A	Zone B	Zone C	Zone D	Zone E	Zone F
Level 1	0	0	0	0	0	0
Level 2	5	49	68	3	35	11
Level 3	42	50	39	106	68	94
Level 4	0	10	2	0	6	4

Table 3. Qualitative and partly quantitative classification of the stepped wedge.

Class	Qualitative description	Porosity (%)
1	Absence of defects	
2	Slightly visible melt flows	
3	Clearly visible melt flows	
4	Melt flows and detectable porosity (Low Level)	0-0.8
5	Micro and macro detectable porosity (Medium Level)	0.8-1.5
6	Distributed micro and macro detectable porosity (High Level)	> 1.5
7	Scraps – crack or incomplete filling	

Visual inspection of the castings led to a qualitative classification based on the scores described in the experimental procedure and synthesised in Table 2.

Level 1 was attributed to castings without defects; *Level 2* was given in the case of roughness change in the surface, caused by metal-die interaction, or slightly visible melt flows; *Level 3* was assigned to castings that had a greater roughness change or if contaminants, cold shots or clearly visible melt flows were present on the surface; *Level 4* was given to incomplete, cracked or blistered castings.

A qualitative classification was defined on the basis of the radiographic inspection of the stepped wedge and was then combined with a quantitative one based on the percentage of porosity detected by means of the image analysis software, as previously described in the experimental procedure. Anyway these classifications are adaptable to various needs on the basis of ASTM E0505-01.[14] In Table 3, this qualitative and partly quantitative classification is shown. As for radiographic testing, *Level 1* was not assigned to any casting because at least slightly visible melt flows were always detected. The first three levels of Table 3 included castings with micro-porosities, which were hard to detect by X-ray device and QWin software; the last four levels of Table 3 were attributed to castings with macroporosities clearly detectable. *Level 7* was directly attributed to incomplete or cracked castings.

To further validate the qualitative and partly quantitative classification developed, some micrographs, shown in Figure 8, were obtained from the stepped wedge.

The equipment installed on the HPDC machine was fundamental in order to define a correlation between the independent variables related to the process and the dependent variables corresponding to the casting quality.

3.2 Correlations between process and quality

The main variables studied in this work were injection velocities, in-cavity temperatures and pressures detected by the sensor network, and casting quality in terms of superficial defects and porosity content due to air/gas or shrinkage, which are the most frequent defects in HPDC.[6, 8, 15]

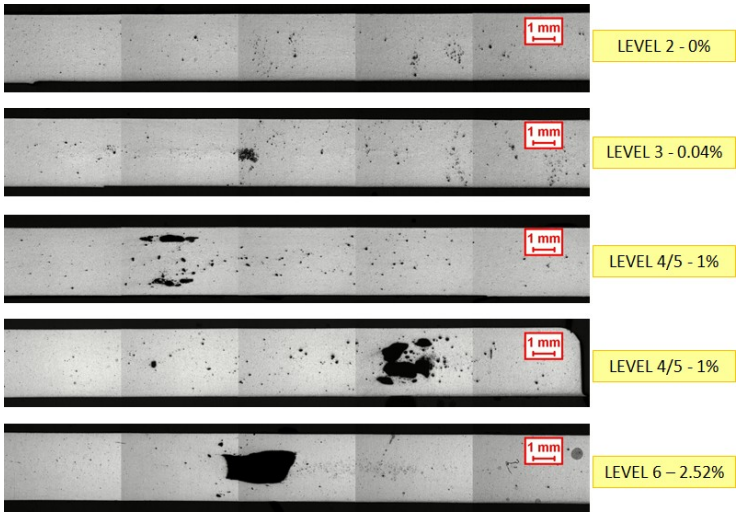

Figure 8. Micrographs of the stepped wedge (zone A); qualitative and quantitative porosity classification.

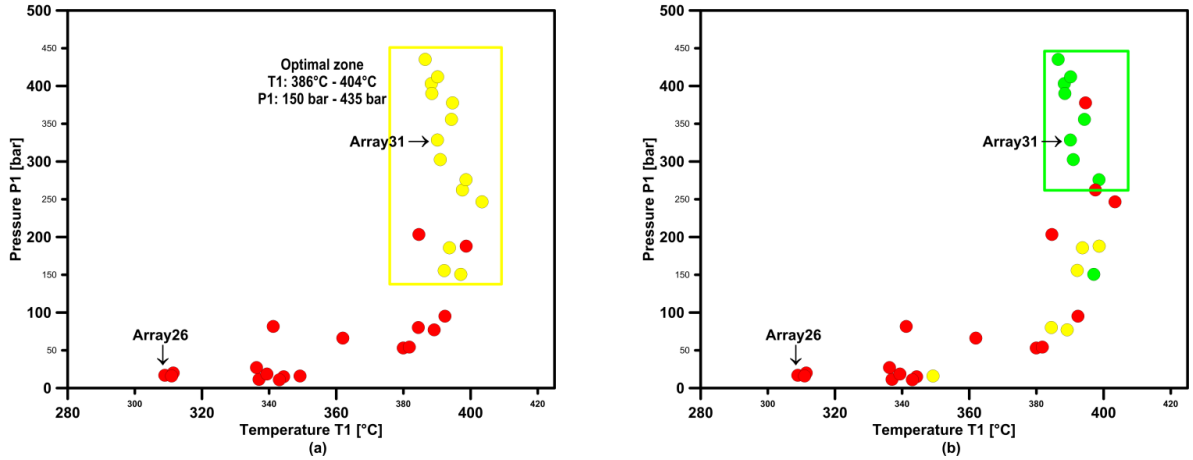

Figure 9. (a) T1 temperature sensor versus P1 pressure sensor: the values in the box correspond to sound castings according to visual inspection; (b) T1 versus P1: the values in the box correspond to castings with low porosity content; red, yellow and green colors are related to increasing level of quality determined as previously explained.

Interesting correlations were obtained between the in-cavity parameters detected by temperature and pressure sensors and the quality of the castings. As shown in Figure 9(a), with the purpose of obtaining sound castings according to visual inspection, the molten metal should reach the end of the stepped wedge of the die (particularly T1 and P1 sensors represented in Figure 3) with relatively high measured temperature (between 380 and 400 °C for these castings) and measured pressure (between 150 and 440 bar) avoiding, in this way, surface defects, cracks and incomplete filling. Porosity content, as the superficial quality of the castings, was related to temperature and pressure values detected from the in-cavity sensors installed in the stepped wedge of the die, as shown in Figure 9(b). The higher the temperature and pressure detected by the sensors, the lower the porosity content.

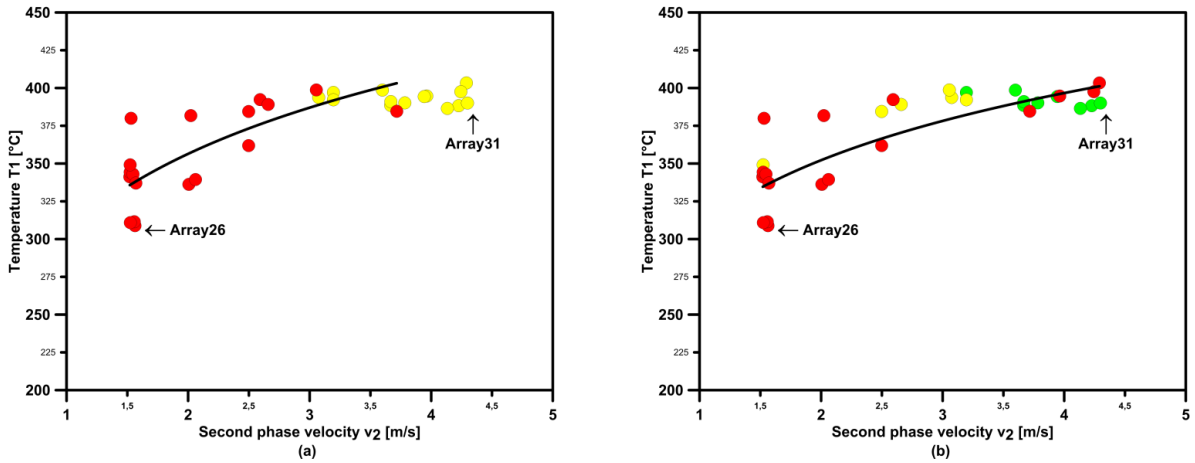

Figure 10. T1 sensor temperature as a function of second phase plunger velocity with reference to (a) visual inspection and (b) porosity content; red, yellow and green colors are related to increasing level of quality. Data present a logarithmic relationship.

Table 4. Comparison between worst and best process parameter configurations. The values of the second phase velocity, temperature measured by T1 and P1 sensors, visual inspection and radiographic testings confirm the correlations proposed.

	V_1 [m/s]	V_2 [m/s]	Switch [mm]	T1 [°C]	P1 [bar]	Visual insp. level	Porosity (x-ray) level [%]
Worst_array 26	0.9 (0.8)	1.5 (1.5)	329 (330)	311	16	4	13.5
Best_array 31	0.2 (0.2)	4.3 (4)	332 (335)	390	329	3	0.5

Note: Nominal values written in brackets

As mentioned above, higher metal temperature detected by the sensor T1 in the stepped wedge of the die cavity may lead to a better quality in terms of porosity content and superficial aspect of the castings, but on the other hand, it may result in splashing and presence of flash, which has to be removed. Also plunger velocity has its own significance, as too low second phase velocity results in a compact metal front, but longer cycle times and incomplete castings (considering the first phase unvaried). Conversely, too high plunger velocity results in higher flash and may cause a sort of spraying behaviour with consequent formation of cold joints and air porosities. Moreover, the piston speed determines the filling time: a faster piston movement leads to a shorter filling time and to a higher heat level of the melt in the die. In Figure 10, higher second phase plunger velocities lead to higher temperatures detected by the T1 sensor and this is reflected in a better superficial quality of the castings and minor porosity content.

To further validate the correlations previously described and displayed in Figures 9 and 10, the process parameters and quality investigation results of the worst and best configurations of process variables are reported in Table 4. These two configurations were chosen among the arrays with high number of castings in order to guarantee a significance of the reported results.

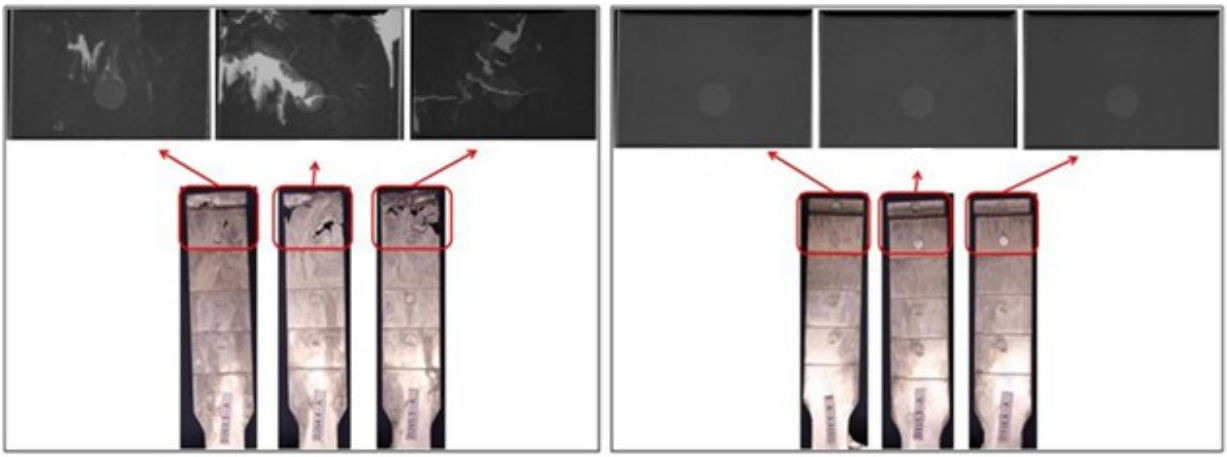

(a) (b)

Figure 11. Pictures and radiographic images of the: (a) worst and (b) best process parameter settings.

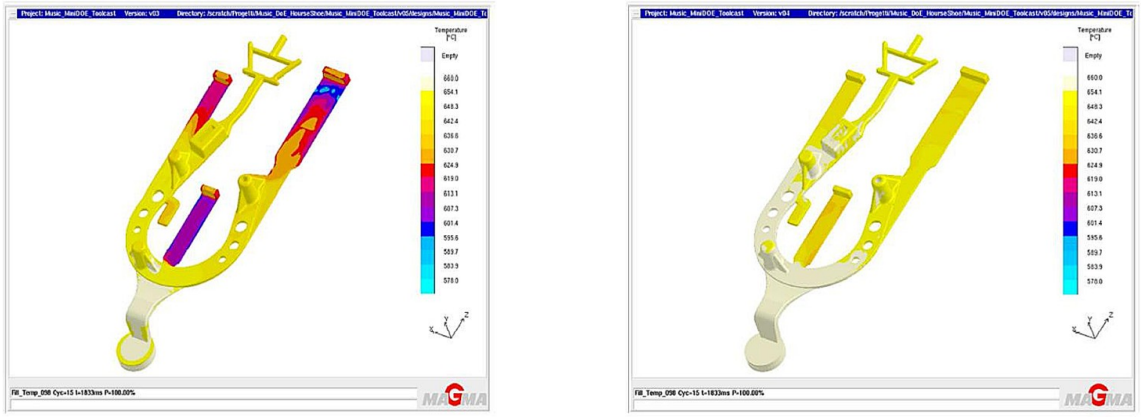

(a) (b)

Figure 12. Simulations of the temperature distribution of the castings obtained by: (a) worst and (b) best process parameter settings.

In Figure 11, pictures and radiographic images of castings obtained by the worst and best configurations of process variables are shown.

In Figure 12, simulations of the two settings are represented: temperature at the end of the filling phase of the best castings is higher than that of the worst ones.

4. Conclusions

HPDC is a complicated manufacturing process with a large number of variables affecting the aesthetic and internal quality of the castings. The main purpose of this work was to introduce and test a new Reference Die for producing the so-called *horse shoe*-shaped castings, and to study some preliminary correlations between process parameters and quality of the castings. The main findings of this work are:

- the *horse shoe*-shaped die is well designed and permits obtaining different defect levels through controlled variations in process parameters;

- the DOE methodology can be effectively applied with the proposed reference die in order to search for correlations between process and quality of the castings;
- second phase plunger velocity, temperature and pressure inside the die cavity show significant influence on surface and internal quality of the castings;
- the best results in terms of surface and internal quality (measured as porosity percentage) of the castings were obtained when high second phase plunger velocity (4 m/s) was used and relatively high temperature (390 °C) and high pressure (329 bar) were detected by the in-cavity sensors mounted in the stepped wedge of the die.

Acknowledgements

This work was developed within European MUSIC project (MUlti-layers control & cognitive System to drive metal and plastic production line for Injected Components, N. 314145).[10] The authors would like to acknowledge Enginsoft, Electronics, Aalen University, MAGMA, Saen, MOTULTECH Baraldi.

References

[1] Bonollo F, Timelli G, Gramegna N. High pressure die casting: contradictions and challenges. J Miner Met Mater Soc Italy. 2015;67:901–908.
[2] Rai JK, Lajimi AM, Xirouchakis P. An intelligent system for predicting HPDC process variables in interactive environment. J Mater Process Technol Switz. 2008;203:72–79.
[3] Kong LX, She FH, Gao WM, Nahavandi S, Hodgson PD. *Integrated optimization system for high pressure die casting processes*. Geelong: Center for Material and Fibre Innovation, Deakin University.
[4] Fiorese E, Bonollo F, Timelli G, Arnberg L, Gariboldi E. New classification of defects and imperfections for aluminum alloy castings. Int J Metalcast Italy-Norway. 2015;9:55–66.
[5] Walkington WG. *Die casting defects – troubleshooting guide*. Arlington Heights (IL): NADCA; 2003.
[6] Information on http://www.stacast-project.org
[7] Twarog DL. *State of die casting industry*. Arlington Heights, IL: NADCA; 2014.
[8] Gariboldi E, Bonollo F, Parona P. *Handbook of defects in high pressure diecasting*. 2nd ed., edited by AIM: Centro di studio pressocolata; 2010.
[9] Timelli G, Capuzzi S, Bonollo F. Optimization of a permanent step mold design for Mg alloy castings. Metall Mater Trans B. 2015;46:473–484.
[10] Information on http://music.eucoord.com/intro/body.pe
[11] Dai X, Yang X, Campbell J, Wood J. Effects of runner system design on the mechanical strength of Al-7Si-Mg alloy castings. Mater Sci Eng. 2003.
[12] UNI EN 1706. *Aluminium and aluminium alloys – casting – chemical composition and mechanical properties*. Brussels: European Committee for Standardization; 2010.
[13] UNI EN 12681. *Founding – radiographic examination*. Brussels:European Committee for Standardization; 2006.
[14] ASTM E0505-01. *Standard reference radiographs for inspection of aluminum and magnesiumdie castings*. West Conshohocken (PA): ASTM International; 2001.
[15] Wang L, Turnley P, Savage G. Gas content in high pressure die castings. J Mater Process Technol Aust. 2011;211:1510–1515.

SUPPLEMENT II

Correlations between defect content, mechanical properties and fractographic investigation of AlSi9Cu3(Fe) alloy reference castings

E. Battaglia, F. Bonollo, I. Tonello, E. Fiorese; Material Science Forum, 2017, pp.193-198

Metarial Science Forum 2017
Trans Tech Publications Ltd

CORRELATIONS BETWEEN DEFECT CONTENT, MECHANICAL PROPERTIES AND FRACTOGRAPHIC INVESTIGATION OF AlSi9Cu3(Fe) ALLOY REFERENCE CASTINGS

E. Battaglia, F. Bonollo, I. Tonello , E. Fiorese
DTG – University of Padova, Stradella S. Nicola 3, Vicenza, Italy

ABSTRACT

High Pressure Die Casting (HPDC) is a foundry process particularly suitable for high production rates and applied in several industrial fields, but the amount of scrap, caused by defects or incomplete filling, is sometimes very high. Thus it is important to know which are the main causes of defect formation and their effects on microstructure and mechanical properties. This paper presents, within the European MUSIC project, the qualitative and quantitative results of a study conducted on AlSi9Cu3(Fe) alloy castings, referred to as *Horse-shoe* Reference Castings, specifically designed to generate different kinds of defects with different severity levels. The work focuses on the correlations obtained between the casting mechanical properties, their defect content in terms of porosity and oxide films and the process parameters adopted, mainly second phase plunger velocity and intensification pressure. The three point bending test was carried out on the four specimens obtained from the two appendixes of the casting. The fracture surfaces were studied by scanning electron microscopy (SEM) and optical microscopy (OM) highlighting that the defect content is clearly correlated to the mechanical properties and the process parameter settings.

Introduction

Among the Aluminum casting processes, High Pressure Die Casting (HPDC) is an efficient, versatile and economic way for producing large number of thin-walled components requiring strict dimensional tolerances and good surface finish. HPDC is a complex process because of the phase transformation that metal undergoes solidifying in the die, the effects of the liquid metal pouring into a metallic shot sleeve, the high melt speed at the gate, the short filling time, the shrinkage porosity that characterizes metal solidification and the elevated pressure applied during the third phase to overcome these physical phenomena [1]. HPDC is widely employed, nevertheless if the process parameters adopted are not adequately controlled, various defects are expected to be generated, resulting in an amount of rejected components sometimes unacceptable [2].

In the existing literature, some correction guide-lines to common casting defects and rules for good castings can be found [3,4]. However, there are no standards for selecting the best solution

according to alloys, process, method and design. As the mechanical properties of die-cast Aluminum alloys are directly influenced by microstructural defects, the understanding of their characteristics, causes and any interaction with the process parameters is fundamental for improving the casting properties. According to the classification of defects recently published as CEN/TR 16749:2014, the most common imperfections normally found in die-cast Aluminum alloys are metal-die interaction flaws, air/gas and shrinkage porosity [2,5,6,7].

The main contribution of this work is to propose the use of the Horse-shoe Reference Casting and the employment of innovative devices installed on the machine to monitor the HPDC process, in terms of piston velocity and displacement, in-cavity temperature and pressure distributions [8,9]. Correlations between data acquired during the process, i.e. second phase plunger velocity and intensification pressure, and defect content, microstructure features and mechanical properties are presented.

Experimental procedure

Within the European MUSIC project [10], a secondary AlSi9Cu3(Fe) cast alloy (EN AB-46000 according to UNI EN 1706) was used to manufacture the *horse-shoe* Reference Casting, already described in previous works [8,9]. Based on a Design of Experiment (DOE) consisting of 32 arrays, i.e. process parameter changes, approximately 150 castings were produced.

Bending test. The three point bending test was carried out, according to ASTM E290-97a, on samples drawn from the two appendixes of the casting, here called B and F respectively. Each appendix was divided into two halves labeled as *upper* and *lower* specimen. All the specimens were 40 mm wide, 75 mm long and 2 mm thick. The three point bending test was employed using a MTS Criterion C43 Test System machine with a load applied to the centerline. The crosshead speed used was 4 mm/min.

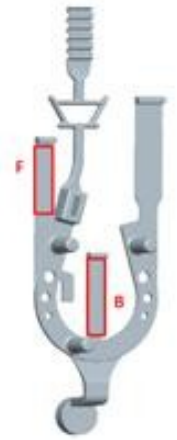

Figure 1. Horse-shoe Reference Casting and the two appendixes for bending test.

Metallography and fractography. At least twelve *upper* samples were subjected to metallographic and fractographic investigations. They were mechanically prepared to a 3 μm finish with diamond paste and polished with a commercial fine silica slurry. The metallographic analyses were carried out using an optical microscope (OM), whereas the fractographic analyses of the fracture surfaces were conducted using a scanning electron microscope (SEM). The quantitative analysis was developed using an image analyzer. Each metallographic section was scanned and divided into 30 images to obtain a statistical average of the porosity distribution.

Results and discussion

Bending test. The bending results, expressed as peak load and displacement to fracture, referred to the upper half of the appendix F. Indeed, since the air entrapment porosity is typically observed far from its origin, an higher amount of defects was assumed to be found in these specimens. According to [11], it was possible to estimate the equivalent stress and strain of the samples under study.

Metallographic analysis. Typical microstructures of the alloy, across the thickness of the die-cast *upper* specimens, show primary Aluminum dendrites, eutectic silicon, oxides, porosities and intermetallics. In Table 1, the process parameters adopted and the quality assessment results of the best and the worst arrays are reported. According to the elaborated DOE, the second phase plunger velocity could vary between 1,5 and 4 m/s and the intensification pressure could fluctuate between 500 and 1000 bar. The appraisal of best and worst configurations is widely explained in [8].

Table 1. Process parameter configurations and quality assessment of best and worst arrays.

Array_ appendix	v_2 [m/s]	P_3 [bar]	Oxides [%]	Porosity [%]	Eq. Stress [MPa]	Eq. Strain [%]
Best-31-F	4	700	0.18	0.06	342.1	0.029
Worst-26-F	1.5	1000	9.12	0.18	285.5	0.014

In Table 1, it is shown that higher second phase plunger velocity corresponds to lower porosity and oxide contents which, in turns, lead to better mechanical properties.

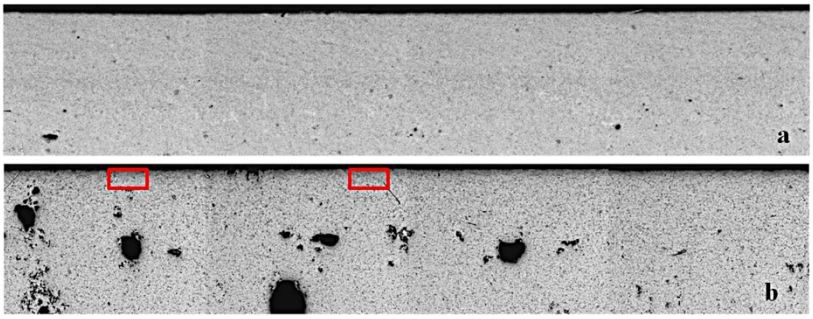

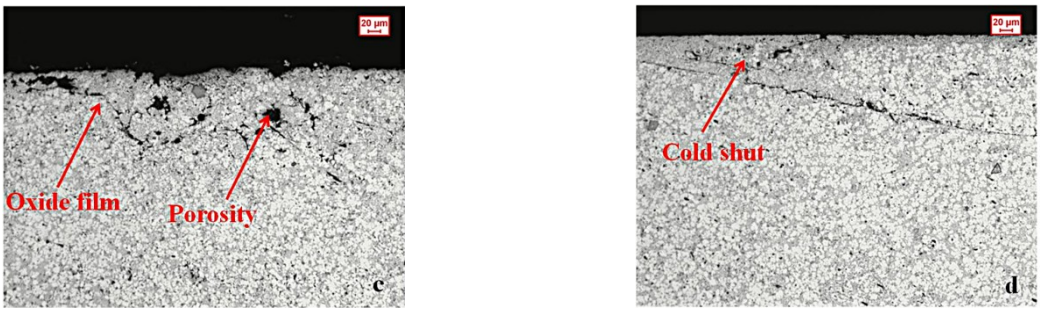

Figure 2. (a-b) Micrographies of array 31 and array 26 respectively. (c-d) Magnifications of array 26 showing the most frequent defects identified.

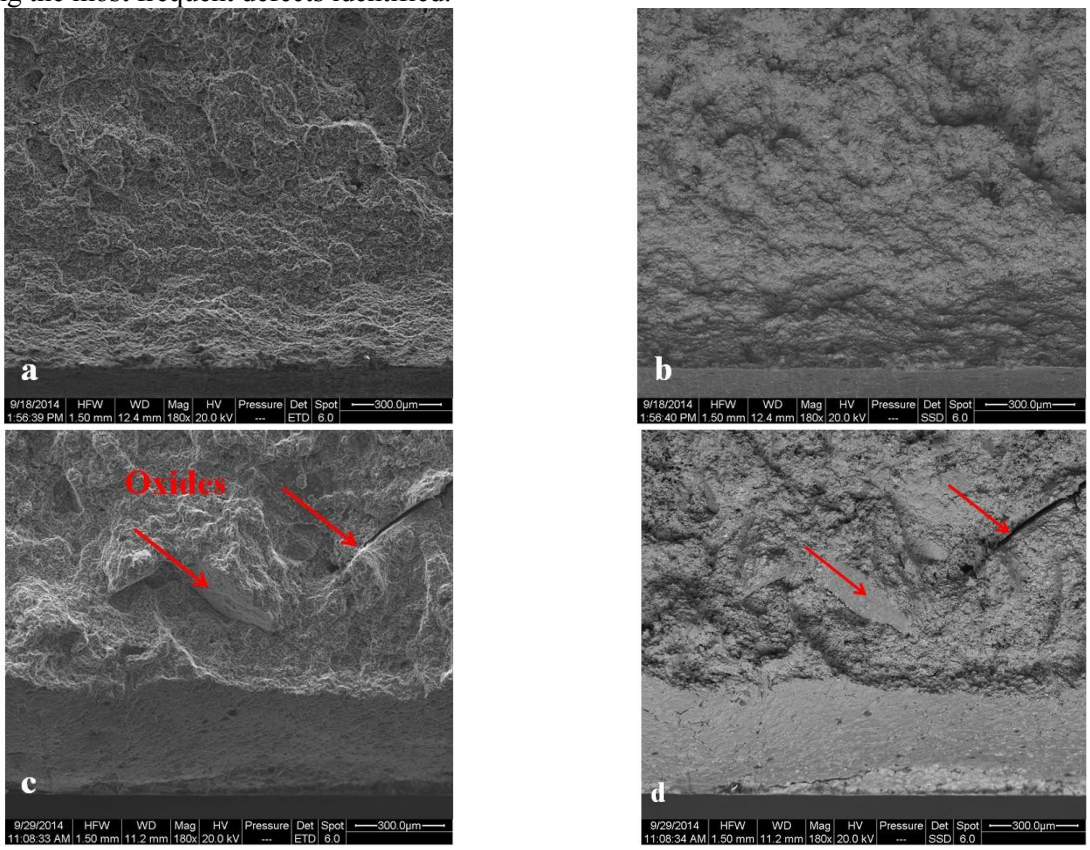

Figure 3. SEM images of best (a-b) and worst (c-d) parameter settings, i.e. Array 26 and 31; the focus is on the side subjected to tensile stress. Secondary electron images on the left, back-scattered electron images on the right.

In Fig. 2a-b, examples of microstructures belonging to the best and the worst parameter settings are shown. It is clear that Fig. 2a shows a better quality than Fig. 2b; Fig. 2c-d, i.e. magnifications of the outermost layer of array 26, support what just stated.

After chemical etching, the analyzed specimens showed an increment of the eutectic percentage moving across their thicknesses, from the inside outward. Indeed, near the surface of the casting the nucleation prevails on the growing mechanism due to the elevated undercooling; therefore, the formation of segregation bands is promoted [12]. The bands of macrosegregation

and porosity are one of the most noticeable microstructural features generated during HPDC and they commonly follow the outer contour of components [13].

Fractographic analysis. In Fig. 3, secondary and back-scattered electron images obtained by means of SEM, of the best and the worst arrays, are compared. Fig. 3a-b show part of the surface layer of array 31 subjected to tensile stress in which there are no defects or inclusions. In contrast, Fig. 3c-d show an example of the oxide films detected in the specimens of array 26; oxides can act as crack initiators leading to sample yielding.

Preliminary correlations between process parameters, defects and mechanical properties. The main variables studied in this work were second phase plunger velocity, bending test properties and casting quality in terms of eutectic, porosity and oxide percentages.

Interesting correlations were obtained between the eutectic and the porosity percentages detected through the micrographic analysis. Fig. 4 reveals that with the increase of the eutectic percentage, an increase of the porosity content is observed. The formation of the eutectic is generally the final stage of the solidification process, thus it is expected to impact the feeding of the casting and consequently the formation of casting defects, in particular porosity [13].

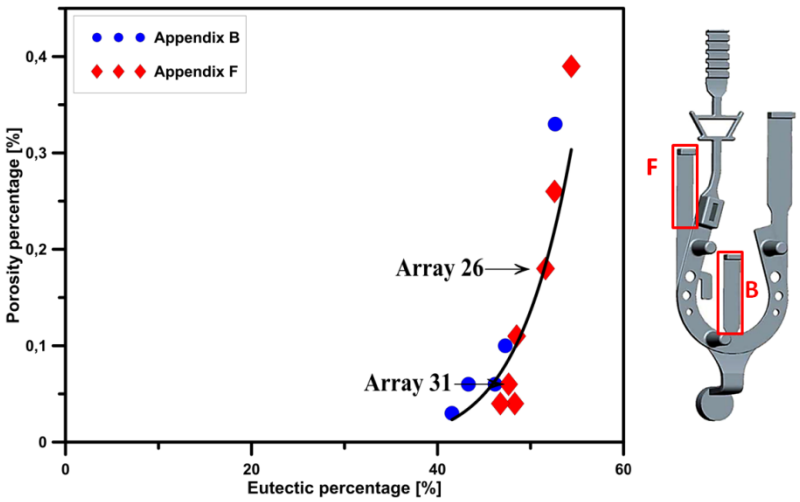

Figure 4. Correlation between eutectic and porosity percentages.

Fracture can nucleate because of internal and surface defects; nevertheless the former are less likely to cause fracture in bending tests. The failure of the specimens is mainly affected by surface microstructural heterogeneities. As it is possible to see in Fig. 5a, the mechanical behavior of the selected specimens is related to the amount of defects detected within 200 μm from the outer surface subjected to tensile stress.

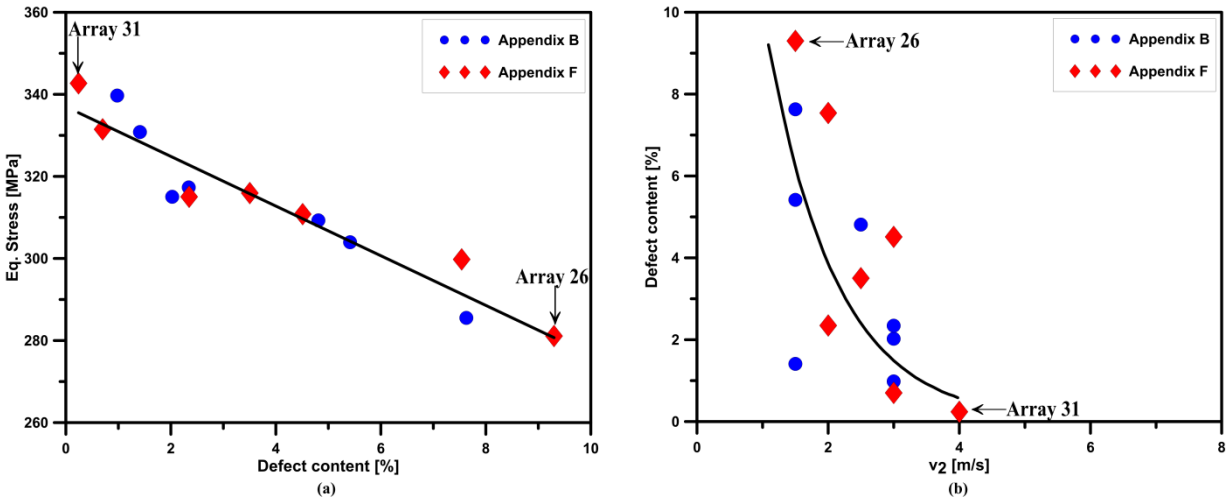

Figure 5. Correlations between (a) mechanical behavior and defect content, i.e. oxides and porosity on the fracture surface; (b) second phase plunger velocity and defect content.

As mentioned above, high defect content leads to poor mechanical properties. In Fig. 5b, the correlation between second phase plunger velocity and defect content, in terms of porosity and oxides, is reported. It is shown that higher plunger velocities lead in this case to a lower defect content, as already reported in [8].

It is generally believed that the effective application of the intensification pressure is crucial to the production of high integrity parts [14].

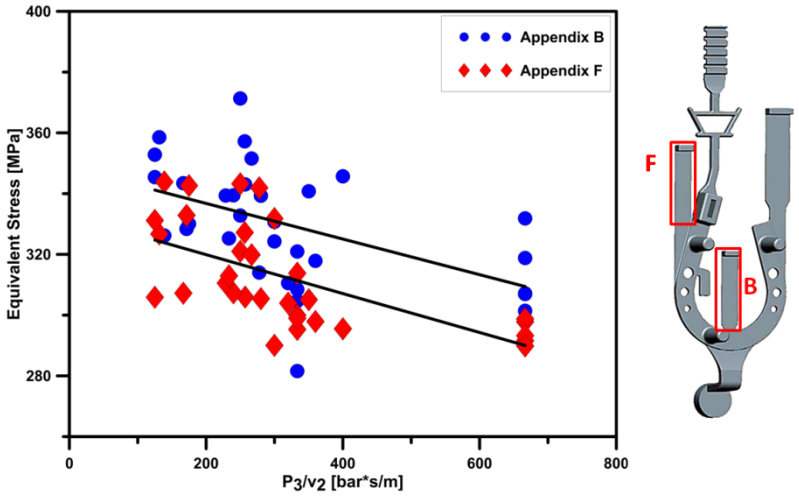

Figure 6. Correlation between intensification pressure-second phase velocity ratio and mechanical behavior.

In Fig. 6, it is possible to see that the filling and the intensification pressure are the most influential phases in HPDC.

Summary

The aim of this work was the identification of some preliminary correlations between HPDC process parameters and casting quality, especially mechanical and internal properties. The main findings obtained, with reference to the *horse-shoe* casting manufactured, are:

- The eutectic segregation affects the feeding mechanisms during the solidification process, causing an increase of porosity;
- the defect content on the fracture surfaces negatively influences the static properties and shows a decreasing trend by increasing the second phase velocity;
- the filling and the intensification pressure are the most influential phases in HPDC.

Acknowledgments

This work was developed within European MUSIC project (MUlti-layers control & cognitive System to drive metal and plastic production line for Injected Components, N. 314145). The authors would like to acknowledge Enginsoft, Electronics, Aalen University, MAGMA, Saen, MOTULTECH Baraldi. The authors are also immensely grateful to G. Mazzacavallo and E. Della Rovere (Department of Management and Engineering, University of Padova).

References

[1] F. Bonollo, G. Timelli, N. Gramegna, High Pressure Die Casting: Contradictions and Challenges, The Journal of the Minerals, Metals & Materials Society (2015) Italy.
[2] E. Fiorese, F. Bonollo, G. Timelli, L. Arnberg, E. Gariboldi, New classification of defects and imperfections for aluminum alloy castings, International Journal of Metalcasting (2015) Italy-Norway.
[3] W.G. Walkington, Die Casting Defects – Troubleshooting Guide, NADCA (2003) Arlington Heights, Illinois.
[4] J. Campbell, The 10 rules for good castings, in: Complete Casting Handbook, second ed. (2015) pp. 535-638.
[5] Information on http://www.stacast-project.org
[6] CEN/TR 16749, Aluminium and aluminium alloys – Classification of defects and imperfections in high pressure, low pressure and gravity die cast products (2014) pp. 1-41.
[7] E. Gariboldi, F. Bonollo, P. Parona, Handbook of defects in high pressure diecasting, second ed., AIM: Centro di studio pressocolata, Italy, 2010.
[8] E. Battaglia, F. Bonollo, G. Timelli, E. Fiorese, G. Kral, Correlation between process, microstructure and properties in High Pressure Die Casting Aluminum-Silicon alloys, AMPT2015 (2015) Madrid, under review.
[9] M. Winkler, L. Kallien, T. Feyertag, Correlation between process parameters and quality characteristics in aluminum high pressure die casting, NADCA Die Casting Congress & Exposition (2015).
[10] Information on http://music.eucoord.com/intro/body.pe

[11] E. Zanini, S. Barison, L. Capra, G. Timelli, F. Voltazza, Microstructure and bending properties of die-casting alloys at various chromium contents, La Metallurgia Italiana (2012) Italy.
[12] L. Lu, K. Nogita, S.D. McDonald, A.K. Dahle, Eutectic solidification and its role in casting porosity formation, JOM, Vol. 56, Issue 11 (2004) pp. 52-58.
[13] C.M. Gourlay, H.I. Laukli, A.K. Dahle, Defect band characteristics in Mg-Al and Al-Si high pressure die castings, Metallurgical and Materials Transactions A (2007) Australia
[14] M. S. Dargusch, G. Dour, N. Schauer, C. M. Dinnis, G. Savage, The influence of pressure during solidification of high pressure die cast aluminium telecommunications components, Journal of Materials Processing Technology, (2006).

SUPPLEMENT III

Overview of the correlations between process parameters, microstructure and mechanical properties of reference castings and industrial demonstrators

E. Battaglia, F. Bonollo, E. Fiorese, G. Kral; Key Engineering Materials, 2016, pp.35-40

Key Engineering Materials 2016
Taylor & Francis online

OVERVIEW OF THE CORRELATIONS BETWEEN PROCESS PARAMETERS, MICROSTRUCTURE AND MECHANICAL PROPERTIES OF REFERENCE CASTINGS AND INDUSTRIAL DEMONSTRATORS

E. Battaglia, F. Bonollo, E. Fiorese and G. Kral
DTG – University of Padova, Stradella S. Nicola 3, Vicenza, Italy

ABSTRACT

Among the Aluminum casting processes, High Pressure Die Casting (HPDC) is an efficient, versatile and economic way for producing large number of components. Nevertheless, because of the elevated amount of rejected castings, it is important to know which are the main causes of defect formation and their effects on microstructure and mechanical properties. This paper presents, within the European MUSIC project, an overview of the preliminary correlations obtained studying both castings with defect generator geometry, referred to as *Horse-shoe* Reference Castings, and industrial demonstrators, referred to as Gear Box Housing. The deduced correlations between static mechanical properties and casting defects highlighted interesting trends in both cases.

Introduction

Aluminum casting processes are very productive and versatile techniques for manufacturing semi- or finished products with complex shapes. The characteristics of these processes are continuously improved and developed in order to satisfy many needs and reach new markets.

Among the casting processes, High Pressure Die Casting (HPDC) is the most demanding in terms of volume. It plays a key role in the manufacturing of *near-net-shape* products with thin wall thicknesses and, therefore, reduced weights. Hence, by all of the biggest customers of the Aluminum foundry industry, there are the Automotive Manufacturers that aim to reduce the weights in order to fulfill the requirements for energy efficiency, cost savings and emission reduction.

The quality of a die cast part is defined by a multitude of parameters, which are hard to check [1]; there are many sequential actions in the three phases of the process that may affect the casting quality, i.e. injection of molten metal, solidification, casting extraction and lubrication system [2-4]. The lack of an adequate control of all the variables, that play a prominent role during the HPDC process, leads to the generation of various defects, which in turn can cause casting rejection. For this reason, the defect classification for HPDC components, introduced in

Ref. [5] and recently published as CEN/TR 16749:2014 [6], has been taken into account; according to this classification and to a recent survey carried out on the European foundry industry, the most common defects and imperfections normally found in die-cast Aluminum alloys are porosity (both due to gas entrapment and shrinkage) and filling-related defects, such as oxides, as shown in Fig. 1[5,7].

The main contribution of the present work, developed within the European MUSIC project [8], is the introduction of an overview on the preliminary correlations between process, casting defects and static mechanical properties obtained analyzing both Reference Castings characterized by a defect generator geometry and already commercialized industrial demonstrators. The former were developed in order to produce castings with different kinds of defects at different levels of severity, while the latter were aimed at applying at industrial scale the acquired findings. The noteworthy innovation adopted within the EU MUSIC project and specifically during the development of this work was the network of in-cavity and plunger sensors installed in the die and in the machine. The aim of these sensors was to monitor the whole process, i.e. pressure and temperature distributions inside the die cavity, besides the plunger motion profiles.

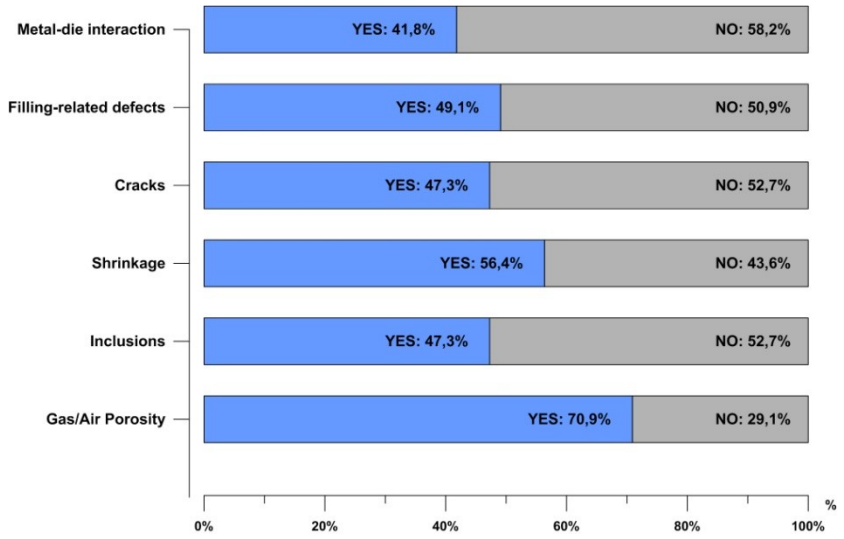

Figure 1. Extent of measurement/quantification of defects in die castings, as estimated by a survey carried out on European HPDC foundries [5,7].

Experimental procedure

Reference Die and industrial demonstrator. In the frame of the European MUSIC project, two test-products were used to produce castings with different injection parameters and hence with different quality characteristics. A Reference Die was designed and realized with the aim of producing Reference Castings with typical HPDC defects and a Gear Box Housing was chosen as industrial demonstrator (see Fig. 2).

Innovative intelligent sensor networks (ISN) [9] were installed in the machine and in the die cavity in positions sensitive to the process parameter variations in order to monitor the evolution of some variables during each manufacturing cycle. The parameters recorded were in cavity temperature and pressure profiles (represented in Fig. 2 with T_i and P_i) and plunger motion profiles.

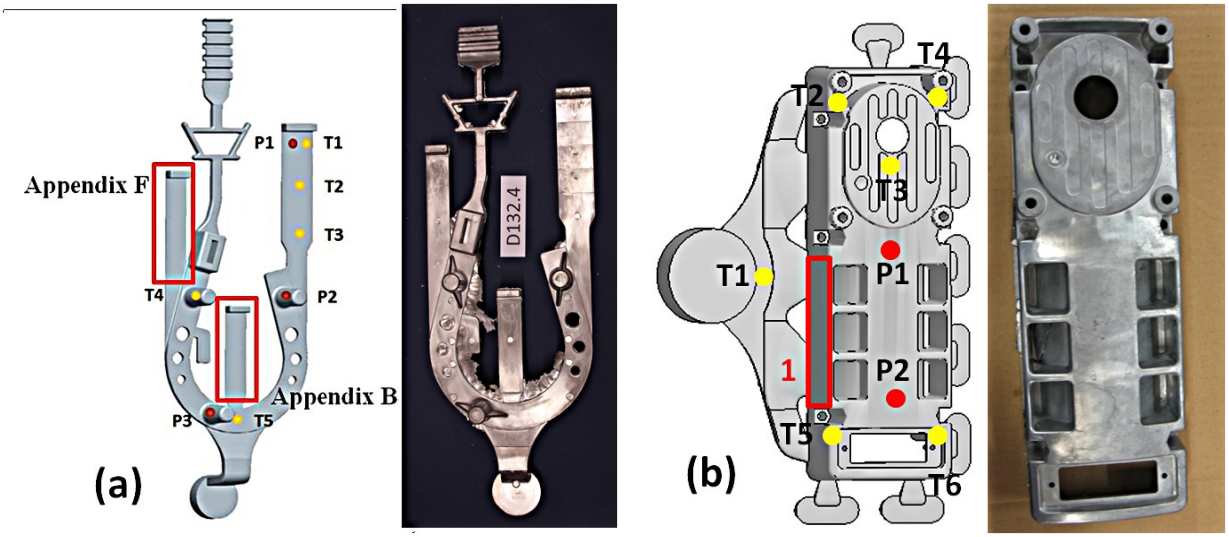

Figure 2. (a) *Horse-shoe* shaped Reference Casting, (b) Gear Box Housing with indicated the positions of the sensors and of the test samples.

Casting trials and quality control procedures. The analyzed castings were produced using two Aluminum alloys belonging to the EN AB-46000 and EN AB-46100 families according to UNI EN 1706. In Table 1, the chemical compositions measured by optical emission spectroscopy on separately poured samples are shown.

Table 1. Chemical compositions of the casting alloys [wt%].

Alloy	Si	Fe	Cu	Mg	Sr	Zn	Cr	Ni	Ti	Pb	Mn	Al
EN AB-46000	8-11	0,6-1,3	2-4	0,05-0,55	-	1,2	0,15	0,55	0,25	0,35	0,55	Bal.
Tested alloy	10,4	0,8	3	0,42	0,0001	0,9	0,04	0,05	0,05	0,06	0,3	Bal.
ENAB-46100	10-12	1,1	1,5-2,5	0,3	-	1,7	0,15	0,45	0,25	0,25	0,55	Bal.
Tested alloy	10,7	0,81	1,65	0,22	0,0001	1,44	0,08	0,06	0,07	0,07	0,22	Bal.

The Design of Experiments (DOE) consisted of 32 and 29 arrays respectively, i.e. process parameter changes, by leading to an overall amount of approximately 150 and 200 castings.

Some samples for mechanical testing and metallographic analysis were obtained from each casting, as indicated in Fig. 2. X-ray NDT investigation and microstructural analysis were performed to identify the defect distribution and morphology that vary with the process parameters used. Three point bending test was carried out according with ASTM E290-97a; more details about the tests executed are reported elsewhere [10,11].

Fractographic analyses were developed using a scanning electron microscope (SEM). The images obtained were investigated through an image analyzer in order to determine the oxide and porosity contents, as shown in Fig. 4.

Results and Discussion

Data extraction from sensors. The key parameters obtained through the manipulation of temperature and pressure sensor profiles were the maximum values and the corresponding time for both castings. Examples of temperature and pressure profiles, with reference to the sensor network installed on the *Horse-shoe* die, are given in Figs. 3a and 3b, respectively. Similar trends were extracted though the analysis of data collected by the sensor network installed on the Gear Box die. With reference to each array, a higher data scattering was associated to less process repeatability and in turn, worse casting quality.

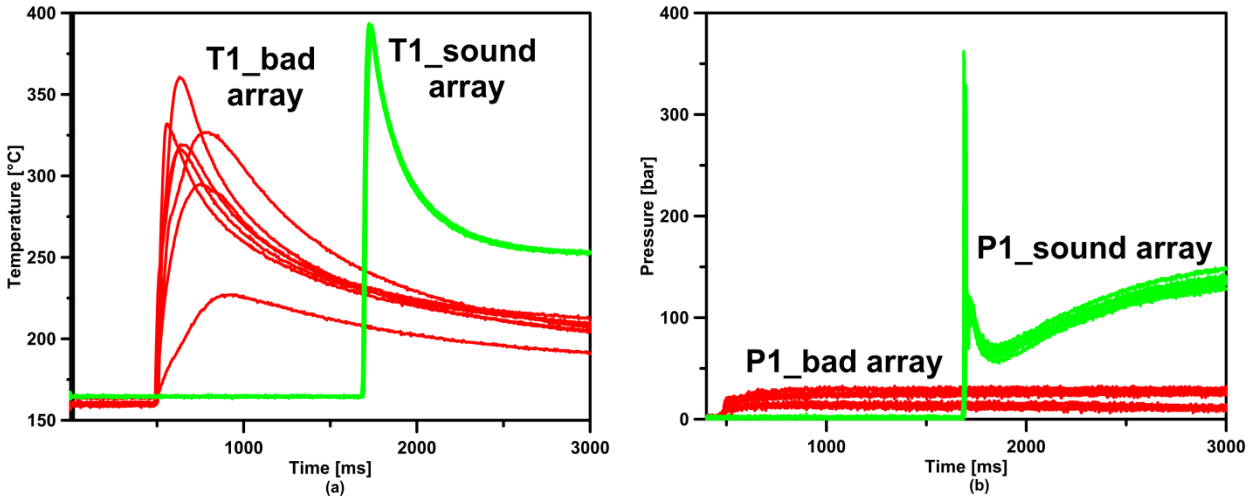

Figure 3. (a) Temperature and (b) pressure profiles of sensors T1 and P1 installed on the *Horse-shoe* die. Worst and best configurations are compared.

Bending tests and fractographic analyses. The details about the bending results, expressed as peak load (PL) and displacement to fracture, are reported in Ref. [10,11]. In Fig. 4, the secondary electron images obtained by means of SEM of the best and worst arrays with regard to both the geometries investigated are shown. The images show the part of the surface layer subjected to tensile stress in which a negligible amount of defects was detected (best cases, Figs. 4a and 4c) or a consistent amount of oxides and porosity was assessed (worst cases Fig. 4b and 4d). Fracture can nucleate because of internal and surface defects; nevertheless, the former are

less likely to cause yielding in bending test. Thus, defects concentrating on the stressed layer act as crack initiators leading to the sample failure [12]. Examples of microstructures belonging to both castings, show primary Aluminum dendrites, eutectic silicon, cold flakes, oxides, porosities and intermetallics (see Figs. 5a-c).

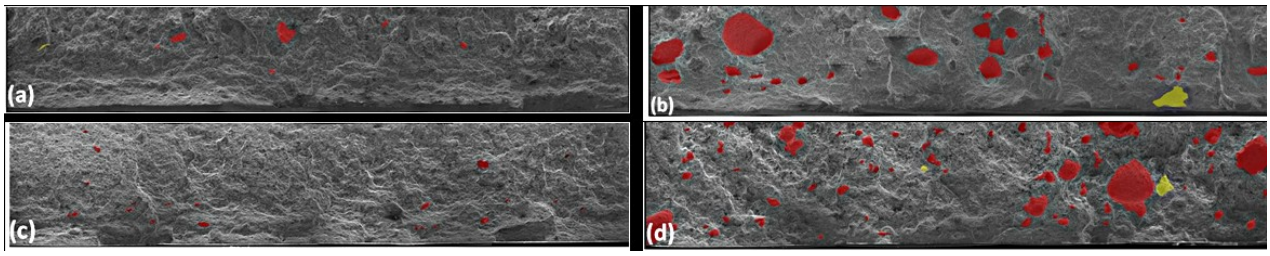

Figure 4. SEM images of best (a-c) and worst (b-d) arrays, referring to the *Horse-shoe* casting and the Gear Box respectively. The focus is on the side subjected to tensile stress.

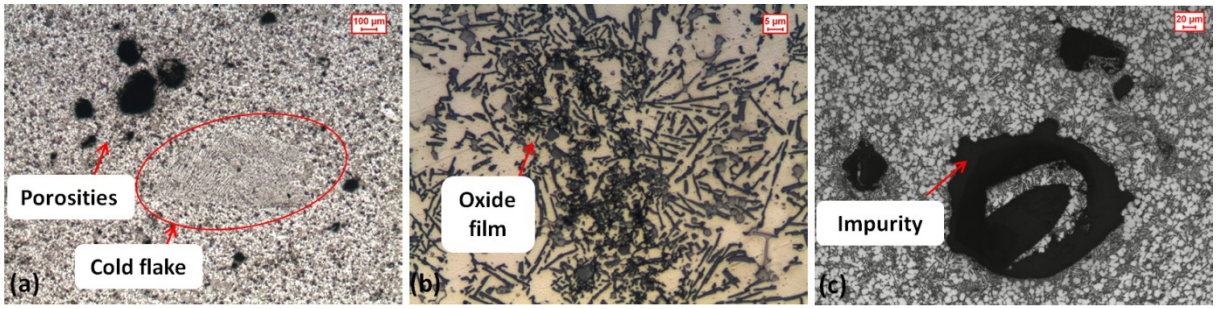

Figure 5. Examples of micrographies showing the most frequent identified defects: (a) porosities and cold flakes, (b) oxide films, (c) impurities (solid inclusions).

In Fig. 6, the preliminary correlations are shown; the main variables studied were bending test properties and casting quality in terms of porosity and oxide percentages. In both cases, the casting mechanical behavior is controlled by the defect content measured on the fracture surfaces. As already stated elsewhere [10,11], higher amounts of oxides and porosity lead to early casting yielding (Figs. 6a,b).

The correlations obtained studying the Reference Casting are more well-defined than those obtained analyzing the industrial demonstrator. The reason is that the former was designed and precisely aimed at generating defects that could be easily controlled, detected and assessed; moreover, the two castings show a different in-gate configuration. A branched gating system like those of the Gear Box gives good potentialities to direct the metal flow in desired zones, that is not true for the single gate. However, the process parameter variation associated with a more or less favorable geometry can cause a more swirling flow which results in more randomly distributed defects and thus in a higher scatter of mechanical results. Hence, the industrial demonstrator, with its more complex shape than the Reference Casting, results in less predictability and repetitiveness of the defect positions, leading again to a higher quality scattering.

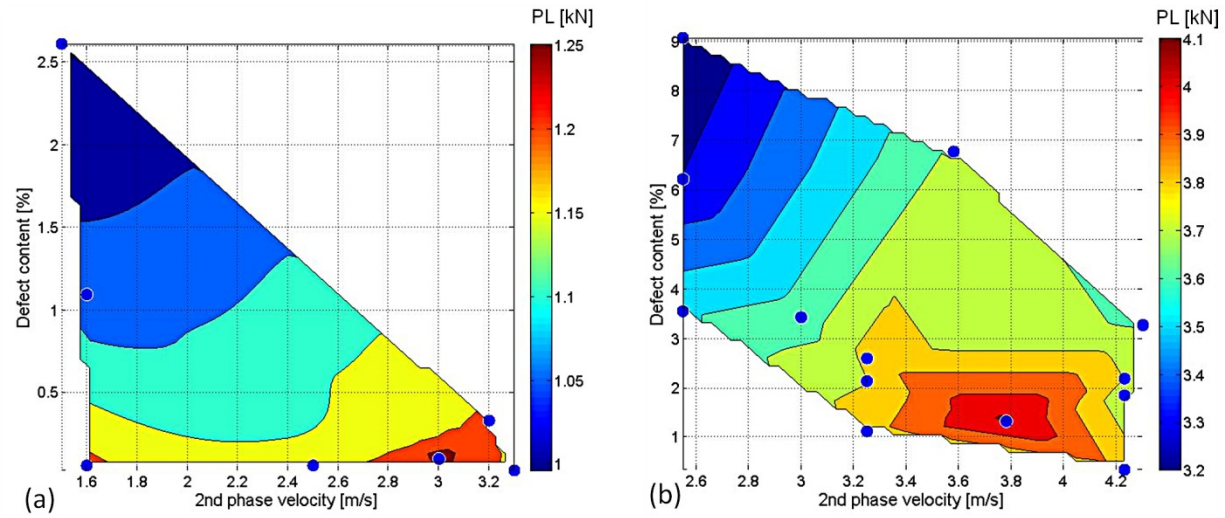

Figure 6. Preliminary correlations between defect content on the fracture surfaces and mechanical properties: (a) *Horse-shoe* casting, (b) Gear Box.

Summary

The aim of this work was to give an overview of the preliminary correlations obtained, within EU MUSIC project, from the study of a Reference Casting designed to generate typical HPDC defects and an already commercialized industrial demonstrator, i.e. Gear Box Housing. Based on the results reported in the present study, the following conclusions can be drawn.

- In both cases the defect content on the fracture surfaces negatively influences the casting mechanical behavior.
- The filling and the intensification pressure are the most influential phases in HPDC.
- The correlations obtained analyzing the Reference Castings can be extended to a real industrial demonstrator.

Acknowledgements

This work was developed in the frame of MUSIC project (MUlti-layers control & cognitive System to drive metal and plastic production line for Injected Components), supported by European Union - FP7-2012-NMP-ICT-FoF] under grant agreement number n°3141. The authors would like to acknowledge Enginsoft, Electronics, Aalen University, MAGMA, Saen, RDS, MOTULTECH Baraldi.

References

[1] M.S. Dargusch, G. Dour, N. Schauer, C.M. Dinnis, G. Savage, The influence of pressure during solidification of high pressure die cast aluminium telecommunications components, J. Mater. Proc. Tech. 180 (2006) 37-43.
[2] F. Bonollo, G. Timelli, N. Gramegna, High Pressure Die Casting: Contradictions and Challenges, J. of Metals 63 (2015) 901-908.
[3] E. Battaglia, F. Bonollo, G. Timelli, E. Fiorese, G. Kral, Correlation between process, microstructure and properties in High Pressure Die Casting Aluminum-Silicon alloys, Proc. AMPT2015 Int. Cong., Madrid (2015).
[4] E. Fiorese, F. Bonollo, E. Battaglia, G. Cavaliere, Improving die casting processes through optimization of lubrication, Int. J. Cast Metals Research (2016).
[5] E. Gariboldi, F. Bonollo, P. Parona, Handbook of defects in high pressure die casting, second ed., AIM, Milano, 2010.
[6] CEN/TR 16749:2014 Aluminium and aluminium alloys – Classification of defects and imperfections in high pressure, low pressure and gravity die cast products (2014) 1-41.
[7] E. Fiorese, F. Bonollo, G. Timelli, L. Arnberg, E. Gariboldi, New classification of defects and imperfections for Aluminum alloy castings, Int. J. of Metal Casting 9 (2015) 55-66.
[8] Information on http://music.eucoord.com/intro/body.pe
[9] U. Gauermann, A. Mazzamuto, N. Gramegna, An Integrated and Intelligent Sensor Network as tool for monitoring HPDC process parameters, Proc. 6th Cong. High Tec Die Casting, Venice (2016), AIM, Milan, paper nr. 69.
[10] E. Battaglia, F. Bonollo, I. Tonello, E. Fiorese, Correlations between defect content, mechanical properties and fractographic investigation of AlSi9Cu3(Fe) alloy Reference Castings, Proc. Thermec'2016 INt. Conf., Graz (2016).
[11] F. Bonollo, E. Battaglia, A. Brotto, G. Kral, A. Mazzamuto, Understanding quality of HPDC Aluminium alloy products from intelligent sensors network, Proc. 6th Int. Cong. High Tech Die Casting, Venice (2016), paper nr. 66.
[12] E. Zanini, S. Barison, L. Capra, G. Timelli, F. Voltazza, Microstructure and bending properties of die-casting alloys at various chromium contents, La Metallurgia Italiana 104 (2012) 3-13.

SUPPLEMENT IV

Experimental damage criterion for static and fatigue life assessment of commercial Aluminum alloy diecastings

E. Battaglia, F. Bonollo, P. Ferro; Metallurgical and Materials Transactions A, 2017, pp. 2574-2583.

Metallurgical and Materials Transactions A 2017
Springer

EXPERIMENTAL DAMAGE CRITERION FOR STATIC AND FATIGUE LIFE ASSESSMENT OF COMMERCIAL ALUMINUM ALLOY DIECASTINGS

E. Battaglia, F. Bonollo, P. Ferro
DTG – University of Padova, Stradella S. Nicola 3, Vicenza, Italy

ABSTRACT

Defects, particularly porosity and oxides, in high-pressure die casting can seriously compromise the in-service behavior and durability of products subjected to static or cyclic loadings. In this study, the influence of dimension, orientation, and position of casting defects on the mechanical properties of an AlSi12(b) (EN-AC 44100) Aluminum alloy commercial component has been studied. A finite element model has been carried out in order to calculate the stress distribution induced by service loads and identify the crack initiation zones. Castings were qualitatively classified on the basis of porosities distribution detected by X-ray technique and oxides observed
on fracture surfaces of specimens coming from fatigue and tensile tests. A damage criterion has been formulated which considers the influence of defects position and orientation on the mechanical strength of the components. Using the proposed damage criterion, it was possible to describe the mechanical behavior of the castings with good accuracy.

1. Introduction

Casting is a process by which almost all kinds of products can be manufactured. This explains why there are many different application areas for castings; furthermore, 100% of castings can be recycled. Among the casting materials, particular importance is put on non-ferrous metals and specifically, on Aluminum alloys.

Among all Aluminum casting technologies, High Pressure Die Casting (HPDC) is one of the most versatile and highly productive process: currently about half of the world production of light metal castings is obtained by this kind of process [1]. For 2020, a global Aluminum foundry production close to 17 million tons is expected [2]. HPDC allows the production of large numbers of near-to-shape components of complex geometry, thin wall thicknesses and very good surface finish and it is very economical for large scale production [3]. Nevertheless, the high number of sequential actions involved in the process may affect the casting quality and compromise its integrity[4-6]. As stated by J. Campbell [7], the directness of the process from the liquid metal to the finished product involves the greatest difficulty as many aspects must be controlled simultaneously.

A critical disadvantage of HPDC is the almost inevitable presence, in the produced castings, of surface and internal defects which are often hard to detect: oxide bifilms and confluence welds [8], porosity, primary intermetallic particles and many others [9-11]. Defect classification for HPDC components, introduced in Ref. [8], has been recently published as CEN/TR 16749:2014 [12]. According to this classification and to a recent survey carried out by the European foundry industry, some of the most common defects and imperfections normally found in high pressure die-cast Aluminum alloys are porosity (due to gas entrapment and shrinkage) and filling-related defects (i.e.: oxides) as illustrated in Fig. 1 [8,13].

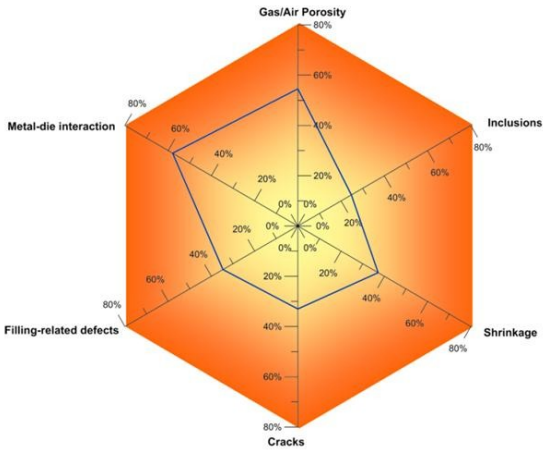

Figure 1. Frequency of defects in die castings, as estimated by European HPDC foundries [8,12,13].

In industry, different methods are used to detect casting defects and assess their quality. Visual inspection, magnetic particle and dye penetrant testing, radiographic analysis, ultrasonic and eddy current testing are the major six non-destructive investigation methods. Among them, the X-ray investigation is the main non-destructive testing (NDT) used within the HPDC foundries.

The influence of defects on both static and fatigue behavior of high pressure die cast Aluminum alloys has been studied by several researchers [14-16]. In literature, many approaches for static and dynamic strength prediction of HPDC magnesium and Aluminum alloys components have been proposed [3,17-21,25].

Gokhale et al. [17] and Timelli et al. [18] demonstrated that the mechanical properties decrease monotonically increasing the area fraction of defects revealed on the fracture surfaces of gravity cast and high pressure die cast Aluminum alloys. It is worth mentioning that even high integrity castings are expected to contain defects and it is thus important to be able to predict their effect on the mechanical properties of the component. Generally, two different ways based on constitutive models or statistical and stochastic approaches are used. Càceres et al. [19] carried out studies on Al-Si-Mg alloy tensile test samples. They showed that the dominant parameter is the area fraction of defect in the cross section, regardless of defect shape, number or distribution, in agreement with the predictions of their proposed analytical model. Timelli [18] studied the influence of casting defects on the static mechanical properties of high pressure

AlSi9Cu3(Fe) die cast samples. It was shown that defects influence only the elastic-plastic portion of the stress-strain curve; moreover, the defects area detected on the fracture surfaces can be used to establish the fracture point along the constitutive equation. Quantitative methods for predicting the relation between defects, notably their size, and fatigue life have been also developed. Skallerud et al. [20] mainly focused on the relation between shrinkage cavities and the fatigue life of an AlSi7Mg(0.4) alloy. They found that porosity makes the fatigue crack initiation period negligible compared to the total fatigue life. Typical fatigue cracks initiate around pores at, or near, the surface due to the high stress concentration generated by the defect itself. Wang at al. [21] carried out an experimental investigation on an A356 (EN AC42000 according with UNI EN 1706) Aluminum alloy concluding that the decrease in fatigue life is directly correlated to the increase of defect size. They also pointed out that flawed castings show a fatigue life of an order of magnitude lower compared to that of defects-free materials.

In this study, a numerical and experimental investigation has been carried out on AlSi12(b) commercial high pressure die castings. The influence of casting defects, i.e. oxides and porosity, on static and fatigue strength of the analyzed components was assessed. A damage criterion was finally proposed which adopts information coming from fractographic analysis and simulated stress distribution bands to describe the mechanical behavior of the castings.

2. Experimental procedure

An AlSi12(b) Aluminum alloy was adopted to produce HPDC fixing elements used in tripods for photographic kits (Fig. 2). The casting includes four appendixes: two are fastened to the tripod leg and two can be opened and closed in order to allow the lengthening of the telescopic leg.

The moving parts of the component were labeled as A- and B-side, as shown in Fig. 3; however, the focus was put only on the B-side since experiments and numerical simulation showed it was the most critical one.

The alloy chemical composition is summarized in Table 1.

Net-to-shape castings were produced using a multicavity die in a horizontal cold chamber high pressure die casting machine whose process parameters were optimized and constant.

Table 1. Chemical composition of the experimental alloy (wt pct); the Composition Limits of AlSi12(b) Alloy (EN AC-44100) are also reported according to EN1706:2010 Standard

Alloy	Si	Fe	Cu	Mg	Mn	Ni	Ti	Zn	Al
EN AC-44100	10.5 - 13.5	0.65	0.15	0.10	0.55	0.10	0.20	0.15	Bal
Tested alloy	13	0.458	0.083	0.023	0.294	0.008	0.032	0.116	Bal.

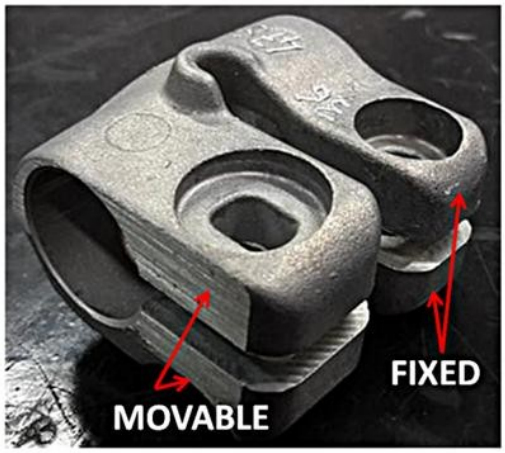

Figure 2. The tested casting used in photographic tripods.

Figure 3. A- and B-sides of the component

2.1.Strain gage analysis

In order to determine the deformation induced by the service loads on the component, two strain gages were placed on the B-side of the component (Fig. 4). The surfaces of interest were cleaned with a grinder and smoothed out to remove debris that might have been created from the grinding. Finally, a solvent specifically designed to prepare surfaces for bonding was used. Once the surface was clean, it was roughened to improve the bonding power by increasing the active surface area. The applied strain gages were metallic foil gages arranged in a grid pattern, HBM 0.6/120 LY41. A tightening torque of 1.8 Nm was applied in order to clamp the casting to the support.

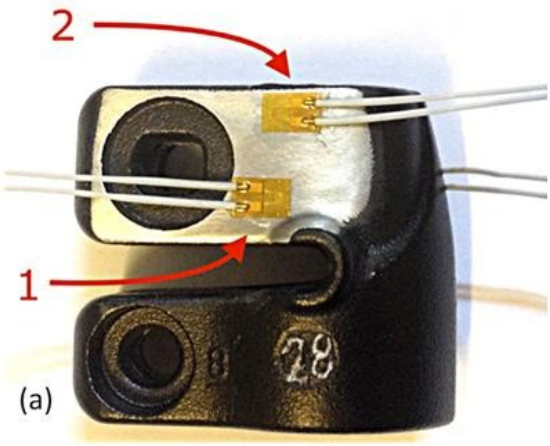

Figure 4. Strain gages locations on the B-side of the component

Table 2. Material characteristics

E [MPa]	ν	ρ [kg/dm^3]
71000	0.33	2.66

2.2.FE analysis

A numerical model was carried out by means of Ansys® Workbench 14.5 in order to calculate the stress and strain distributions induced by service loads on the component.

Elastic and elastic-plastic properties of AlSi12(b) at room temperature were evaluated by means of preliminary static tensile tests on standard specimens, according to ASTM E8-04. The material was assumed to be isotropic and the true stress-strain curve obtained from tensile tests was implemented in the numerical model; Young modulus (E), Poisson's ratio (ν) and material density (ρ) are listed in Table 2.

In order to accurately capture the 3D stress distribution, a higher mesh density was applied on the hole contact surfaces and close to the critical point shown in Fig. 5a. After few convergence tests, the optimized mesh showed a total of 59586 tetrahedral elements. It is worth observing (Fig. 5b) that the portion of the tripod on which the component had to be fastened during service was also modelled.

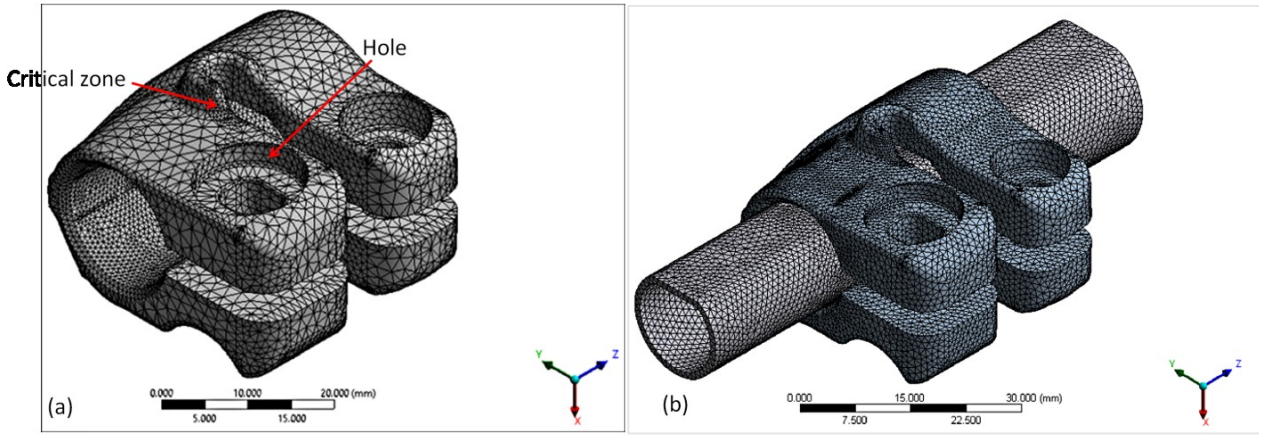

Figure 5. (a) Geometry and mesh division of the 3D finite element model; (b) final model with steel support.

Due to the presence of an initial gap between casting and support and their subsequent contact after the load application, a *symmetric frictionless* contact type was defined between the internal surface of the component and the external surface of the support. The *Augmented Lagrange* was chosen as solver algorithm; it is a penalty-based approach described by Equation (1):

$$p = k_n x_n + \lambda \tag{1}$$

where k_n is the contact stiffness, x_n is the resulting penetration which, during the Newton-Rapson iterations is checked against an automatically-calculated maximum allowable penetration tolerance ϵ_n and p is the contact pressure. If $x_n \geq \epsilon_n$ then λ is increased and a message is printed indicating the number of contact points that have excessive penetration.

Fig. 6 shows the applied forces (A-D) and the constraints (E-G) imposed on the four ends of the component.

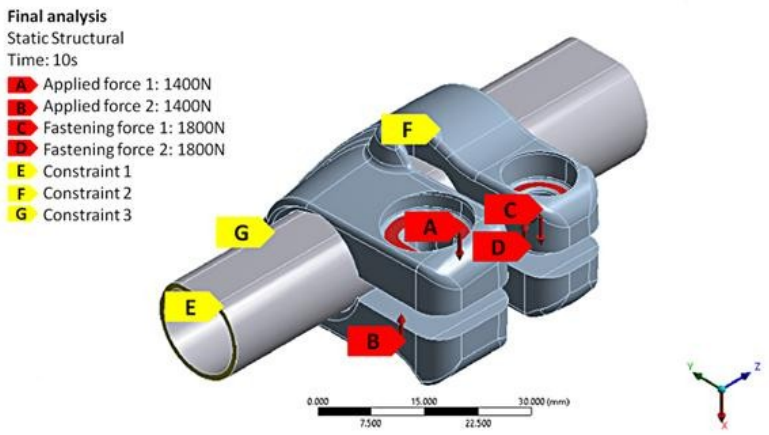

Figure 6. Applied loads and constraints.

2.3.Stress distribution mask elaboration

The main focus was put on the B-side of the component since experiments showed it to be the weakest part. The fracture surface turned out to be the section near the geometrical critical point, identified by a sudden change in the casting thickness (Fig. 7). For this reason, the stress distribution on that was deeply analyzed.

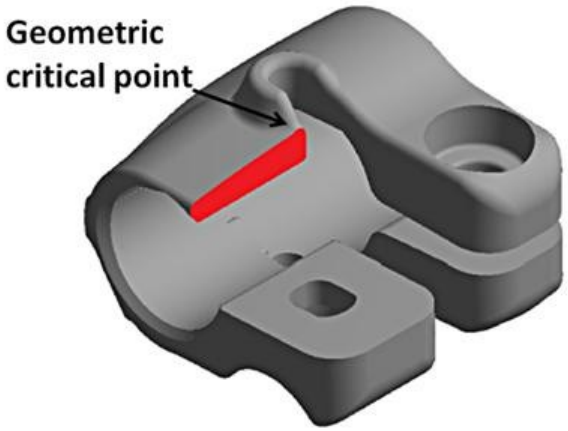

Figure 7. Position of the stress distribution mask

2.4. X-ray analysis, mechanical testing and fractographic investigation

Radiographic examinations were performed in order to detect possible inner defects before subsequent destructive tests. A micro-focus radiographic inspection was carried out, according to UNI EN 12681:2006 [22] and focusing on the geometrical critical area of the casting, in order to detect the presence of porosities due to gas/air entrapment or shrinkage. A current and a voltage of 100 μA and 78.9 kV respectively, were adopted for all the radiographies captured, one for each component. The X-ray images were then analyzed in order to define a casting qualitative classification base on the highlighted porosities.

The static mechanical tests were carried out on a computer controlled tensile testing machine MTS Criterion C43; the crosshead speed was 2 mm/min. The component was clamped by means of the fixed appendixes (Fig. 2) on a framework (Fig. 8) specifically designed with a tightening torque equal to 1.8 Nm; the load was then applied, via the crosshead, on the position shown in Fig. 8, so as to reproduce the real service force. Thirteen specimens were tested.

Figure 8. Static mechanical test

The fatigue tests were conducted on a servo-hydraulic MTS 858 Mini Bionix test system with a load cell capacity of 25 kN. The load-controlled fatigue tests were carried out at room temperature and a constant frequency of 5 Hz; the nominal load ratio, R, was kept constant and equal to 0.1. Two load ranges were adopted (1125 N and 1350 N) and ten specimens were tested. The component was clamped on the same framework used during the static tests and shown in Fig. 8.

The fracture surfaces of all the tested specimens were analyzed by using a scanning electron microscope (SEM). The normal stress distribution mask obtained from the FE model was superimposed to each fractographic image (Fig. 9). The obtained images were analyzed by means of an image analysis software; porosities and oxides on the fracture surface were quantified in terms of their projected areas and distances from the stress concentration zone near the geometry discontinuity, as illustrated in Fig. 9.

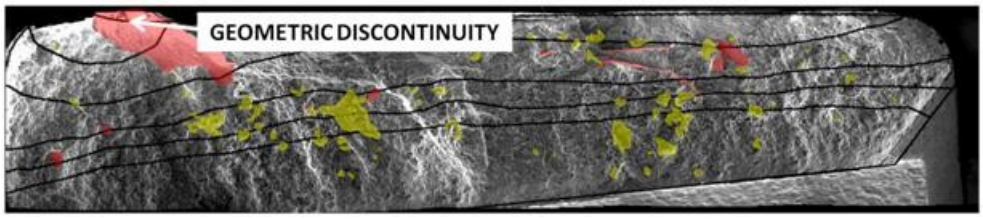

Figure 9. Oxide and porosity quantification.

3. Results and discussion

3.1 Experimental and numerical results

The maximum von Mises stresses were found to be approximately 208 MPa and 261 MPa, corresponding to the applied forces of 1000 N and 1400 N respectively, as shown in Figs. 10a

and 10b. The choice of these two force values was made in agreement with those normally used to fix the telescopic leg.

As expected, a stress concentration was found near the region characterized by a severe thickness variation. Due to the bending effect induced by the clamping forces, tensile stresses were calculated in that zone. In both load-cases the peak value exceeded the material yield stress (i.e. 125-165 MPa according to standard UNI 4514 and preliminary tensile tests) leading to permanent deformation and casting failure during its service.

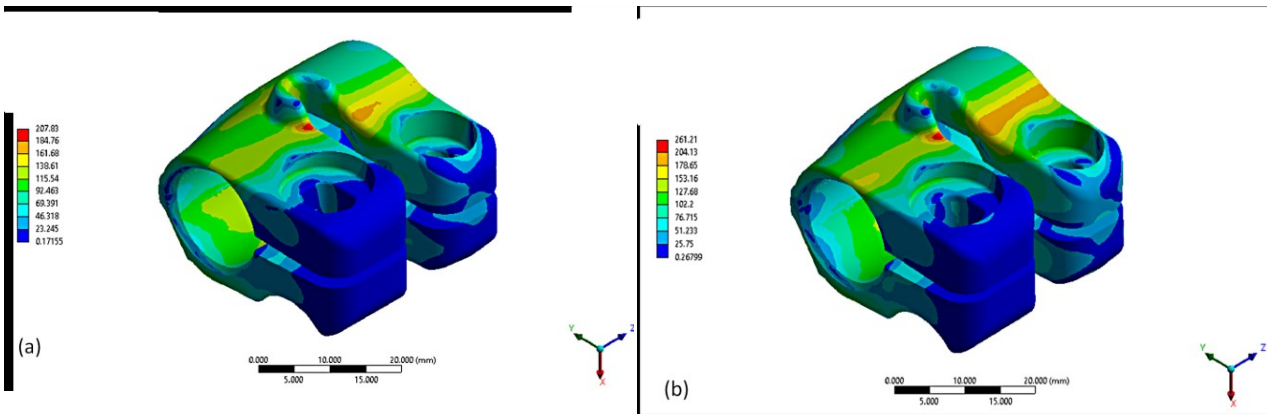

Figure 10. Equivalent Von-Mises stress distributions with an applied force of (a) 1000 N and (b) 1400 N.

The reliability of the model was verified by comparing the με values registered through the strain gages and those calculated by the model. Results are summarized in Table 3.

It can be noted that there is a good match between experimental and simulated results as the disagreement between the obtained values can be considered negligible.

Table 3. Comparison strain gage-Fe results

Strain gage	Experimental με	FE με	Error [%]
1	4800	4810	0.2
2	4500	4420	1.8

3.2 X-ray qualitative classification

A casting qualitative classification was carried out on the basis of the radiographic investigation, according with ASTM E0505-01 [23]. Castings were divided into three classes as shown in Figs. 11(a-c): (a) *good* castings presented no defects close to the geometric critical point, (b) *acceptable* castings showed small or negligible defects, (c) *bad* castings were characterized by a significant amount of defects detected within the area of interest. The micro-focus radiographic investigation can detect only porosities due to entrapped air/gas, shrinkage or local filling problems. Indeed, intermetallic compounds and oxide films are often difficult, if not

impossible, to be detected since they are characterized by very small dimensions, sometimes negligible, and a density close to that of the surrounding material.

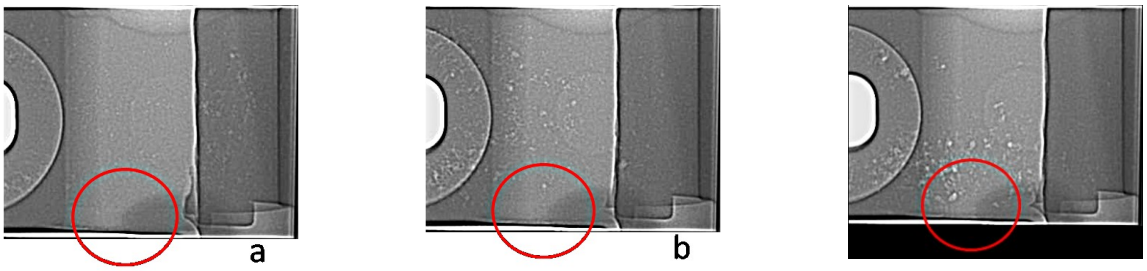

Figure 11. Qualitative classification according to x-ray inspection: (a) good, (b) acceptable and (c) bad casting.

In Table 4 the total amount of inspected castings and their qualitative classification are reported.

Table 4. X-ray qualitative classification results

Analyzed samples	Good	Acceptable	Bad
69	35%	51%	14%

3.2 Static and fatigue mechanical testing and fractographic results

The maximum load at break [kN] and the corresponding displacement [mm] ranged from 3.34 to 5.43 kN and from 1.21 to 1.64 mm, respectively. In Fig. 12a the maximum load at break-displacement data are plotted as a function of qualitative casting classification; it should be noted how the casting quality prediction based only on the x-ray investigation is misleading. Indeed, many castings showing the best properties concerning the x-ray qualitative classification, proved to be the worst regarding the mechanical behavior and vice versa [24].
Fig. 12b shows the number of cycles to failure as a function of qualitative casting classification.

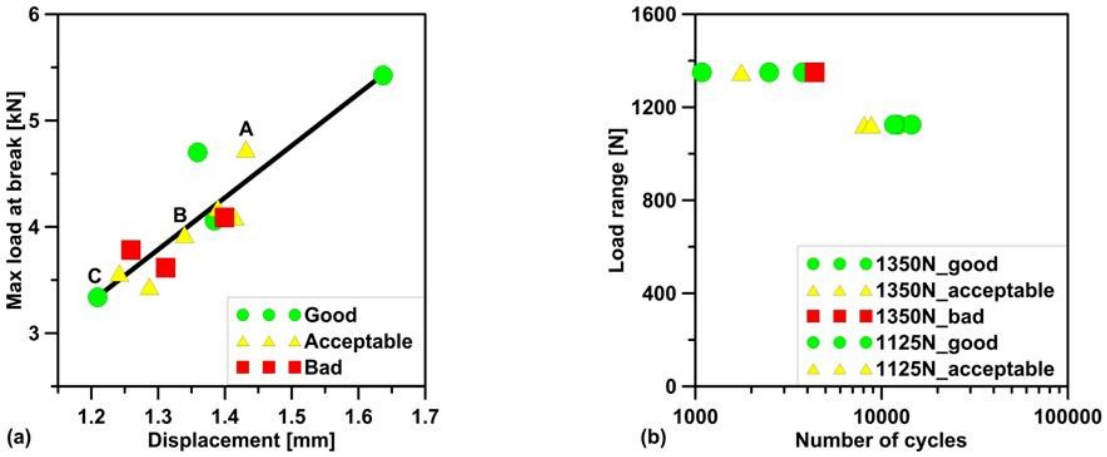

Figure 12. Mechanical results of (a) static and (b) fatigue tests with reference to the x-ray qualitative

classification

Similarly to static tests, the disagreement between radiographic and fatigue properties is due to the fact that, even though radiography is one of the oldest and most widely used methods of non- destructive testing, oxides are more difficult to be observed than porosities which, on the contrary, were adopted as qualitative discriminating element. X-ray analysis uses radiation energy to penetrate the casting and assess variations in thickness or density, generating a 2D shadowgraph of a 3D object; therefore, information in depth and volume can only be obtained observing the object with several orientations, when possible. In this regard, the x-ray equipment is not the most precise device to reveal the presence of all the defects and their relative orientation and position towards the critical point. In Figs. 13(a,b) it can be observed, as stated by Campbell [7], that a large pore in a low-stressed area of the casting may be far less detrimental than a small bifilm near the sharp corner subjected to a high tensile stress.
Furthermore, as it is well known [20, 25], the fatigue life of cast Aluminum alloys is significantly influenced by fatigue cracks initiated from defects near the surface; the region where the fracture initiates is much more important than the propagation one.

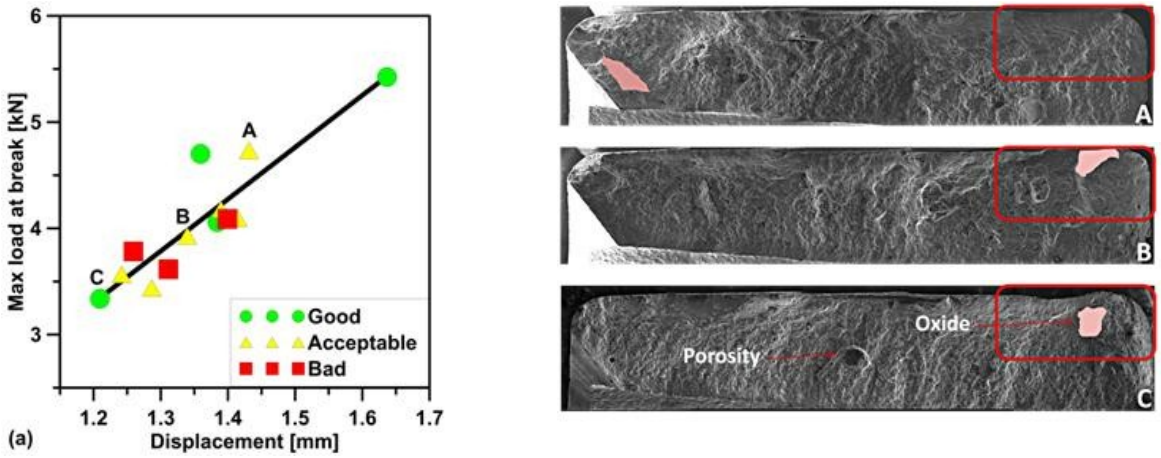

Figure 13. (a) Misleading casting quality prediction only based on the x-ray investigation; (b) fracture surfaces (oxides film are marked in red)

Negative contribution to the casting mechanical properties is given also by oxide orientation; the surface of an oxide parallel to the fracture surface has the most detrimental effect on the casting mechanical behavior. As a matter of fact, oxide films act similarly to cracks in terms of stress concentration and load-bearing area reduction; they easily propagate if critically oriented with respect to the applied load (pure Mode I of crack opening) [26].

In the fracture surfaces of castings A, B and C shown in Fig. 13b, the critical area is identified with a red square. Despite casting C is classified as good according with the x-ray analysis, it shows poor mechanical properties; on the contrary, casting A, judged as acceptable,

reaches a good mechanical resistance. Casting A actually shows a big oxide film located far from the critical area and not parallel to the fracture surface. Moreover, the oxide film detected in casting B, even though detected within the red square, has a less harmful effect on the mechanical properties compared to that observed in casting C because of its orientation less favorable to crack propagation.

3.3 Damage criterion elaboration

Since the casting's mechanical behavior is strongly influenced by oxide and porosity dimension [19,27], shape, orientation and position towards the critical region, a damage criterion was elaborated in order to take simultaneously into account all these features.

The stress distribution at the fracture surface, obtained from the FE model, was used to give each defect a precise weight according to its position.

The 9 bands or zones displayed in Fig. 14a, were inferred from the FE normal stress distribution; each band was characterized by a stress interval. Notably, because of the geometrical stress concentration effect, the bands closer to the critical corner showed the highest stress values. Such values gradually decrease moving towards the compression zone (bands 6 to 9).

In the proposed damage criterion, the five bands subjected to tensile stress were the only ones taken into account (active bands) as only the defects located within those regions were supposed to degenerate and lead to the component failure.

The superimposition of the stress band distribution mask and the actual fracture surface (Fig. 14b), allowed the calculation of a Penalty Index as defined in Eq. (2).

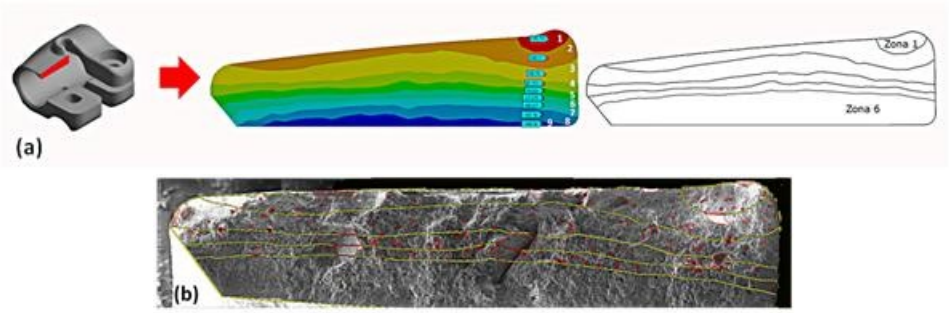

Figure 14. (a) Normal stress band distribution mask, (b) defect detection through mask superimposition.

$$PI = \sum_{z=1}^{N} \left[\frac{A_D}{(A_{SB})_z} * (W)_z \right] \qquad (2)$$

In Eq. (2) projected area, orientation and position of all defects were taken into account simultaneously; z refers to the stress band (1 to 5 as already mentioned); N is the number of active bands (N = 5); A_D is the projected area of each defect detected on the fracture surface by

means of an image analysis software; A_{SB} refers to the area of the z^{th} stress band and W is the weight attributed to each stress band and determined according to Eq. (3).

$$W_z = \frac{(\sigma)_z}{(\sigma)_5} \quad (3)$$

In Eq. (3) the σ is the average normal stress of each z^{th} band (1-5, active bands). The calculated values are plotted in Table 5.

Table 5. Weight values for the Penalty Index calculation

	Zone 1	**Zone 2**	**Zone 3**	**Zone 4**	**Zone 5**
Average stress value [MPa]	182	142	102	61	20
W	9.1	7.1	5.1	3.05	1

In Tables 6 and 7 the static and fatigue strength results, expressed in terms of Maximum load at break and Cycles to failure respectively, are listed together with the Penalty Index values. It is observed that the proposed damage criterion provides good results; indeed, sounder castings (i.e. B and D) show better mechanical properties and lower PI values because of their lower defects content or dangerousness.

Table 6. Penalty Index results of A (Worst) and B (Best) castings according to static testing

Casting	**Peak Load [kN]**	**PI parameters**	**Zone 1**	**Zone 2**	**Zone 3**	**Zone 4**	**Zone 5**	**PI**
A Worst	3.44	DA [mm^2]	0.496	0.555	0.258	0.192	0.049	3.844
		SBA [mm^2]	1.48	8.35	10.64	5.94	4.87	
		W	9.35	7.25	5	3	1	
B Best	4.73	DA [mm^2]	0	0.043	0.294	0.092	0.313	0.286
		SBA [mm^2]	1.48	8.35	10.64	5.94	4.87	
		W	9.35	7.25	5	3	1	

Table 7. Penalty Index results of C (Worst) and D (Best) castings according to fatigue testing

Casting	Cycles to failure-1350 N Load range	PI parameters	Zone 1	Zone 2	Zone 3	Zone 4	Zone 5	PI
C Worst	1084	DA [mm^2]	0.05	0.626	0.999	0.721	0.4	1.816
		SBA [mm^2]	1.46	8.21	10.33	5.79	4.61	
		W	9.35	7.25	5	3	1	
D Best	4380	DA [mm^2]	0	0.198	0.297	0.264	0.153	0.489
		SBA [mm^2]	1.46	8.21	10.33	5.79	4.61	
		W	9.35	7.25	5	3	1	

In Figs. 15 a,b the mechanical results are plotted as a function of the Penalty Index; best and worst castings are also pointed out.

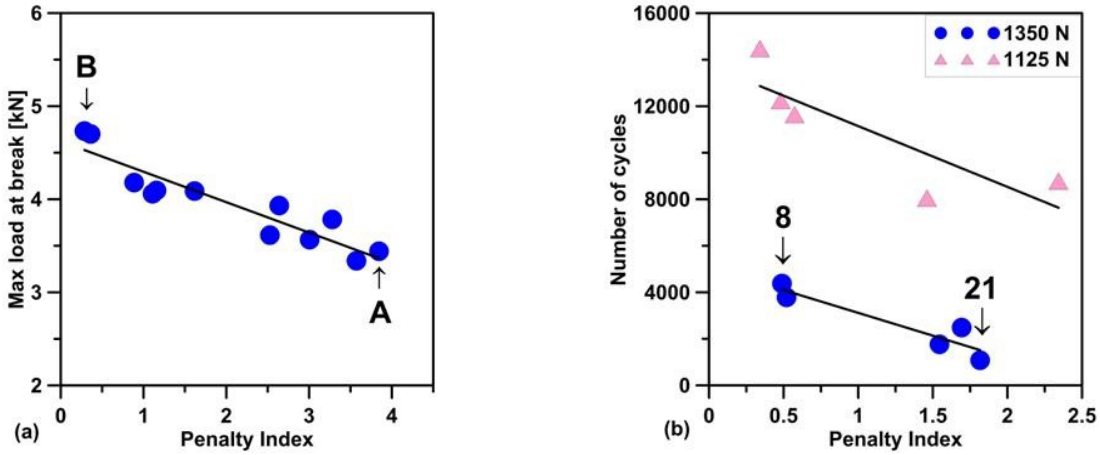

Figure 15. Correlations between the penalty index and (a) static and (b) fatigue mechanical properties

Figs. 15a and 15b confirm that both oxides and porosities control the casting mechanical behavior which is well described by the Penalty Index.

With regard to the fatigue life, the defects that initiated the crack were those located within the region that showed the typical fatigue slip bands displayed in Figs. 16a-c (i.e. bands 1 and 2 with reference to Fig. 14a). In agreement with the proposed criterion, a more penalizing factor was attributed to these defects as already described.

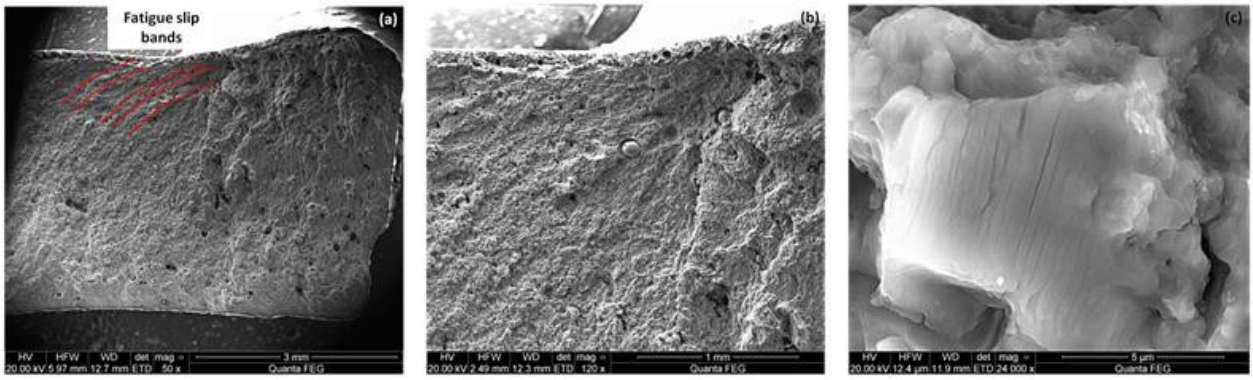

Figure 16. (a) SEM image of the region where the fatigue crack initiates, the fatigue slip bands are highlighted, **(b)** higher magnification of (a) and **(c)** Al matrix with visible fatigue slip bands; no evidence of these bands far from this region

Even if X-ray investigation is widely used in controlling the quality of the castings, it was shown that it is often not sufficient to assess the real quality of the components. As a matter of fact, it was not able to detect all kinds of defects (i.e.: oxide films) which are very detrimental for the mechanical properties of the castings.

In this regard, the proposed damage criterion is able to quantify the effect of defects on the mechanical properties of the castings. The main drawback is that it is a "post-mortem" approach and it can be implemented only after the component testing. Anyway, it is expected that, thanks to the wider diffusion of industrial high resolution Computer Tomography (CT) techniques, the proposed criterion can be adopted also for predictive analyses.

Finally, it is authors' opinion that the proposed damage criterion can be used also for different casting geometries characterized by blunt notches, prior suitable FE analysis of the real in-service behavior. Further works are necessary to evaluate also the effect of stress singularity induced by sharp (zero radius) V notches.

4. Conclusions

In this study, a numerical and an experimental investigation have been carried out on AlSi12(b) commercial high pressure die castings. Static and fatigue tests were carried out in order to both assess their mechanical properties under in-service conditions and validate the numerical model. Fractographic analyses were preformed in order to evaluate the defects influence on mechanical properties of the castings by means of the definition of Penalty Index.

The following conclusions can be drawn from this work:

1. the casting mechanical behavior cannot be predicted only on the basis of porosity content detected through the radiographic equipment;
2. oxides are difficult to be observed using x-ray analysis since they are characterized by a material density close to that of the Aluminum alloy and tiny dimensions;

3. casting defects have a detrimental effect both on static and fatigue life: the deterioration of the mechanical properties is directly correlated to defects projected area and their relative position towards the stress concentration zone;
4. the elaborated damage criterion based on FE model and fractographic investigation, gives satisfactory predictions of both static strength and fatigue life of castings containing defects.

Acknowledgements

The authors are indebted to Eng. A. Cenghialta for his support during the experimental work and to G. Mazzacavallo (Department of Management and Engineering, University of Padova, IT) for valuable discussions and comments.

References

[1] Bonollo F., Gramegna N. and Timelli G.: *JOM*, 2015, vol. 67 (5), pp. 901-908.
[2] PRESS DPT. GIFA 2015, Proc. 13th Int. Foundry Trade Fair, Dusseldorf (2015), Germany, Art. n1
[3] Avalle M., Belingardi G., Cavatorta M.P. and Doglione R.: *International Journal of Fatigue*, 2002, vol. 24, pp. 1-9.
[4] Fiorese E., Richiedei D., Bonollo F.: *International Journal of Advanced Manufacturing Technology*, 2016, pp. 1-10.
[5] Fiorese E., Bonollo F.: *Metallurgical and Materials Transactions A*, 2016, pp. 1-13.
[6] Fiorese E., Richiedei D., Bonollo F.: *Metallurgia Italiana*, 2016, 108 (6), pp. 21-24.
[7] Campbell J.: *Castings*, 2nd edn., Butterworth-Heinemann, Bodmin, 2003, pp. 352.
[8] Gariboldi E., Bonollo F. and Parona P.: *Handbook of defects in high pressure die casting*, 2nd ed., AIM, Milano, 2010.
[9] Laukli H.I., Gourlay C.M. and Dahle A.H.: *Mater. Sci. Eng. A*, 2005, vol. 413-414, pp. 92-97.
[10] Timelli G. and Bonollo F.: *Mat. Sci. Eng. A*, 2010, vol. 528, pp. 273-282.
[11] Laukli H.I., Gourlay C.M. and Dahle A.H.: *Met. Mater. Trans. A*, 2005, vol. 36, pp. 805-818.
[12] CEN/TR 16749:2014 Aluminium and aluminium alloys – Classification of defects and imperfections in high pressure, low pressure and gravity die cast products 2014;1-41.
[13] Fiorese E., Bonollo F., Timelli G., Arnberg L. and Gariboldi E.: *Int. J. of Metal casting*, 2015, vol. 9, pp. 55-66.
[14] Battaglia E., Bonollo F., Tonello I., Fiorese E.: *Materials Science Forum*, 2017, 879, pp. 193-198.
[15] Battaglia E., Bonollo F., Fiorese E., Kral G.: *Key Engineering Materials*, 2016, 710, pp. 35-40.
[16] Sanna F., Fabrizi A., Ferraro S., Timelli G., Ferro P., Bonollo F.: *Metallurgia Italiana*, 2013, 105 (4), pp. 13-24.
[17] Gokhale A.M. and Patel G.R.: *Scripta Mater*., 2005, vol. 52, pp. 237-241.
[18] Timelli G. and Bonollo F.: *Metal.Sci Tech.*, 2008, vol. 26, pp. 2-8.
[19] Caceres C.H. and Selling B.I.: *Mater. Sci. Eng. A*, 1996, vol. 220, pp. 109-116.

[20] Skallerud B., Iveland T. and Harkegard G.: *Eng. Fract. Mech.*, 1993, vol. 44, pp. 857-874.
[21] Wang Q.G., Apelian D. and Lados D.A.: *J. of Light Metals*, 2001, vol. 1, pp. 73-84.
[22] UNI EN12681, Founding – Radiographic Examination, European Committee for Standardization, Brussels, 2006.
[23] ASTM E0505-01, Standard Reference Radiographs for Inspection of Aluminium and Magnesium Die Castings, ASTM International, United States, 2001.
[24] Battaglia E., Bonollo F., Ferro P., Cenghialta A. and Mazzacavallo G.: *Metallurgia Italiana, 2016, vol. 108 (6), pp.*61-64.
[25] Lados D.: Ph.D thesis, WPI, Worcester USA, 2004.
[26] Campbell J.: *Complete Casting Handbook*, 2nd ed., Elsevier, Oxford, 2015.
[27] Timelli G.: *Metal. Sci. and Tech.*, 2010, vol. 28-2, pp. 9-17.

SUPPLEMENT V

Effect of heat treatment on commercial AlSi12Cu1(Fe) and AlSi12(b) Aluminum alloy diecastings

E. Battaglia, F. Bonollo, P. Ferro, A. Fabrizi; Submitted to Metallurgical and Materials Transactions A, 2017.

Submitted to **Metallurgical and Materials Transactions A 2017**
Springer

EFFECT OF HEAT TREATMENT ON COMMERICAL AlSi12Cu1(Fe) and AlSi12(b) ALUMINUM ALLOY DIECASTINGS

E. Battaglia, F. Bonollo, P. Ferro, A. Fabrizi
DTG – University of Padova, Stradella S. Nicola 3, Vicenza, Italy

ABSTRACT

High Pressure Die Castings (HPDCs) cannot normally be heat treated at high temperature because of the presence of inner air/gas or shrinkage pores that may lead to the formation of undesired surface blisters. In the present paper, an unconventional heat treatment is proposed. Two secondary Al-Si alloys, i.e. an AlSi12(b) and an AlSi12Cu1(Fe) alloy, have been stabilization heat treated at 624 K (350 °C) with a soaking time ranging from 1 to 8 hours. The enhancement of both static and dynamic mechanical propertieshas been found to be related to the fragmentation of the interconnected eutectic Si particles and the smoothing of coarser crystals.The achievement of more ductile alloysis confirmed by the decrease in Si particles roundness and hardness properties. The formation of Si precipitates within the α-Al matrix has been also highlighted.

1. Introduction

Worldwide, Aluminum foundries benefit from the trend towards light-weight construction since Aluminum combines low density with reasonable strength. For 2020, the global Aluminum foundry production is expected to reach 17 million tons[1]. It is therefore fundamental to benefit from economically suitable processes that can give high production rates, light-weight products with close dimensional tolerances and smooth surface finishes. Among them, approximately more than 60% of the global production of Aluminum alloys castings is obtained by High Pressure Die Casting (HPDC) which is the manufacturing process that better fulfills all the requirements. Moreover, one of its advantages including a higher production rate than that achieved with gravity or low-pressure die casting processes and the ability to produce castings with close dimensional tolerances, is also the reduced machining operations required[2,3].

However, several operations and processes are involved in the whole HPDC technology from the liquid metal to the finished shape [4].Due to the complexity of the process, HPDC castings generally contain undesired features such as pores due to entrapped gas or shrinkage, oxide skins or cold shuts, hard primary intermetallic particles and others [5–9].

It is known that in HPDC the molten metal experiences an extreme turbulent flow as it is forced into the die at high speed and a very rapid solidification rate is reached. Consequently, the inevitable internal porosity is one of the prevalent defects in HPDCs that makes, for instance, producing pressure tight parts difficult. Moreover, the presence of gaseous phases under high pressure (Figure 1) has the disadvantage that conventionally produced HPDC components cannot subsequently be heat treated at high temperatures without causing undesirable flaws, particularly blisters [10].

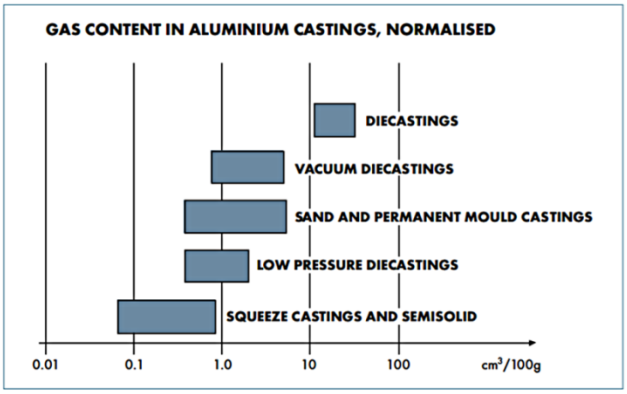

Figure 1. Comparative gas contents arising from different casting processes. Reprinted with permission from [2].

This confirms that the variables affecting the microstructure and defects generation include not only alloy composition and production process, but also heat treatment.

Recently it has been illustrated that conventional HPDC castings can be heat treated without causing unacceptable surface blisters or compromising their mechanical properties. Lumley et al. [7,11,12]demonstrated that lower solution-treatment temperatures and shorter times than those normally used for Al-Si based alloy should effectively produce a good age hardening response without surface blistering. In the same studies [7,11,12], it was shown that significant mechanical responses were possible even reducing the solution temperature to values as low as 714 K (440 °C) and to less than 15 min of total heat treatment.

It is well-established that Si particles undergo significant changes in size and shape during solution treatment and they normally require a time up to 16 hours to achieve complete homogenization within Al grains and spheroidization. However, the use of lower temperatures and much shorter times has proven to be effective.

By adopting such heat treatments, the mechanical properties, which are strongly influenced by the characteristics of eutectic silicon particles in Al-Si based alloys, can be adequately improved, often by more than 100%, with a consequent cost saving and weight reduction. Indeed, the eutectic Si particles play an important role in determining the fatigue and tensile properties. In the as-cast condition, the eutectic Si crystals typically display an acicular or lamellar morphology, which is often modified in a more fibrous one since it is more favorable in terms of fatigue strength and elongation [13]. For this reason, besides the use of common chemical

modifiers, i.e. Sr and Na, specific heat treatments are also applied to change the eutectic Si morphology from a coarse, flake-like form to a fine fibrous one [14].

In the present work, the mechanical response and the microstructure of an AlSi12Cu1(Fe) Aluminum alloy were examined after stabilization heat treatment at 624 K (350°C) for times ranging from 1 to 8 hours. Although the selected treatment times can be considered short to achieve a complete spheroidization of eutectic Si, it was found that they were sufficient to show a considerable mechanical improvement compared to the as-cast conditions. Optical Microscopy (OM) and Transmission Electron Microscopy (TEM) confirmed the evolution of Si particles morphology after heat treatment; in addition, the TEM allowed to observe the fine precipitation within the α-Al matrix, in part responsible for the mechanical improvement.

The formation of Si precipitates within the Al matrix after heat treatment was also observed in literature [15–17]: many researches tried to investigate the factors leading to the formation of Si precipitates within the Al matrix in different Aluminum alloys; however, the causes of their formation and the consequences on the HPDCs' mechanical behavior must be deeply understood.

Static and fatigue mechanical tests and hardness assessment confirmed the changes due to heat treatment. A selected heat treatment was carried out also on AlSi12(b) alloy components in order to verify its effectiveness through subsequent static and fatigue tests and hardness assessment.

Finally, according to the presented findings, in the authors' opinion, a heat treatment shorter than that commonly applied in industry could be the desirable choice for HPDC Al-Si components since the costs are minimized due to the low temperature adopted and the shorter duration of the thermal cycle, allowing for substantial energy savings, and the mechanical properties are enhanced.

2. Experimental procedure

In the present work, two recycled Al-Si based alloys (AlSi12(b) and AlSi12Cu1(Fe))were taken into account; the alloy chemical compositions are listed in Table I. The alloys were adopted to produce commercial HPDC components (supports for electronic devices) and a detailed description of the component geometry (see Figure 2) and its production process is reported elsewhere [19].

Table 1. Chemical composition of the experimental alloys (wt%); the composition limits of AlSi12(b) (EN AC-44100) and AlSi12Cu1(Fe) (EN-AC47100) alloys are also reported according to EN1706:2010 standard [18].

Alloy	Si	Fe	Cu	Mg	Mn	Ni	Ti	Zn	Al
EN AC-44100	10.5-13.5	0.65	0.15	0.10	0.55	0.10	0.20	0.15	Bal.
Tested alloy	13	0.458	0.083	0.023	0.294	0.008	0.032	0.116	Bal.
EN AC-47100	10.5-13.5	1.3	0.7-1.2	0.35	0.55	0.30	0.20	0.55	Bal.
Tested alloy	11.6	0.85	0.849	0.082	0.199	0.051	0.049	0.45	Bal.

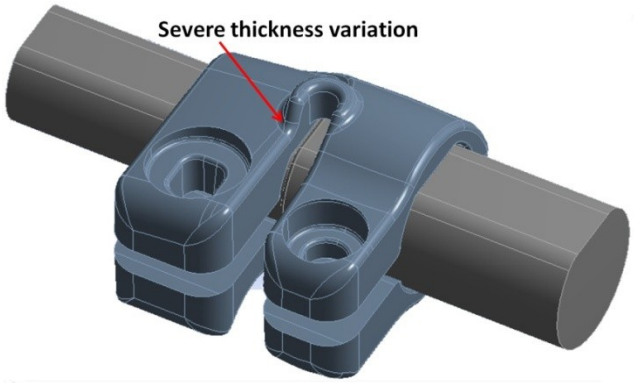

Figure 2. Geometry of the component with highlighted geometrical critical point

The as-cast AlSi12Cu1(Fe) alloy components were heat treated at a stabilization temperature equal to 624 K (350°C), with soaking times of 1, 2, 4 and 8 hours in order to improve their static and dynamic mechanical behaviors. The duration of the various heat treatments represents the actual time of heat treatment (i.e. time to heat up is not included); their durations were chosen according to previous tests conducted on secondary high ductility and high strength AlSi alloys [20].

As a remarkable improvement of mechanical properties in the AlSi12Cu1(Fe) castings was observed already after 1 hour at 624 K (350°C), the AlSi12(b) castings were also heat treated at the same stabilization time and temperature in order to study the mechanical consequences on this alloy which will show a better tensile and fatigue response in the as-cast condition.

In order to analyze the tensile properties of the two alloys, several flat bone-like specimens were produced and tested. Tensile tests were carried out according to ASTM B557M-15 [21], on a MTS Criterion C43 tensile testing machine; the crosshead speed was 2mm/min. Stress-strain curves were obtained using an extensometer (25 mm) attached to the gauge length of the

specimens. Test data of at least three replicates for each alloy were used to obtain the ultimate tensile strength (UTS), the yield strength (YS) and the elongation at fracture (A%).

Stabilization heat treatment at 624K (350°C) for 1 h were performed on both alloys in order to investigate its effect on the tensile properties of the alloys.

Static and dynamic mechanical tests were carried out on the as-cast and heat treated commercial diecastings, of both Aluminum alloys. The static mechanical tests were performed on the same computer controlled machine MTS Criterion C43; the crosshead speed was 2mm/min. The component was clamped on a framework (Figure 3) specifically designed with a tightening torque equal to 1.8 Nm; the load was applied *via* the crosshead. The dynamic tests were conducted on a servo-hydraulic MTS 858 Mini Bionix test system with a load cell capacity of 25 kN. The load-controlled fatigue tests were performed at room temperature with a constant frequency of 5 Hz; the nominal load ratio, R, was kept constant and equal to 0.1. As regards the heat treated components, a single and heavy burden load range was adopted (1350 N), and at least three components of both alloys were tested.

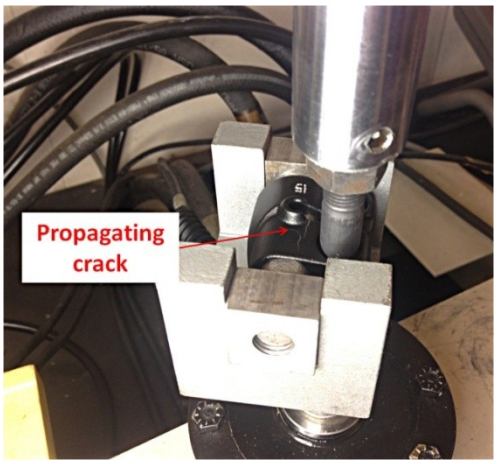

Figure 3. Ongoing dynamic mechanical test

Brinell hardness measurements were performed on ground and polished samples drawn near the fracture surfaces; the tests were carried out using a load of 62.5-kgf. Each data point represents the average of three or more hardness tests. Results clearly affected by the presence of porosity were discarded and the measurement repeated. The hardness outcomes were adopted to reveal trends in changes in the alloy due to time increase during heat treatment rather than as values representative of the bulk material.

Samples for metallographic investigations were cut near the critical point described in Figure 2 [19]. They were mechanically prepared to a 3-µm finish with diamond paste and, finally, polished with a commercial 0.04-µm silica colloidal suspension. Microstructural observations were carried out using an OM (Leica® DMLA) and a field emission gun-environmental scanning electron microscope (FEG-ESEM, FEI® QUANTA 250) equipped with an energy-dispersive spectrometer (EDS, EDAX®). OM and SEM micrographs were processed by image analysis software and various microstructural parameters were investigated and measured, such as

eutectic Si particle size and roundness (ρ). For a deeper evaluation of the eutectic Si morphology, electron back-scatter diffraction (EBSD, EDAX®) investigations were performed on the sample surfaces.

Some samples were also deeply etched in a concentrated NaOH solution, as reported by Timelli et al. [22], in order to remove Aluminum and reveal the 3D morphology of eutectic Si crystals.

Specimens for TEM observations were taken from thin slices; discs with 3-mm diameter were cut and then mechanically ground to 20-30 μm, followed by low-angle ion milling. TEM investigations were carried out using a JEM 2000 EX II microscope (JEOL©), operating at 200 keV.

3. Results and discussion

3.1 Tensile tests

The tensile test results and the corresponding standard deviations are plotted in Table II. It should be noted that both UTS and YS decrease after heat treatment, whereas the elongation at fracture increases due to the enhanced ductility reached with the stabilization heat treatment.

Table 2. Average mechanical properties of as-cast AlSi12(b) and AlSi12Cu1(Fe) alloy tensile testing specimens.

Alloy	Condition	YS [MPa]	UTS [MPa]	A [%]
AlSi12(b)	As-cast	123 ± 3	244 ± 20	2.1 ± 0.5
	Heat treated	104 ± 2	195 ± 21	2.4 ± 1.6
AlSi12Cu1(Fe)	As-cast	138 ± 2	236 ± 26	1.4 ± 0.5
	Heat treated	111 ± 1	234 ± 20	2.4 ± 0.1

More interesting is the different elongation enhancement between the two alloys after heat treatment. Despite a better as-cast mechanical response and a lower content of Fe and other elements such as Cu and Mg, the AlSi12(b) shows a less outstanding ductility improvement compared to AlSi12Cu1(Fe)alloy.

The same behavior was observed in the commercial components and the reasons must be connected to a slightly different microstructure between the two alloys, as further explained.

3.2 Mechanical response

The results obtained from previous analyses conducted on the as-cast components [19,23] highlighted that a stress concentration was found near the region characterized by a severe thickness variation. This led to permanent deformation and component failure during its service.

In Figures 4a,b, the mechanical properties of the tested as-cast components are shown and compared in terms of static and fatigue behavior; in Table III the average mechanical results with the corresponding standard deviations are listed.

Table 3. Average mechanical properties of as-cast AlSi12(b) and AlSi12Cu1(Fe) alloy components.

Alloy	Max load at break [kN]	Displacement [mm]	Load range [N]	Num. of cycles	HB
AlSi12(b)	4.07 ± 0.59	1.36 ± 0.11	1350	5583 ± 3585	76 ± 1
			1125	11041 ± 2629	
AlSi12Cu1(Fe)	3.48 ± 0.61	1.04 ± 0.08	1350	78 ± 20	
			1125	231 ± 54	77 ± 1

AlSi12(b) alloy shows a better mechanical response than AlSi12Cu1(Fe) alloy. This can be explained, to some extent, by the lower amount of Fe present in the former alloy; Fe is the most detrimental impurity of Al-Si alloys since it forms brittle and complex intermetallic compounds [24–26]. In addition, in the AlSi12(b) alloy the amount of Mn, that is the most common alloying element introduced to suppress the development of needle particles by promoting the formation of a thermodynamically stable α-phase, is sufficient to keep the Fe:Mn ratio lower than 2 which is the value recommended to encourage the α-phase precipitation [27]. To be precise, the Fe:Mn ratio in the AlSi12(b) alloy reaches 1.18, whereas in the AlSi12Cu1(Fe) alloy it achieves 2.36.

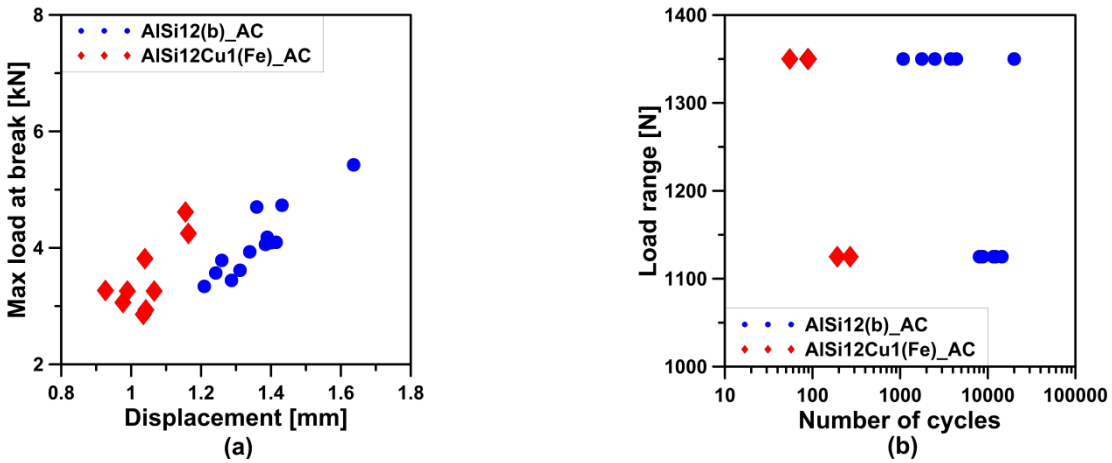

Figure 4. Mechanical results of (a) static and (b) fatigue test in as-cast conditions. Reprinted from [19]

Nevertheless, die soldering which is a serious detractor in the casting industry, represents an important issue with the AlSi12(b) [28,29]. Indeed, due to the lower amount of Fe in this alloy, a surface reaction can take place and molten metal sticks to the surface of the metallic die mold during the casting process, causing casting operation interruptions in order to repair or replace the die.

Hence, heat treatments were largely conducted only on AlSi12Cu1(Fe) HPDCs, with the aim of improving their mechanical response without excessively affecting the costs. In Figures 5a and 5b the mechanical responses of the AlSi12Cu1(Fe) alloy castings after heat treatment are displayed and compared to the as-cast properties of both AlSi12Cu1(Fe) and AlSi12(b) alloys. In Table IV the average mechanical results and the corresponding standard deviations are listed.

Table 4. Average mechanical properties of AlSi12Cu1(Fe) alloy components after heat treatment

HT duration	Max load at break [kN]	Displacement [mm]	Load range [N]	Number of cycles	HB
1h	7.09 ± 0.15	2.05 ± 0.20	1350	11295 ± 2636	69 ± 0.6
2h	7.66 ± 0.34	2.14 ± 0.18	1350	10641 ± 374	66 ± 0.6
4h	8.58 ± 0.08	2.64 ± 0.08	1350	17942 ± 2910	64 ± 0.6
8h	7.46 ± 0.48	2.51 ± 0.21	1350	20000 ± 0	60 ± 2.1

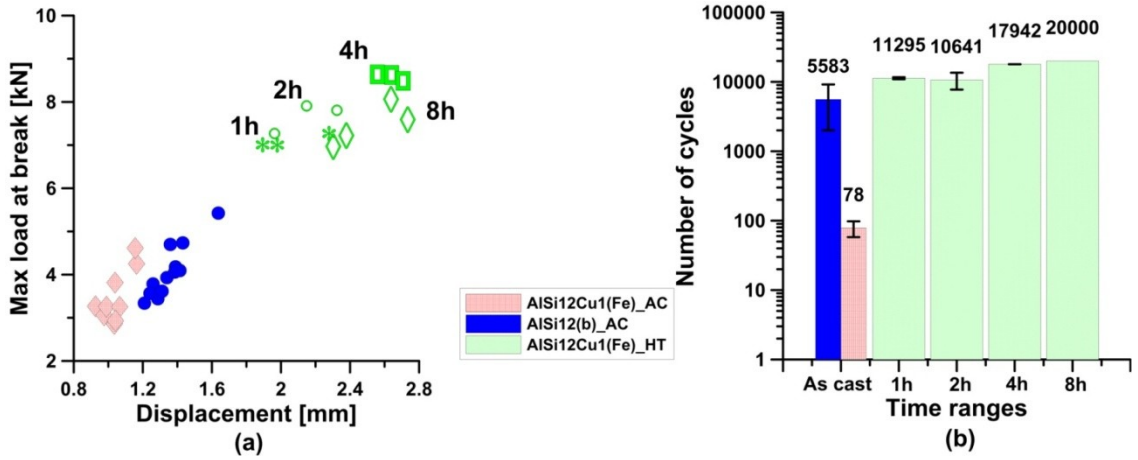

Figure 5. Mechanical results of (a) static and (b) fatigue test in as cast and heat treated conditions

As evidenced from Figure 5, after heat treatment the mechanical properties are significantly improved both in terms of static and fatigue responses. The mechanical improvement is much more outstanding in terms of fatigue life. As can be seen, the AlSi12Cu1(Fe) alloy does not reach 100 cycles in the as-cast condition, on the other hand, the AlSi12(b) alloy exceeds 5000 cycles in the same status. After 1 hour heat treatment, the dynamic mechanical response of the former alloy is much better than the as-cast AlSi12(b) alloy.

This improvement can be related to changes in microstructure, primarily to the morphological changes of the Si crystals in the eutectic areas [30], also described below. Moreover, the formation of Si precipitates within the α-Al matrix and the interruption of Si continuity within eutectic colonies also affect the mechanical improvement.

The more outstanding static and dynamic mechanical improvement after heat treatment of the AlSi12Cu1(Fe) alloy compared to the AlSi12(b) alloy has many reasons. Solidification conditions, nucleant characteristics and alloy chemistry strongly influence the microstructure of the Al-Si eutectic grains. Common ternary alloying elements such as Cu, Mg and Fe may influence the nucleation and growth dynamics of the eutectic and thus the final microstructure [31]. They can induce a more refined eutectic Si morphology and thus make the Si particles

fragmentation easier. Indeed, in the case of the AlSi12Cu1(Fe) alloy, the eutectic Si shows the aforementioned Si network which, in as-cast condition, has a detrimental effect on the mechanical response of the components. Nevertheless, after heat treatment, the thinner Si crystals branches of the network tend to fragmentize more easily than coarser particles. This partially justifies the more outstanding mechanical improvement, after heat treatment, of the AlSi12Cu1(Fe) alloy compared to the AlSi12(b) one. Unlike typical modifying elements as Sr, Na and Sb, little research has been devoted to understanding the effect of the Al-Si microstructure of common alloying elements.

After more than 2 hours of heat treatment, a change in the breaking point position was observed due to the elevated ductility reached by the alloy (Figure 6). Figure 6b shows the new location of the breaking point after 4 hours of heat treatment. This change is representative of the lessened sensitivity of the alloy, after heat treatment, to the sudden thickness reduction. It represents a drawback since, even if the number of cycles are enhanced, the component undergoes a permanent deformation, during its service, that prevents any further employment.

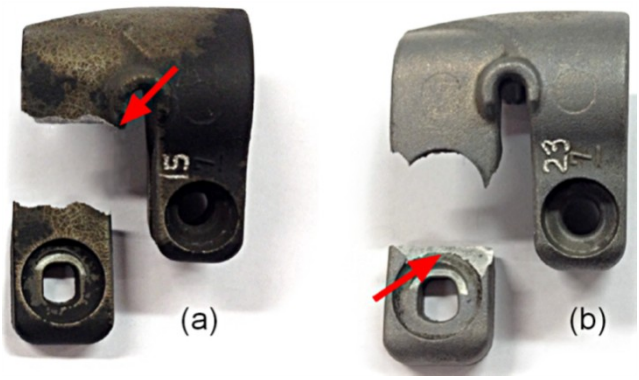

Figure 6. Change of the breaking point in the fatigue-tested AlSi12Cu1(Fe) components in the (a) as-cast condition and (b) after 4-h heat treatment.

The heat treatment does not only affect the mechanical properties in terms of maximum load at break and number of cycles, but also the hardness, as can be seen in Figures 7a,b and in Table IV.

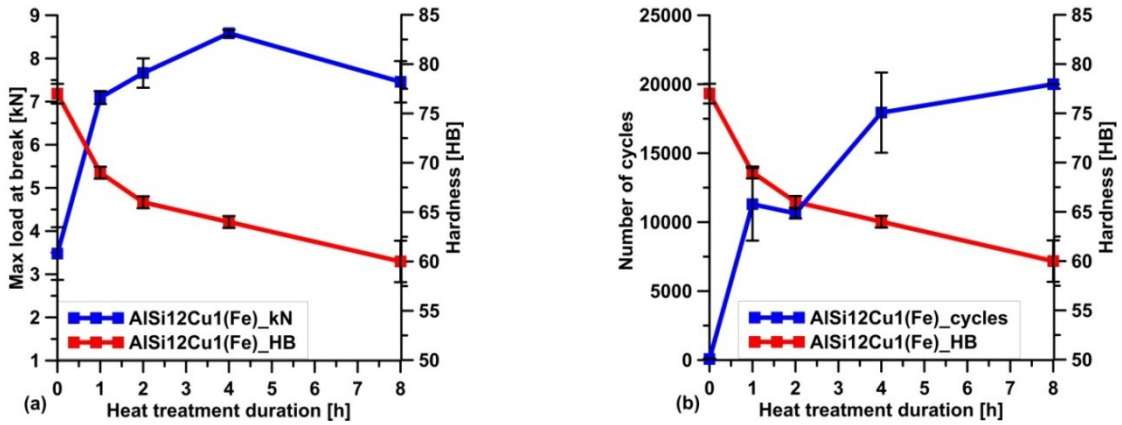

Figure 7. Hardness and (a) maximum load at break, (b) number of cycles of AlSi12Cu1(Fe) alloy, as functions of increased heat treatment duration.

Since the mechanical improvement is already visible after 1 hour of heat treatment and the drawback shown in Figure 6 takes place after more than 2 hours, the shortest heat treatment duration was chosen as the best solution. As aforementioned, the static and dynamic mechanical properties of the AlSi12(b) alloy heat-treated at 624 K (350°C) for 1h were measured for comparison with the as-cast conditions; they are shown in Figures 8a,b.

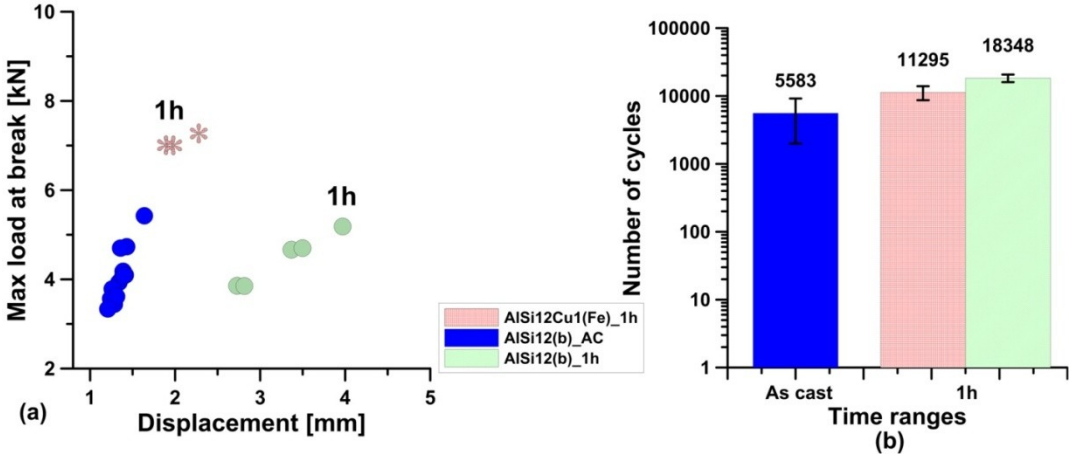

Figure 8. Mechanical results of (a) static and (b) fatigue tests conducted on AlSi12(b) alloy after 1 hour of heat treatment at 624 K. The AlSi12(b) as cast results are also displayed.

The AlSi12(b) mechanical response shown in Figure 8 confirms the effectiveness of the heat treatment.

It should be highlighted, as anticipated, that the dynamic mechanical improvement of the AlSi12Cu1(Fe) alloy, after heat treatment, is noteworthy. Only after 1 hour soaking time at 624 K (350°C), its fatigue mechanical behavior is 145 times better compared to the as-cast condition; on the contrary, the AlSi12(b) alloy shows a fatigue mechanical response 3 times higher than the starting as-cast condition.

Moreover, AlSi12(b) components show a noticeable enhancement of their ductility rather than an improvement of the maximum load at break; on the contrary, AlSi12Cu1(Fe) HPDCs show a

shift of the maximum load at break. These different behaviors can be attributed, on one hand, to a similar modification that eutectic Si crystals undergo, i.e. the Si "network" fragmentizes and coarser crystals smooth their edges during heat treatment and, on the other, to the slightly different chemical compositions of the two alloys. In particular, AlSi12Cu1(Fe) alloy shows higher amounts of strengthening alloying elements, such as Cu and Mg (see Table I), that contribute to peak load improvement.

3.3 Eutectic Si "network" in AlSi12Cu1(Fe) alloy

As shown in Figure 9, heat treatments tend to break the eutectic Si particles into smaller ones or, for shorter times, tend to smooth and round their edges. As already observed by Pedersen et al. [30], in as-cast conditions, the Si crystals are coarse; on the other hand, even a short heat treatment can cause the fragmentation of small Si crystals and the curvature of their edges.

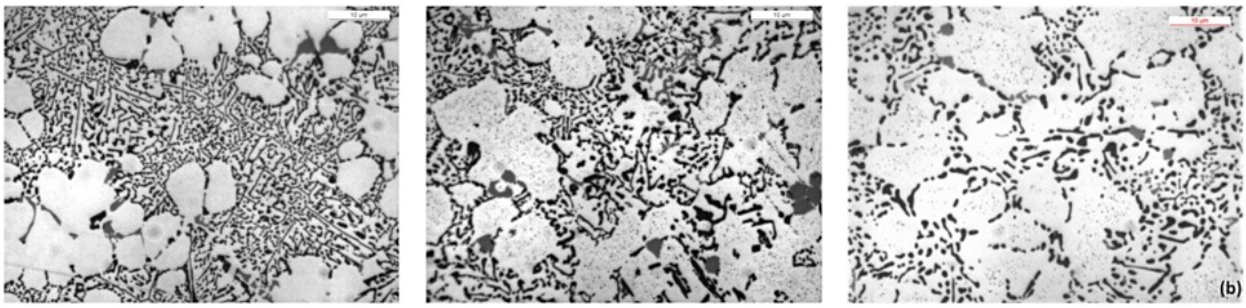

Figure 9. Eutectic Si morphology of AlSi12Cu1(Fe) alloy (a) in as cast condition, (b) after 1 hour and (c) after 4 hours of heat treatment at 624 K

In Figures10a,b the as-cast Si structure, after deep-etching, is shown. It can be observed that the areas of the structure that appear like a sort of eutectic Si "network" are indeed more or less connected to each other. This interconnection is confirmed by Figures11a,b in which a SEM micrograph and the corresponding EBSD grain-orientation maps, are shown.

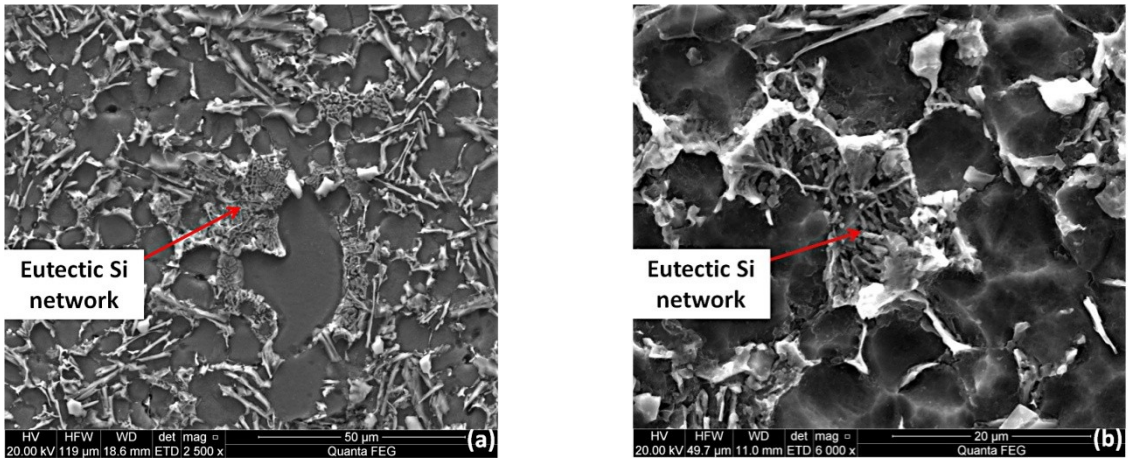

Figure 10. Si crystals in the eutectic region of AlSi12Cu1(Fe) alloy. Images obtained with secondary

electrons: (a) 2500x, (b) 6000x. The material has been deep etched.

From the Inverse Pole Figures (IPF) in Figure 11b, it appears that the Si particles of the eutectic "network" areas of AlSi12Cu1(Fe) alloy form colonies that show preferential crystal orientations that are therefore reasonable to be considered connected.

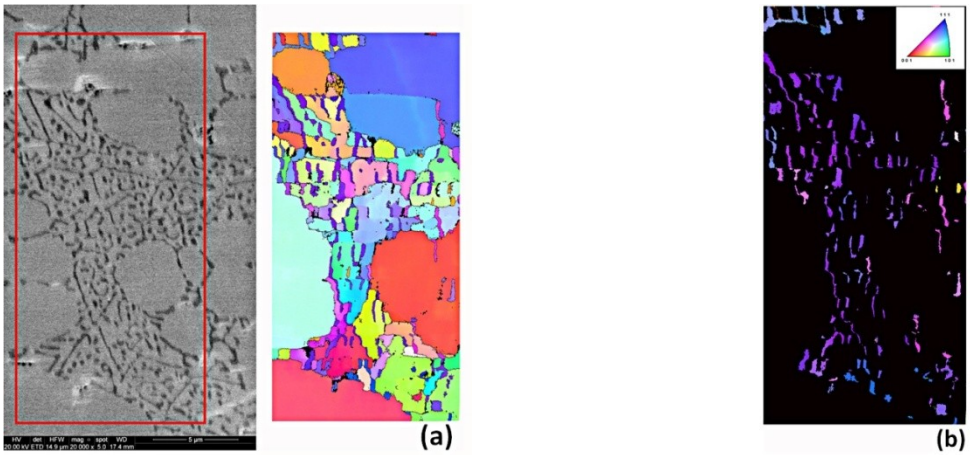

Figure 11. (a) SEM micrograph of eutectic Si "network" and corresponding IPF map; (b) IPF map of the Si phase.

It can be assumed that shorter heat treatments, i.e. up to 2 hours, only lead to a rounding of coarser plates' edges while finer plates start to fragmentize. Thus, it can be concluded that the ductility of the components strongly depends on Si crystals' size and morphology. The as-cast structure, characterized by coarse Si plates or an interconnected "network" leads to a rapid reduction of the load-bearing area during the component use and the crack can propagate rapidly through the structure. On the contrary, as confirmed in literature by Pedersen et al.[30], when the size of the silicon crystals is reduced and the fragmentation has taken place, the casting failure is less instantaneous as the crack has to propagate through the ductile Aluminum matrix.

In order to confirm the effect of heat treatment duration on Si smoothing and fragmentation, the roundness (ρ) of eutectic Si crystals was calculated as follows:

$$\rho = \frac{p^2}{4\pi A} \tag{1}$$

where P is the perimeter and A is the area of each particle. According to the Eq. (1), the minimum value of ρ is 1 corresponding to a circle shape. The mean roundness values for the experimental AlSi12Cu1(Fe) alloy, reported in Table V, point out a morphological variation after heat treatment which can be correlated to the hardness decrease as shown in Figures 12a,b.

Table 5. Mean roundness values of eutectic Si particles for AlSi12Cu1(Fe) alloy in as cast condition and after 1 and 4 hours of heat treatment.

Time range [h]	ρ	Standard deviation
As cast	8.7	0.6
1	7.2	0.4
4	4.3	0.5
8	3.4	0.1

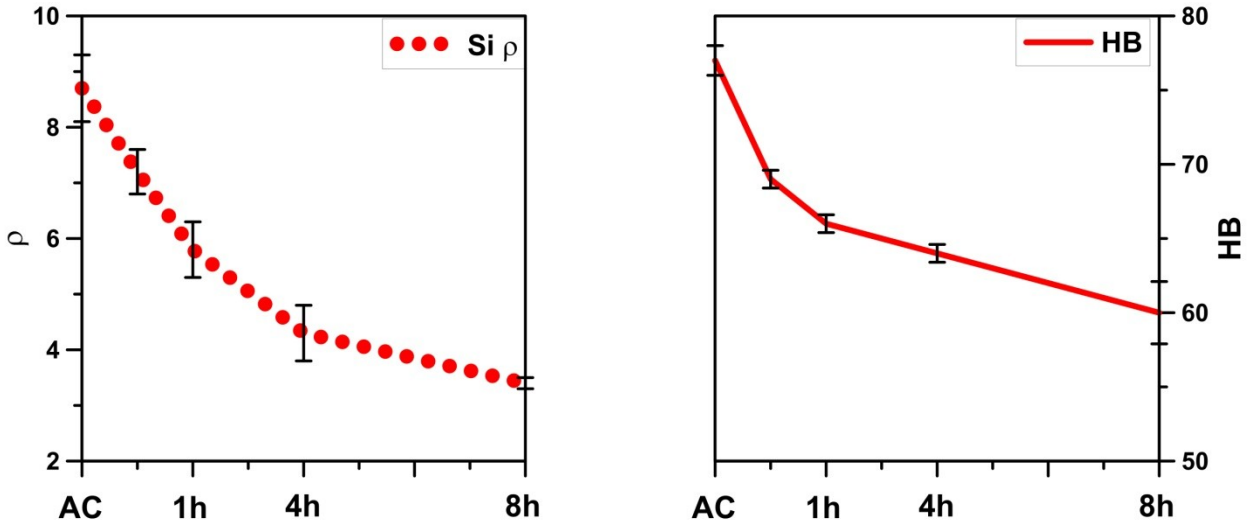

Figure 12. (a) Si particles roundness trend and (b) hardness trend for AlSi12Cu1(Fe) alloy.

As already observed by Manente and Timelli [32], increasing the heat treating time the interparticle distance increases; since Rayleigh instability occurs, Si crystals undergo necking and are broken down into fragments. The instability generated and the reduction in the total interface energy lead to eutectic Si spheroidization and coarsening. As stated by Greenwood [33], coarsening and spheroidization, evaluated through roundness assessment, are diffusion-controlled processes so they are directly proportional to heat treating time (temperature is kept constant in this study).

3.4 Si precipitates within α-Al matrix of AlSi12Cu1(Fe) alloy

Another phenomenon that takes place after heat treatment and that must be taken into account is the precipitation of a Si phase within the α-Al matrix, which seems to be less widely investigated in literature. Several researchers studied the precipitation behavior of Mg-containing precipitates from solid solution in Al-Mn-Fe-Si (3xxx) and Al-Mg-Si-Mn (6xxx) wrought alloys during heating and homogenization processes[16,17,29,34].Li et al. [17] focused on a DC-cast AA3003 alloy and highlighted the formation of very fine precipitates with sizes of about several nanometers, only after heating the alloy at 573 K (300°C). They also noticed a size evolution of

the precipitates controlled by nucleation, growth, coarsening and dissolution. Chen et al. [15] investigated the mechanism of the precipitation a Si-containing phase and its hardening effect for an AlSi7Mg alloy. They concluded that the supersaturated Si concentration in the matrix leads to the precipitation of Si particles after the completion of solidification; an increase in size, but a slight decrease in the number per area was also observed after long time heat treatments. Moreover, as it was also observed in the present study, a precipitate-free zone (PFZ) near the eutectic was recognized.

The evolution of size and number per area of Si precipitates after 1 h and 8 h of stabilization heat treatment is shown in Figures 13a,b, respectively. The size of precipitates increases with holding time, however nothing can be said about their number per area.

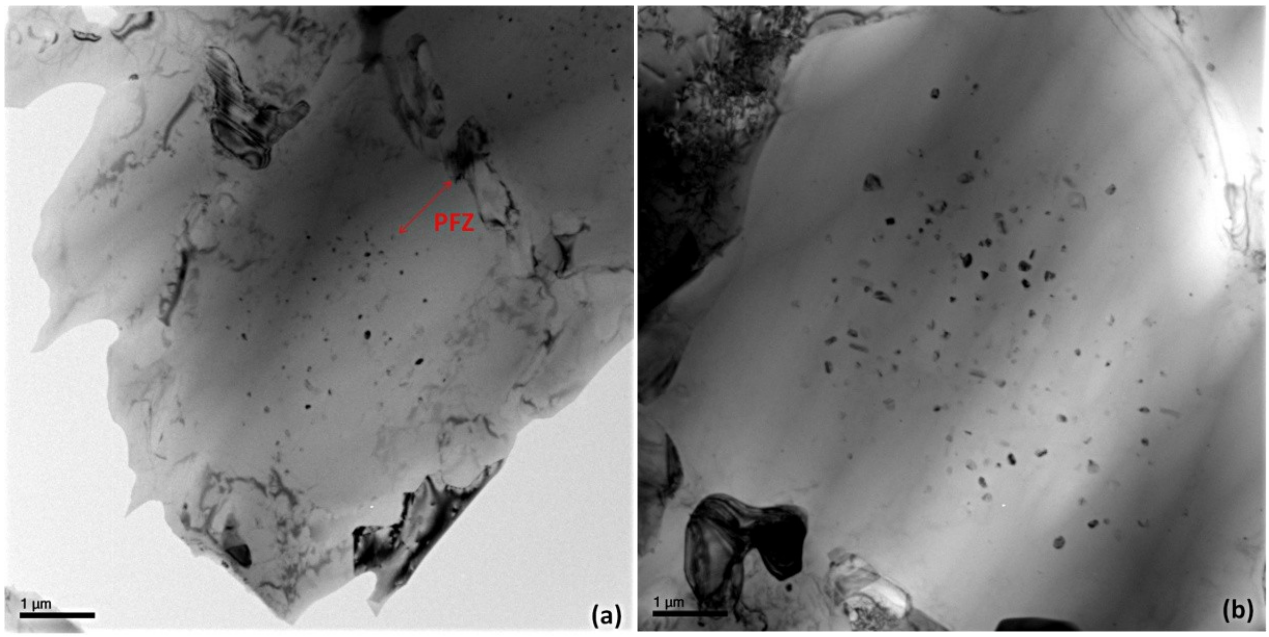

Figure 13. Al grain with evident Si precipitates after (a) 1h and (b) 8 h of heat treatment

As shown in Figures 14a and 14b, most of the precipitates formed in the vicinity of dislocations probably because (i) heterogeneous nucleation at dislocations can reduce the nucleation energy barrier of precipitates [35,36] and (ii) solid state diffusion (in this case, of Si atoms) is made easier by the presence of dislocations.

Dislocations, as well as vacancies, grain boundaries, stacking faults, inclusions and free surfaces are suitable nucleation sites since they increase the free energy of the material and contribute to reduce the total strain energy of the embryo. Nucleation on dislocations may also be promoted by solute segregation which can rise the composition of the matrix to nearer that of the precipitate [31,35].

However, an in-depth analysis is necessary to understand rather their influence or not on the mechanical response of the analyzed diecastings.

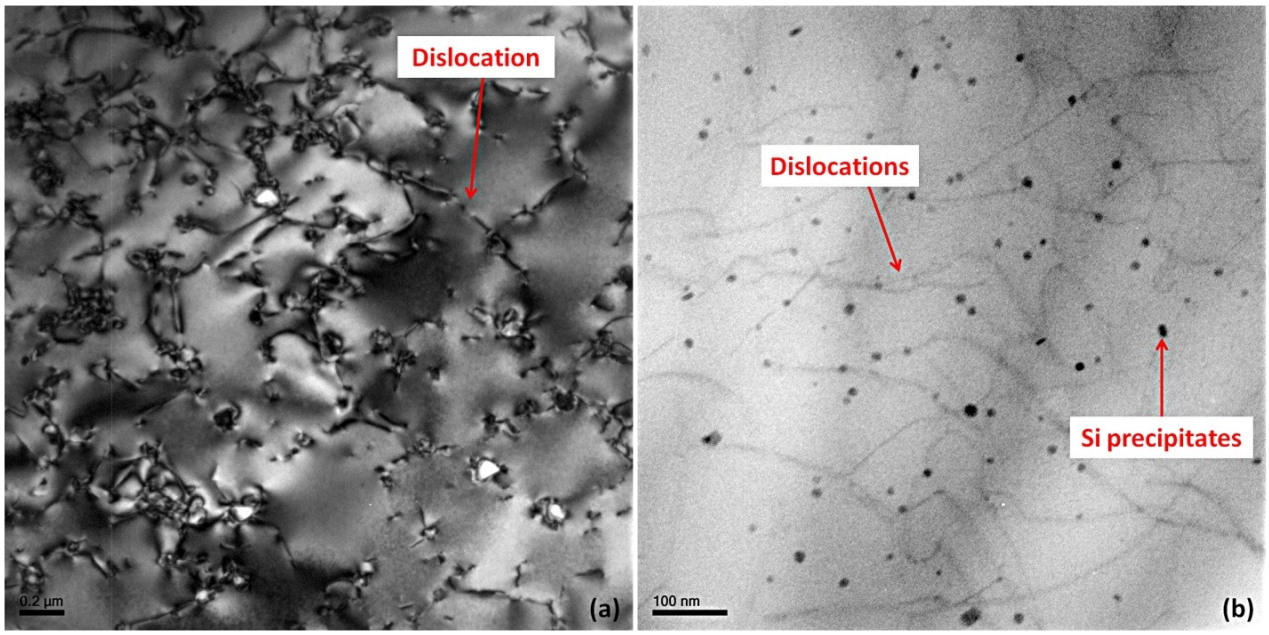

Figure 14. Si precipitates in the vicinity of dislocations after (a) 1 h and (b) 8 h of heat treatment.

Conclusions

The effect of stabilization heat treatment on the mechanical response and microstructure of AlSi12Cu1(Fe) high pressure die castings has been investigated. It was the authors' choice to test different heat treatment durations only on this alloy, in order to improve its mechanical properties and make it competitive with an alternative solution, constituted by the AlSi12(b) alloy [19].

Based on the results obtained in the present study, the following conclusions can be drawn.

- The developed procedure allows to heat treat HPDCs without causing surface blistering or component distortion. It involves stabilization heat treating at 624 K (350°C) for 1 to 8 h.
- The alloy displays visible mechanical improvements in terms of both static and dynamic response. Especially ductility is enhanced over the as-cast condition, but exceeding 2 hours of heat treatment can cause undesirable drawbacks.
- The improved ductility is determined both by size and shape of silicon crystals and by strengthening alloying elements in the chemical composition.
- Silicon particles fragmentize or smooth their edges after heat treatment leading to a less instantaneous failure.
- Heat treatment also leads to the precipitation of silicon within the α-Al. Causes and consequences of Si precipitates within the matrix are not completely clear: further analyses must be carried out.
- It's the authors' opinion that 1 hour heat treatment is enough to obtain good mechanical properties, avoid undesirable drawbacks and limit extra costs. The same heat treatment was also developed on AlSi12(b) alloy castings in order to validate its effectiveness.

Acknowledgements

The authors are indebted to Eng. A. Cenghialta for his support during the experimental work and to G. Mazzacavallo (Department of Management and Engineering, University of Padova, IT) for valuable discussions and comments.

References

[1] H.J. Buchner and J. Glossner: *Proc. 13th Int. Foundry Trade Fair*, Dusseldorf (2015), Germany, pp. 1-31.
[2] F. Bonollo, J. Urban, B. Bonatto and M. Botter: *Metall. Ital.*, 2005, Vol. 6, pp. 23-32.
[3] W.A. Butler, G. Timelli, E. Battaglia and F. Bonollo: *Ref. Modul. Mater. Sci. Mater. Eng.*, Elsevier, 2016, pp. 1-10.
[4] J. Campbell: *Castings*, 2nd edition., Butterworth Heinemann, Oxford (UK), 2003, pp. 1-335.
[5] F. Bonollo, N. Gramegna and G. Timelli:*JOM*, 2015, vol. 67 (5), pp. 901-08.
[6] E. Fiorese, F. Bonollo, G. Timelli, L. Arnberg and E. Gariboldi: *Int. J. Met.*, 2015, Vol. 9 (1), pp. 55-66.
[7] R.N. Lumley, R.G. O'Donnell, D.R. Gunasegaram and M. Givod: *Metall. Mater. Trans. A*, 2007, Vol. 38, pp. 2564-2574.
[8] G. Timelli and F. Bonollo: *Mater. Sci. Eng. A*, 2010, Vol. 528, pp. 273-282.
[9] E. Battaglia, F. Bonollo, G. Timelli, E. Fiorese and G. Kral: *Adv. Mater. Process. Tech.*, 2016, Vol. 698, pp. 1-14.
[10] E.J. Vinarcik and J. Wiley: *High Integrity Die Casting Processes*, John Wiley & Sons Inc., Hoboken NJ, 2003, pp. 1-223.
[11] R.N. Lumley, D.R. Gunasegaram, M. Gershenzon and R.G. O'Donnell: *Int. Heat Tret. Surf. Eng.*, 2010, Vol. 4, pp. 25-32.
[12] R.N. Lumley, I.J. Polmer and P.R. Curtis: *Metall. Mater. Trans. A*, 2009, Vol. 40, pp. 1716-1726.
[13] Q. Wang: *Metall. Mater. Trans. A*, 2003, Vol. 34, pp. 2887-2899.
[14] M.F. Ibrahim, E.M. Elgallad, S. Valtierra, H.W. Doty and F.H. Samuel: *Materials*, 2016, Vol. 9, pp. 1-17.
[15] R. Chen, Q. Xu, Z. Jia and B. Liu: *Mater. Des.*, 2016, Vol. 90, pp. 1059-1068.
[16] R. Hu, T. Ogura, H. Tezuka, T. Sato and Q. Liu: *J. Mater. Sci. Technol.*, 2010, Vol. 26, pp. 237-243.
[17] Y.J. Li and L. Arnberg: *Acta Mater.*, 2003, Vol. 51, pp. 3415-3428.
[18] European Standard EN 1706, Aluminium and aluminium alloys – Castings – Chemical composition and mechanical properties, CEN-CENELEC, Brussels (2010).
[19] E. Battaglia, F. Bonollo and P. Ferro: *Metall. Mater. Trans. A*, 2017, Vol. 48, pp. 2574-2583.
[20] R. Zambelli, P. Parona, F. Bonollo, E. Battaglia: *La Metallurgia Italiana*, 2016, Vol. 108, pp.157-160.
[21] ASTM B557M-15: *Standard Test Methods for Tension Testing Wrought and Cast Aluminum- and Magnesium- Alloy Products (Metric),* 2015, USA.
[22] G. Timelli, A. Fabrizi, S. Capuzzi, F. Bonollo and S. Ferraro: *Mater. Sci. Eng. A*, 2014, Vol. 603, pp. 58-68.

[23] E. Battaglia, F. Bonollo, P. Ferro, A. Cenghialta and G. Mazzacavallo: *Metall. Ital.*, 2016, Vol. 108, pp. 61-64.
[24] S. Ferraro, A. Fabrizi and G. Timelli: *Mater. Chem. Phys.*, 2015, Vol. 153, pp. 168-179.
[25] H. Zhu, X. Zhang, M.J. Couper and A.K. Dahle: *Mater. Chem. Phys.*, 2009, Vol. 113, pp. 401-406.
[26] C. Yang, S. Lee, C. Lee and J. Lin: *Mater. Chem. Phys.*, 2005, Vol. 93, pp. 412-419.
[27] S. Ji, W. Yang, F. Gao, D. Watson and Z. Fan: *Mater. Sci Eng. A*, 2013, Vol. 564, pp. 130-139.
[28] K. Domkin, J.H. Hattel and J. Thorborg: *J. Mater. Process. Technol.*, 2009, Vol. 209, pp. 4051-4061.
[29] S. Shankar and D. Apelian: *Metall. Mater. Trans. B*, 2002, Vol. 33, pp. 465-476.
[30] L. Pedersen and L. Arnberg: *Metall. Mater. Trans. A*, 2001, Vol. 32, pp. 525-532.
[31] A. Darlapudi, S.D. McDonald, S. Terzi, A. Prasad, M. Felberbaum, D.H. StJohn:*J. of Crystal Growth*, 2016, Vol. 433, pp. 63-73.
[32] A. Manente, G. Timelli: *Recent trends in processing and degradation of aluminum alloys,* www.intechopen.com
[33] Greenwood G.W.: *Acta Metallurgica*, 1956, Vol. 4, pp. 243-248.
[34] Q. Du, W.J. Poole, M.A. Wells and N.C. Parson: *Acta Mater*, 2013, Vol. 61, pp. 4961-4973.
[35] A.W.F. Muggerud, E.A. Mortsell, Y. Li and R. Holmestad: *Mater. Sci. Eng. A*, 2013, Vol. 567, pp. 21-28.
[36] D. Porter, K.E. Earsterling and M. Sherif: *Phase Transformations in Metals and Alloys*, 3rd Edit., Taylor & Francis Group, Abingdon (UK), 2009.